Molecular Imaging of Prostate Cancer Using Biomarker-Guided Strategies

A DISSERTATION

SUBMITTED TO THE FACULTY OF THE GRADUATE SCHOOL

OF THE UNIVERSITY OF MINNESOTA

BY

MARIYA SHAPOVALOVA

IN PARTIAL FULFILLMENT OF THE REQUIREMENTS

FOR THE DEGREE OF

DOCTOR OF PHILOSOPHY

Advisor

Aaron LeBeau, PhD

August 2019

© Mariya Shapovalova

Acknowledgements

There are many people I would like to thank for helping me get to this point in my life. This was a team effort. The PhD process challenged me in every way possible. I can honestly say that my way of thinking has been changed about science and medicine.

First, I would like to thank my wonderful family. My parents came to the United States from Ukraine in hopes of a better future for me. Without the move, this would not have been possible. I remember moving to NYC when I was 5. It was a difficult time in our lives, but I am forever grateful for my parents' hard work to get established here in the United States. My parents are a constant source of support and are the main reason I was able to earn my PhD. Thank you, Mom and Dad, for everything. Thank you to all of the relatives in Ukraine, particularly grandma and grandpa for being my biggest fans and sincerely believing that I can do anything, even become the president of the U.S., which truly shows they believe I can do anything because I was not born in the U.S.! Also, thank you to my sister Nastya, for visiting me in Minnesota every summer and brightening every day she was with me. I am a lucky to have my amazing family, I love you all very much.

A PhD can often be challenging intellectually and emotionally. The amount of hard work that I put in sometimes made it very difficult to handle the failures. Luckily, I had an advisor that understood how to see the positivity in failure and was always supportive of me, no matter what kind of day I was having. Thank you, Aaron, for being a source of knowledge, mentorship, and incredible support. I came into this lab relatively inexperienced and now I can honestly say that the research has turned me into a critical thinker.

My accomplishments could not have been possible without my partner in life, Sean. Sean and I remained in a long-distance relationship throughout my PhD. As if the PhD is not challenging enough, we also had to juggle international visits because he is from Canada! Sean, thank you for listening to all of my rants about cells dying, bacteria not growing, weird results, and so much more. Of course, there were also positive conversations, but Sean's support always came through when things weren't working in my favor. I am incredibly grateful for all of your support, love, and patience.

I may not have a biological twin, but Melyssa, my best friend is my spiritual twin. She and I ended up going to graduate school at the same time, in Pharmacology, only at different schools. She ended up at Case Western, Ohio. She understood this time of my life like no other. She was a rock throughout this entire PhD adventure and the only person that actually comprehended my scientific rants. Thank you Melyssa for supporting me from day one.

Lastly, I would like to thank my colleagues, my committee, and the animals involved in my studies. Thanks Hallie and Paige for being a resource in the lab. We were the first members in our lab which came with extra challenges. I couldn't have asked for more dependable co-workers. I'd like to thank my committee for guiding me through this degree. My committee consisting of Hiroshi Hiasa, PhD, Cheuk Leung, PhD, Greg Metzger, PhD, and of course my PI Aaron LeBeau, PhD helped shape my experience and my research. Lastly, I would like to acknowledge the mice that helped contribute to my research. Thank you to all of the animals, because without them, the medical field would not be the same.

Dedication

I dedicate this to my parents Kateryna Shapovalova and Vladyslav Shapovalov.

Abstract

Prostate cancer affects 1 in 9 men in their lifetime. While disease that is detected early can be very treatable, recurrence affects about 30% of the patients. Imaging is an important tool for detecting and assessing therapeutic regimens for prostate cancer patients. Patients with advanced stages of prostate cancer, typically those who have had a recurrence and are forming resistance to hormone therapy, are in a great need for a more accurate assessment of the extent of their disease for a better understanding of its aggressiveness. Clinical imaging offers physicians information about the location and extent of disease. Unfortunately, conventional imaging methods often lack the sensitivity needed to detect some lesions properly, especially when the disease is no longer localized and has spread outside of the prostate, which leads to insufficient information that is needed for proper diagnosis and treatment planning. Most of the current imaging techniques are not specific for tumor physiological processes. Therefore, a clinical need remains for new imaging agents that can target prostate tumors more specifically and sensitively. My PhD research focused on using molecular-genetic imaging approaches to develop imaging agents *in vitro* and *in vivo* that can detect prostate cancer using the cancer's unique regulatory genetic differences from normal cells. I investigated the expression two prostate cancer-specific genes, *AMACR* and *PEG10* and used the genes' unique transcriptional regulations in the prostate cancer cells to induce prostate cancer-specific expression of reporter proteins. Specifically, I used the promoters of AMACR and PEG10 in adenovirus and plasmid DNA vectors upstream of various reporter genes to induce expression of reporter proteins in prostate cancer cells. By using the prostate cancer-specific promoters, I was able to image prostate cancer *in vivo* using various vectors and different modes of imaging such as

bioluminescence/fluorescence and positron emission tomography imaging. My results strongly support that prostate cancer specific promoters can induce prostate cancer specific gene expression and may have the potential to be used for imaging purposes.

Table of Contents

List of Figures

List of Tables

Chapter I: Introduction

Prostate Cancer

In the United States (US), prostate cancer (PCa) is the second most common cause of cancer in men, surpassed only by non-melanoma skin cancer [1]. In 2019, approximately 170,000 men will be diagnosed with PCa, and over 30,000 men are estimated to lose their lives to PCa [2]. PCa takes a long time to develop and most patients are asymptomatic at diagnosis since the Food and Drug Administration (FDA) approval of prostate-specific antigen (PSA) blood screening test in 1994 [3, 4] which allows for more timely detection of the disease.

The Prostate

The prostate is a walnut-sized gland [5] located in the pelvis anterior to the rectum and inferior to the bladder. The urethra runs through the center of the prostate and while lymph nodes are found throughout the body, some of them are in the pelvic area, near the prostate [6]. The prostate gland is a male sex organ that produces and secretes seminal fluid to protect the sperm and may facilitate sperm motility, however, the function of the organ is not fully understood. The prostate is divided into four lobes; anterior, middle, lateral, and posterior lobes [7]. The prostate consists of branching glands with ducts, which are lined with secretory epithelial cells and basal cells as well as scattered neuroendocrine cells [8-10]. The secretory epithelial cells (luminal cells) depend on androgen for growth and production of PSA. These secretory cells are derived from the transitional cell population (intermediate cells). The basal cells are not androgen-dependent and rarely express the

androgen receptors (AR). Basal cells give rise to the intermediate cells, from which the luminal cells will form. The gland is also surrounded by stroma that consists of fibroblasts, smooth muscle, nerves, and lymphatics [9]. A schematic of the different cellular compositions found in the prostate can be seen in **Figure 1-1.** The relevance of the lymph nodes is that PCa can often spread to them because of their close proximity to the prostate.

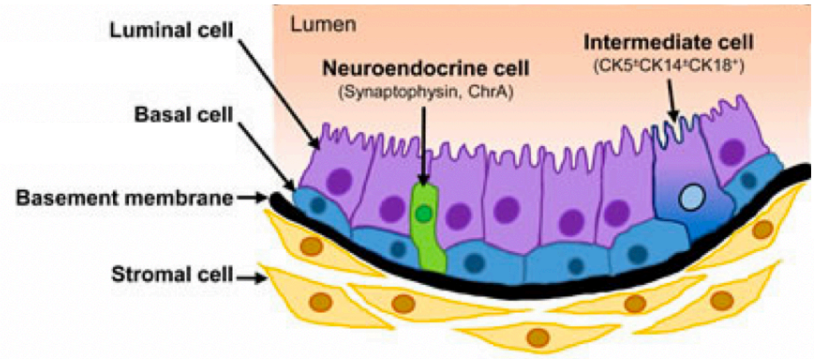

Figure 1-1. Schematic of the cellular composition of the prostate epithelium.

The prostate epithelium consists of inner secretory luminal cells and surrounding basal cells. The basement membrane is the barrier between the epithelium and stromal sections. Intermediate cells derived from basal cells give rise to luminal cells. Neuroendocrine cells are scarcely scattered throughout the lumen. The image was extracted/adapted from reference [10]. Permission to reuse and reprint the article are allowed as long as the original authors are cited.

Because PCa grows slowly and remains asymptomatic, the disease is often detected at various stages of progression. Localized disease, or cancer that has not spread outside of the prostate [11], has the highest potential for treatment response. Around 77% of new PCa cases are diagnosed as localized disease [12]. Regional PCa is defined as having spread

outside of the gland into nearby structures or lymph nodes [11]. Approximately 13% of PCa cases at diagnosis are regional disease [12]. Distant metastasis means the PCa has spread beyond the pelvis. The bones, liver, and lungs are common sites of PCa metastasis [13]. About 6% of PCa at diagnosis is metastatic disease [12]. Unknown/upstaged PCa account for the remaining 4% of diagnoses [12].

Screening

PCa 5-year survival rate for men diagnosed with local or regional PCa is nearly 100%. However, the 5-year survival rate for men diagnosed with distant metastasis plummets to around 30% [11]. These statistics reiterate the importance of screening since the early detection of asymptomatic, localized PCa. Timely treatment could prevent cancer from developing into metastatic disease and therefore reduce the morbidity associated with PCa. The current standard of care uses the PSA blood test to screen for PCa with or without the digital rectal exam. If a PSA test is suspicious, the patient is further evaluated via a biopsy to determine the final diagnosis [14].

Screening Guidelines

The PSA test has revolutionized PCa screening since its FDA approval in 1994. There is clear evidence that the PSA test reduces the number of deaths from PCa [15] and the benefits of screening are clear in cases where malignant. Despite the proven benefits, some still question if the test does more harm than good. PCa is often so slow-growing that it may not cause a man any problems in his lifetime [16]. The PSA test has led to an increase in the detection of these slow-growing or benign tumors (indolent) and has resulted in the

overtreatment of some patients. These patients experience the adverse side effects associated with PCa treatment such as urinary, bowel, and sexual function [3] with little to no benefit. Several organizations have established similar guidelines for PCa screening that are aimed to distinguish between malignant and benign disease. Therefore, it is more likely that only patients that require treatment receive it. The controversy in screening lies in the overdiagnosis of clinically insignificant tumors, which leads to a related issue of cost versus benefit [17].

Memorial Sloan Kettering Cancer Center's guidelines follow three principles [18]:

- PCa can benefit from active surveillance. A diagnosis of PCa is information used to make decisions, but not an indication for immediate treatment.
- Compliance with screening will increase if men are informed about their risk level.
- There needs to be a balance between the harms and benefits of screening.

There are some risk factors that determine how early men should start their PSA screening:

1. **Age**: The risk of PCa increases with age. After the age of 50, the chances of having PCa increases [19]. Men age 50 and above are recommended to have their PSA level checked annually [20]. 60% of PCa cases are diagnosed in men over the age of 65[2].
2. **Race**: It is not understood why, but African-American men have a higher risk of developing PCa, and the disease tends to be more aggressive [21].
3. **Family History**: If a close family member was diagnosed with PCa before the age of 65, the risk of developing PCa is increased [22].

4. **Inherited Gene Mutations**: BRCA1 and BRCA2 are associated with PCa risk [22].
5. **Diet**: High animal fats and low vegetables in a diet may increase the risk of PCa [23].

PSA

PSA is an androgen-regulated serine protease that is produced by prostate epithelial cells and secreted into the seminal fluid by normally functioning prostates [24]. The functional role of PSA is to cleave semenogelins in the seminal coagulum to increase sperm motility and dissolve cervical mucus [25, 26]. A low level of inactive PSA is released into the bloodstream where it circulates in its unbound state. Active PSA that enters the bloodstream gets quickly bound to protease inhibitors [25]. A PSA concentration of less than 4.0 ng/mL is considered normal, but if a man produces more than 4.0 ng/mL of PSA, a digital rectal exam is performed and a biopsy is recommended to evaluate the lesion using Gleason scoring which will be discussed further in this chapter [27]. Higher levels of PSA are associated with PCa because PSA production is increased in rapidly dividing PCa cells and the presence of cancer disrupts the barriers between the lumen and the capillary causing the release of more PSA into the bloodstream [28]. The PSA test was originally intended to monitor progression of disease in men who have already been diagnosed with PCa. In 1994, the PSA blood test was approved to be used with the DRE to screen asymptomatic men, although men with PCa symptoms are also tested for PSA levels to help physicians evaluate disease progression. After the approval of the PSA test in 1994, disease detection increased dramatically [29].

An elevated PSA result does not always mean a PCa diagnosis. There are other factors that can cause a rise in PSA levels in the blood. PSA naturally increases with age, can be higher in men with a noncancerous condition called benign prostatic hyperplasia (BPH), and can increase with inflammation of the prostate, which is a condition called prostatitis. A needle biopsy of the prostate needs to be performed before any definitive diagnosis is made. The biopsy is used to determine the Gleason score of the tumor, which is a scoring of the cell differentiation [30]. Due to the lack of specificity that comes with PSA screening, there is a clinical need for new detection methods that are less invasive than biopsy to detect prostate cancer and differentiate between life-threatening PCa that requires treatment from indolent disease that does not require treatment [31-33].

Active surveillance is an approach many physicians choose over treatment. If the cancer is not causing symptoms, expected to grow slowly based on the Gleason score (6 or less), is small and localized, then active surveillance may be a good choice [34]. The surveillance includes a bi-annual doctor visit with a PSA test (with or without DRE). Prostate biopsies may be done annually as well. Treatment is considered if significant changes take place in the PSA test/biopsy [35].

PSA monitoring is used to determine the effectiveness of the PCa treatment. Generally, PSA levels decrease after successful treatment, however, PSA levels do not change immediately and can stay elevated in the blood for weeks after treatment. Following treatment, PSA tests are administered every few months and the frequency is determined by the physician [36]. Detectable PSA after treatment does not necessarily mean that cancer cells are still present. Physicians should use their discretion to investigate the elevated PSA result post-treatment and determine if further therapy is necessary. A dramatic increase in

PSA levels can be an indicator of recurrent disease; however, as the PCa becomes more advanced, PSA becomes less effective at indicating PCa recurrence because PCa can become androgen-independent and since PSA expression is dictated by the androgen receptor (AR), AR-negative PCa does not benefit from PSA testing. There is a clinical need for more effective tests and tools for detecting recurring PCa because low PSA can be found in patients with very aggressive recurrent disease [37-39].

In summary, the PSA tests measure the level of PSA protein made by cells in the prostate gland that is released into the man's bloodstream. The presence of PCa can increase PSA levels, however, PCa is not the only culprit responsible for elevated levels. PSA levels can also rise from slow-growing benign PCa or other noncancerous conditions. PSA alone is not a diagnosis, but a sign that the man should be referred for additional testing to determine a diagnosis whether it's PCa related or not.

PCa Diagnosis

Adenocarcinomas from the epithelial cells make up 95% of PCa cases. Other cases are rare and include mucinous or signet-ring cell carcinomas, adenoid cystic carcinomas, carcinoid tumors, large prostatic duct carcinomas, and small-cell undifferentiated cancers [40]. The degree of differentiation is proven to be critical for determining PCa prognosis. The standard for grading tumors based on their patterns of gland formation was developed by Gleason, and now PCa tumor biopsies are evaluated based on the "Gleason Score" [30]. Current procedures call for a biopsy evaluation after a suspicious screening results from the PSA test and digital rectal exam.

The biopsy is performed using ultrasound to guide the biopsy needle placement and remove a small piece of tissue from the suspect areas. This procedure is referred to as transrectal ultrasonography (TRUS)-guided needle biopsy [41]. The biopsy is sent to pathologists for analysis where a Gleason score is given to grade the tissue. The pathologist performs Hematoxylin and eosin (H&E) staining to reveal the anatomy of the cells. The pathologist determines where the cancer is more prominent (the primary pattern) and assigns that region a primary grade (1-5, 5 being the most aggressive). The pathologist then determines the next prominent area and assigns that region a secondary grade. The "Gleason score" is the sum of the primary and secondary grades. A biopsy with normal looking cells would have a Gleason score below six. The highest Gleason score is a 10 (5+5). The grading is primarily based on the level of differentiation of the cells. The less differentiated the cells look and less glandular the tissue appears under the microscope, the higher the score [42]. **Figure 1-2** shows a schematic of the Gleason pattern scoring.

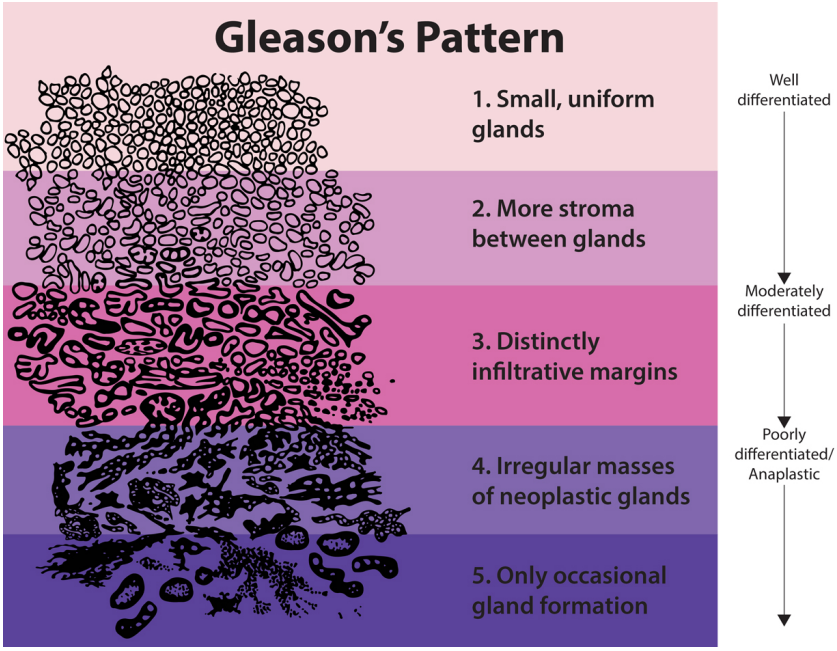

Figure 1-2. Gleason Pattern Schematic.

The less differentiated the biopsy tissue is, the higher it's Gleason score. A Gleason score of 7 and above is considered significant thus requiring medical intervention. The image was obtained from a SEER Training Site. NCI has asked that it was mentioned that since this may be an old figure due to updates in their content, there may have been changes in the grading scheme. The major change is that the cribriform glands that were previously grade 3 are now in grade 4. NCI has asked to make this disclaimer. [43].

If the pathologist determines that the biopsy contains malignant cells, physicians are likely to recommend a diagnostic imaging test to locate the tumor and determine the extent of the disease. The common imaging methods used are multi-parametric magnetic resonance imaging (MRI) for general inquiry, radionuclide bone scan to determine if PCa has spread to the bones and a positron emission tomography (PET) scan to determine if the PCa has spread to other parts of the body [44]. The diagnostic imaging is a crucial component for determining the right treatment plan.

PCa Staging

PCa staging is done to assess how much cancer is in the body and where it's located. Staging helps determine the optimal treatment plan. The most widely staging system for PCa is the American Joint Committee on Cancer **TNM** system The **TNM** stands for the: T-tumor category, whether the PCa spread to the lymph nodes – N category, and whether the PCa has metastasized to other parts of the body- M category).

T Category:

1. Clinical T category (**T**) : The physician's estimate of the extent of disease based on the physical exam, which includes the DRE, biopsy, and imaging results.
2. Pathologic T (**pT**) : This evaluation is assigned after the prostate has already been removed (if it's been removed). The pT is more accurate than the T because it is done after the prostate has been examined in the lab.

Numbers or letters after the T, N, M are used to provide more detail about each of these categories. The higher the number after the letter, the more advanced the cancer is. The categories are combined with the PSA level and grade group (Gleason score) to determine the overall stage of the cancer. The main stages of PCa range from I to IV. A higher number means indicates the extent of the cancer spreading. **Table 1-1** summarizes the different categories and severity in each category. **Table 1-2** groups the categories into stages [45].

Table 1-1. PCa staging categories based on AJCC 7th edition.

Clinical Tumor (T)	
TX	Primary tumor cannot be assessed
T0	No evidence of primary tumor
T1	Clinically inapparent tumor
T1a	Tumor incidental histologic finding in more 5% or less of tissue
T1b	Tumor incidental histologic finding in more than 5% of tissue
T1c	Tumor identified by needle biopsy
T2	Tumor confined within prostate
T2a	Tumor involves one half of one lobe or less
T2b	Tumor involves more than one half of one lobe but not both lobes
T2c	Tumor involves both lobes
T3	Tumor extend through the prostate
T3a	Extracapsular extension
T3b	Tumor invades seminal vesicles
T4	Tumor is fixed or invades structures other than seminal vesicles such as rectum, sphincter, bladder, levator muscles, and/or pelvic wall
Pathologic Tumor (pT)	
pT2	Organ confined
pT2a	Unilateral, one half of one side or less
pT2b	Unilateral, involving more than on half but not both sides
pT2c	Bilateral
pT3	Extraprostatic extension
pT3a	Extraprostatic extension or microscopic invasion of bladder neck
pT3b	Seminal vesicle invasion
pT4	Invasion of rectum, levator muscles, and/or pelvic wall
Regional Lymph Nodes (N)	
NX	Regional lymph nodes were not assessed
N0	No regional lymph node metastasis
N1	Metastasis in regional lymph nodes
Distant Metastasis (M)	
M0	No distant metastasis
M1	Distant metastasis
M1a	Non-regional lymph node(s)
M1b	Bone(s)
M1c	Other site(s) without or without bone disease

The table is based on the American Joint Committee on Cancer Prostate Cancer Staging and permission was obtained to use [46] .

Table 1-2. Prostate Cancer Staging.

AJCC Stage	Stage Grouping	Description
I	cT1, N0, M0 Grade Group 1 (Gleason score 6 or less) PSA less than 10	The physician can't feel the tumor or see it with an imaging test such as transrectal ultrasound (it was either found during a transurethral resection of the prostate (TURP) or was diagnosed by needle biopsy done for a high PSA) [cT1]. The cancer has not spread to nearby lymph nodes [N0] or elsewhere in the body [M0]. The Grade Group is 1, and the PSA level is less than 10.
	cT2a, N0, M0 Grade Group 1 (Gleason score 6 or less) PSA less than 10	The tumor can be felt by digital rectal exam or seen with imaging such as transrectal ultrasound and is in one half or less of only one side (left or right) of the prostate [cT2a]. The cancer has not spread to nearby lymph nodes [N0] or elsewhere in the body [M0]. The Grade Group is 1, and the PSA level is less than 10.
	pT2, N0, M0 Grade Group 1 (Gleason score 6 or less) PSA less than 10	The prostate has been removed with surgery, and the tumor was still only in the prostate [pT2]. The cancer has not spread to nearby lymph nodes [N0] or elsewhere in the body [M0]. The Grade Group is 1, and the PSA level is less than 10.
IIA	cT1, N0, M0 Grade Group 1 (Gleason score 6 or less) PSA at least 10 but less than 20	The physician can't feel the tumor or see it with imaging such as transrectal ultrasound (it was either found during a transurethral resection of the prostate (TURP) or was diagnosed by needle biopsy done for a high PSA level) [cT1]. The cancer has not spread to nearby lymph nodes [N0] or elsewhere in the body [M0]. The Grade Group is 1. The PSA level is at least 10 but less than 20.
	cT2b or cT2c, N0, M0 Grade Group 1 (Gleason score 6 or less) PSA less than 20	The tumor can be felt by digital rectal exam or seen with imaging such as transrectal ultrasound and is in one half or less of only one side (left or right) of the prostate [cT2a]. OR the prostate has been removed with surgery, and the tumor was still only in the prostate [pT2].The cancer has not spread to nearby lymph nodes [N0] or elsewhere in the body [M0]. The Grade Group is 1. The PSA level is at least 10 but less than 20.
	cT2b or cT2c, N0, M0 Grade Group 1 (Gleason score 6 or less) PSA less than 20	The tumor can be felt by digital rectal exam or seen with imaging such as transrectal ultrasound. It is in more than half of one side of the prostate [cT2b] or it is in both sides of the prostate [cT2c]. The cancer has not spread to nearby lymph nodes [N0] or elsewhere in the body [M0]. The Grade Group is 1. The PSA level is less than 20.

IIB	T1 or T2, N0, M0 Grade Group 2 (Gleason score 3+4=7) PSA less than 20	The cancer has not yet spread outside the prostate. It may or may not be felt by digital rectal exam or seen with imaging such as transrectal ultrasound [T1 or T2]. The cancer has not spread to nearby lymph nodes [N0] or elsewhere in the body [M0]. The Grade Group is 2. The PSA level is less than 20.
IIC	T1 or T2, N0, M0 Grade Group 3 or 4 (Gleason score 4+3=7 or 8) PSA less than 20	The cancer has not yet spread outside the prostate. It may or may not be felt by digital rectal exam or seen with imaging such as transrectal ultrasound [T1 or T2]. The cancer has not spread to nearby lymph nodes [N0] or elsewhere in the body [M0]. The Grade Group is 3 or 4. The PSA level is less than 20.
IIIA	T1 or T2, N0, M0 Grade Group 1 to 4 (Gleason score 8 or less) PSA at least 20	The cancer has not yet spread outside the prostate. It may or may not be felt by digital rectal exam or seen with imaging such as transrectal ultrasound [T1 or T2]. The cancer has not spread to nearby lymph nodes [N0] or elsewhere in the body [M0]. The Grade Group is 1 to 4. The PSA level is at least 20.
IIIB	T3 or T4, N0, M0 Grade Group 1 to 4 (Gleason score 8 or less) Any PSA	The cancer has grown outside the prostate and might have spread to the seminal vesicles [T3], or it has spread into other tissues next to the prostate, such as the urethral sphincter (muscle that helps control urination), rectum, bladder, and/or the wall of the pelvis [T4]. It has not spread to nearby lymph nodes [N0] or elsewhere in the body [M0]. The Grade Group is 1 to 4, and the PSA can be any value.
IIIC	Any T, N0, M0 Grade Group 5 (Gleason score 9 or 10) Any PSA	The cancer may or may not be growing outside the prostate and into nearby tissues [any T]. It has not spread to nearby lymph nodes [N0] or elsewhere in the body [M0]. The Grade Group is 5. The PSA can be any value.
IVA	Any T, N1, M0 Any Grade Group Any PSA	The tumor may or may not be growing into tissues near the prostate [any T]. The cancer has spread to nearby lymph nodes [N1] but has not spread elsewhere in the body [M0]. The Grade Group can be any value, and the PSA can be any value.
IVB	Any T, any N, M1 Any Grade Group Any PSA	The cancer may or may not be growing into tissues near the prostate [any T] and may or may not have spread to nearby lymph nodes [any N]. It has spread to other parts of the body, such as distant lymph nodes, bones, or other organs [M1]. The Grade Group can be any value, and the PSA can be any value.

Table adapted from the American Cancer Society webpage [45]. Permission obtained from Springer Nature, AJCC 7th edition to adapt table from the webpage.

PCa Treatment

There are many forms of PCa therapy that can be used alone or in combination with other treatments. The treatment plan is determined by the physician and the patient based on the PCa extent, aggressiveness, and patient preference.

- Active Surveillance: If a tumor is determined to be slow-growing, the physician may recommend to not take any direct action but to monitor the disease. [34]
- Radical Prostatectomy: This is a surgery to remove the prostate, some surrounding tissue, and the seminal vesicles. Each surgery is unique, tailored to the location, size, and other aspects of the cancer. The lymph nodes are inspected to determine whether the cancer has spread and whether the patients should also go through another form of therapy following the surgery [47]. Surgery is recommended if [48]:
    - The diagnosis is early stage/localized where active surveillance is not appropriate. The surgery alone may be sufficient to eliminate the cancer.
    - The patient has rising PSA after initial focal therapy, which would be indicative of incomplete cancer eradication.
    - The tumor alone cannot be safely removed with surgery.
- Radiation Therapy: This approach uses high-energy beams or radioactive seeds to eliminate tumors. The type of radiation treatment chosen depends on the disease. Radiation therapy can be combined with hormone therapy, as a monotherapy, or after surgery. There are two types of radiation therapy for PCa:

- *Internal*: Also referred to as brachytherapy, such as a radioactive seed implantation. This is an outpatient procedure and can come in low-dose rate and high-dose rate forms. The dose rate refers to the seed at which the dose is delivered, not the dose itself. Brachytherapy uses seed implant which are radioactive sources. The seeds are inserted directly into the prostate and give off localized radiation. Brachytherapy is only indicated for men whose PCa is early stage and is slow growing (low-grade) [49, 50]. The two different forms of brachytherapy are:
    - **Low-dose-rate (LDR) brachytherapy:** These seeds are permanent and meant only for local PCa. The seeds are typically made of iodine-125 or palladium-103 [51]. The radioactive seeds are attached to needles that are inserted into the prostate and are left in prostate and the needles are removed. These seeds give off radiation for weeks or months. Because the seeds are so small, they are left in the prostate even after the radioactive material is done emitting [50].
    - **Hight-dose-rate (HDR) brachytherapy:** The seeds are temporary placed for a few minutes (5-15 minutes) and then removed. The treatment can be repeated over the course of two days. This is often given with a form of EBRT. The seeds are typically made of iridium-192 or cesium-137. The seeds are attached to hollow needles that are inserted directed into the prostate. Catheters are placed in these needles, the needles are removed, and then seeds are

placed in the catheters. The catheters are then removed after the last treatment [50, 52].

- *External*: Image-guided radiation therapy and radiosurgery. This is also known as external-beam radiation therapy (EBRT). EBRT aims the radiation directly at the prostate from the outside of the body using a linear accelerator. This approach can be used alone or in combination with other treatments for more aggressive disease. There are different types of EBRT [53]:
  - **Image-guided, Intensity-Modulated Radiation Therapy (IG-IMRT)**: Before the start of the therapy, the prostate is physically marked with "fiducial markers" which are made of gold and allow the CT scanner to locate the tumor and prostate very accurately. The marking is done to prevent inaccuracy due to natural body movements which can shift the prostate. The patient is imaged before each session. The linear acceleratory is used to generate the high energy photons, or x-rays. The duration of this therapy involves multiple sessions [54]. At Memorial Sloan Kettering for example, IG-MRT is given over a period of 9 weeks in about 48 treatment sessions if administered alone. IG-MRT is recommended for patients who have urinary problems prior to treatment initiation [55]. This procedure can be performed without the repeated imaging scans, this is known as IMRT.

- **Proton Therapy**: This is an advanced form of radiation therapy that uses protons rather than x-rays (which are the form of energy used in traditional radiation therapy) [56]. The benefit of proton therapy over IG-IMRT is unclear [57].
- **Stereotactic surgery*:*** Also known as stereotactic radiation therapy (SBRT), uses radiation entering the body through various angles and intersecting at the target. SBRT delivers higher doses of radiation compared to the MRT in a span of five visits. SBRT is more cost-effective due to its shorter length of duration. The main difference between SBRT and IMRT is the use of unique beam angles to deliver higher radiation. SBRT requires higher accuracy that IMRT [58, 59].

Memorial Sloan Kettering Cancer Center has the following recommendations for which radiation therapy to use based on the diagnosis [53]:

<u>Radiation therapy for localized PCa:</u>

- LDR brachytherapy
- IG-MRT
- Stereotactic surgery

<u>Radiation therapy for regional (also known as locally advanced) PCa</u>

- LDR brachytherapy with short-course of daily IG-IMRT
- IG-IMRT with hormone therapy
    - In this case, hormone therapy is typically administered before the radiation therapy begins and is continued after radiation.

- HDR brachytherapy with short course of daily IG-IMRT

Radiation therapy after prostatectomy

- After radical prostatectomy if there are indications several years after surgery that the cancer has returned.
- The tumor was not fully eradicated by the surgery.
- The tumor was found protruding outside of the prostate during surgery.

  In these situations, IG-IMRT is recommended, which can also be combined with hormone therapy.

- Focal Therapy: This term is used for non-invasive techniques that can kill small tumors confined within the prostate. The advantages of focal therapy are that it can kill the cancer while preserving prostate tissue and function while reducing side effects [60]. There are a few different types of focal therapy [61, 62]:
  - **Focal Cryoablation**: A probe is used to deliver liquid nitrogen that surrounds the tumor and freezes it.
  - **High Intensity Focused Ultrasound (HIFU):** Guided by MRI, HIFU uses sound wave energy directed at the tumor.
  - **Irreversible Cryoablation:** Electrical currents are passed through the tumor and the electricity created pores in tumor cells, killing them.
  - **Photodynamic Therapy:** This therapy uses an intravenous injection of a photosensitizer (padeloporfin) which when exposed to light of a specific wavelength at the tumor site, releases cytotoxic oxygen species which

causes intravascular thrombosis. This is a novel technique that is still in clinical trials.

- Systemic Therapies: Metastatic patients have numerous treatment options that take advantage of the biology of the PCa for targeting cancerous cells. These therapies are called "systemic" because they circulate the entire body and attack the cancer at distant metastatic sites. To appreciate the way these therapies work, it is important to understand the key signaling pathway involved [63]. Androgen receptor signaling drives survival and progression of the disease and is discussed in more detail in the section titled "Androgen Receptor Signaling in PCa [64]." The current systemic therapies available are:
    - **Hormone Therapy:** The male sex hormone, testosterone, is classified as an androgen (male hormones, but are not exclusively only active in males) and promotes PCa growth. Hormone therapy, also known as androgen-deprivation therapy (ADT), includes several small molecules that decrease the production of testosterone or inhibit its binding abilities in the cancer cells. Hormone therapy is recommended for patients with recurrent or metastatic disease and also for patients that have a high Gleason score or PSA level and are receiving radiation therapy. Hormone therapy is also referred to as chemical castration. An alternative to chemical castration is surgical castration (orchiectomy). Surgical castration is more difficult for PCa patients to accept as it requires the removal of the testicles [65, 66]. **Figure 1-3** is a representation of the pathway targeted by the hormone therapies.

- **LHRH Agonist:** Luteinizing hormone-releasing hormone (LHRH) agonists work as agonist of the gonadotropin-releasing hormone (GnRH) receptor [67]. The GnRH is released by the hypothalamus. Binding of GnRH to the GnRH receptor causes the release of the follicle stimulating hormone (FSH) and the luteinizing hormone (LH) from the pituitary gland. LH binds to receptors in the testes, particularly in Leydig cells. The binding of LH to its receptor cause the Leydig cells to synthesize and secrete testosterone [68]. LHRH agonists work by inhibiting the release of LH by the pituitary gland. LHRH are GnRH receptor agonists, which means the agonist could activate the GnRH receptor like the biological GnRH; the continued stimulation of the GnRH receptor causes it to desensitize to the effects of GnRH. The initial stimulation of the GnRH does cause a flare in LH and a rise in testosterone. After the flare-up, the desensitization occurs, and testosterone levels go down due to the lack of LH being released from the pituitary [67]. The flare-up can be avoided by co-administering anti-androgens when starting the LHRH agonists. There are multiple LHRH drugs available [69].
- **LHRH Antagonist:** This drug works by antagonizing the GnRH receptor and avoids the initial flare up. There is only one such drug called Degarelix [70].
- **CYP17A Inhibitor**: This drug blocks the enzyme CYP17, which converts dehydroepiandrosterone (DHEA) to testosterone in the

adrenal glands, testes, and prostate cancer cells [71]. This drug, called abiraterone, is used on patients that have high risk cancer (spread to several spots) or their cancer is castration resistant prostate cancer (CRPC), which means the cancer continues to grow despite of the low testosterone levels from an LHRH agonist, LHRH antagonist, or orchiectomy) [72]. Prednisone must be administered with abiraterone because abiraterone lowers the level of other hormones in the body [73].

- **Anti-androgens**: These drugs prevent dihydrotestosterone (DHT), a more potent derivative of testosterone, from binding to the androgen receptor (AR). Anti-androgens are used for CRPC. The most common FDA approved anti-androgen is enzalutamide. Enzalutamide binds to the ligand-binding domain (LBD) of the AR, which is where DHT would bind. This action not only prevents the AR from binding its targets in the nucleus, but also prevents the translocation of the receptor to the nucleus [74]. Enzalutamide is considered to be a second-generation anti-androgen. First-generation bicalutamide does not prevent the translocation of AR into the nucleus [75, 76]. Enzalutamide has higher efficacy than the first-generation anti-androgen bicalutamide [77]. Apalutamide (approved 2018) and darolutamide (completed Phase III March 2019) are other examples of second-generation anti-androgens [78, 79].

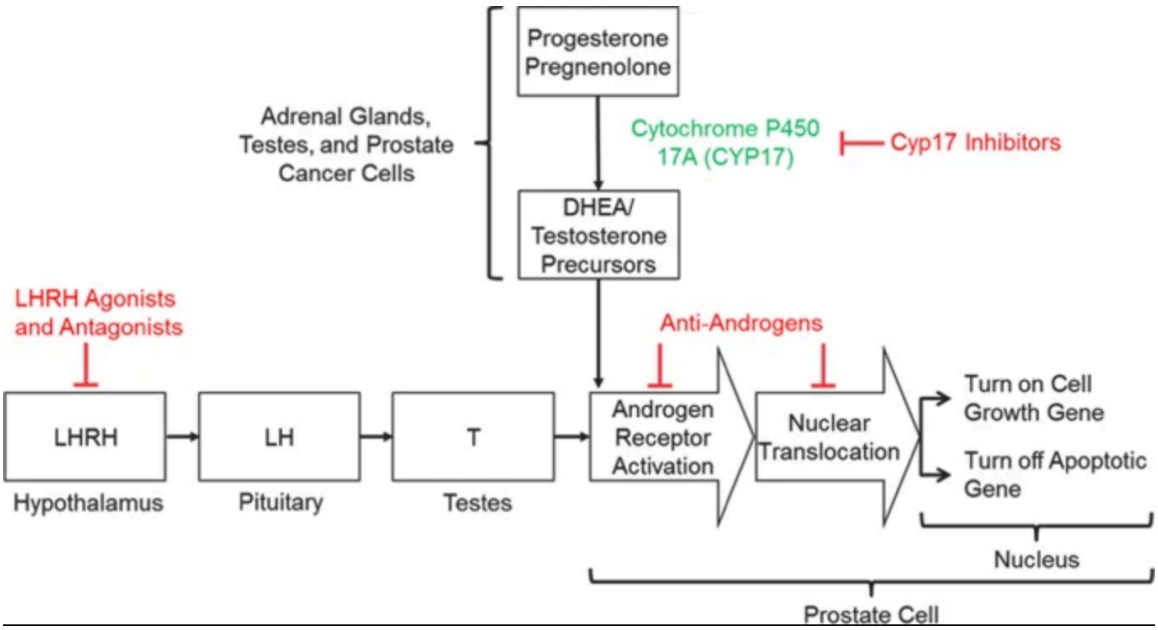

Figure 1-3. Hormone therapy targeting pathway.

Figure obtained from [66]. Permission to use figure is not required as long as it is references and a link is provided to the Creative Common License: http://creativecommons.org/licenses/by/4.0/

- Chemotherapy: When CRPC becomes unresponsive to hormonal therapy, chemotherapy is indicated. Taxanes, such as docetaxel, are often used to bind and stabilize the microtubules in dividing cells [80]. This stabilization causes the dividing cells to arrest in the G(2)M phase and eventually leads to apoptotic cell death [81].

Androgen Receptor Signaling in PCa

The androgen signaling pathway is the most targeted pathway in PCa because the androgen receptor (AR) plays a significant role in PCa progression. The AR is a steroid hormone nuclear receptor, like the estrogen receptor. The AR acts as a transcription factor when it binds to its major ligand 5α-dihydrotestosterone, (DHT), dimerizes, and translocates to the nucleus. AR binds to specific sequences in DNA known as androgen response elements to regulate gene transcription which promotes the growth and survival of prostate cells [82].

Testosterone is primarily synthesized by the Leydig cells in the testes (~90%) and some is synthesized by the adrenal cortex (~10%) and is the precursor to DHT. Testosterone has two precursors, dehydroepiandrosterone (DHEA) and androstenedione. DHEA and androstenedione have precursors as well, that are converted into DHEA and androstenedione by CYP17A. CYP17A is the target of abiraterone. By inhibiting the actions of CYP17A, abiraterone is able to prevent the synthesis of testosterone precursors, thus abiraterone prevents DHT from being formed and binding the AR [83]. **Figure 1-4** is a schematic of the pathway abiraterone targets.

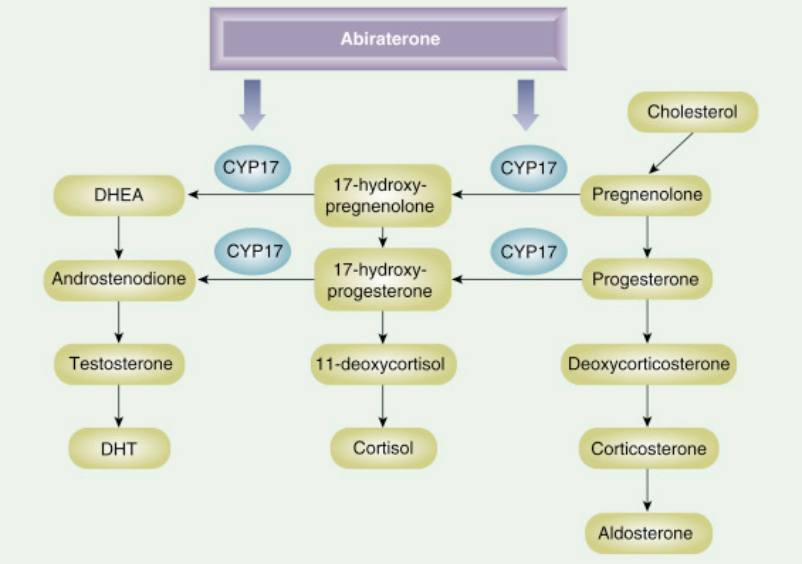

Figure 1-4. Pathway of DHT precursors.

Permission to use figure was obtained from Elsevier [84].

The AR consists of three domains: NH2 terminal transactivation domain, DNA binding domain (DBD), and ligand-binding domain (LBD). DHT binds to the LBD, which leads to a conformational change in the receptor. The receptor can then relocate to the nucleus and dimerize. The dimers can bind to the androgen-response elements of the promoters and the enhancers of target genes using the DBD. AR regulates the transcription of a large number of genes. Examples of such genes are KLK3 (codes for PSA), NKX3 and FOXP1 (transcription factors), UBE2C and TACC2 (cell cycle regulators), IGF1 and APP (growth stimulators), and many more. AR can both activate and repress transcription [82].

AR is the main target of ADT and anti-androgens but it has many mechanisms of resistance:

1. AR amplification: The PCa cells make more AR than normally [85]. The cells amplify the gene, which can lead to AR overexpression and allow the cancer cells to continue androgen-dependent growth in low levels of androgens after castration [86]. The amplification can cause the cells to be hypersensitive to the low level of androgens [87].
2. AR mutations: Mutations can result in various AR functions. Mutations can lead to loss-of-function and gain-of-function AR. A known AR mutation, AR-T877A can be activated not only by androgens but also by the anti-androgen drug flutamide, estrogen, and progesterone [88]. Mutations in the LBD can cause resistance to anti-androgens [89, 90].
3. Aberrant activation: Androgen independent activation of AR leads to resistance to ADT. Altered levels of AR coregulators and their function can cause resistance. Activation by the coregulators leads to ligand-independent signaling pathways. AR can also be activated by growth factors as a mechanism of resistance [91].
4. AR splice variants (AR-Vs): Alternative splicing leads to AR that is not responsive to therapy. For example, AR-V7 lacks the LBD, therefore anti-androgens cannot bind to it. AR-V7 is located in the nucleus and is constitutively active [91].

The AR pathway is very important for the development of improved PCa therapies.

Recurrence

After patients are treated for their localized PCa, there can be an intermediate state of disease where the PSA has risen, but the cancer either has not formed or cannot be located using standard diagnostic tools. This intermediate state is known as biochemical recurrence (BCR). BCR may be an indication for starting ADT; however, it's not always the case. Physicians face a difficult decision when deciding whether to treat the patient with BCR who is asymptomatic because the side effects of the medication may outweigh the benefits, but on the other hand, the therapy may prevent or delay the onset of metastatic disease [92]. The proportion of patients affected by BCR compared to the proportion of patients who actually develop metastatic disease is shown in **Figure 1-5.** It is clear from this figure that a large population of patients BCR would not need further treatment, but current clinical tools lack the sensitivity needed to differentiate between PSA rising that will lead to metastasis and PSA rising that will not lead to metastasis.

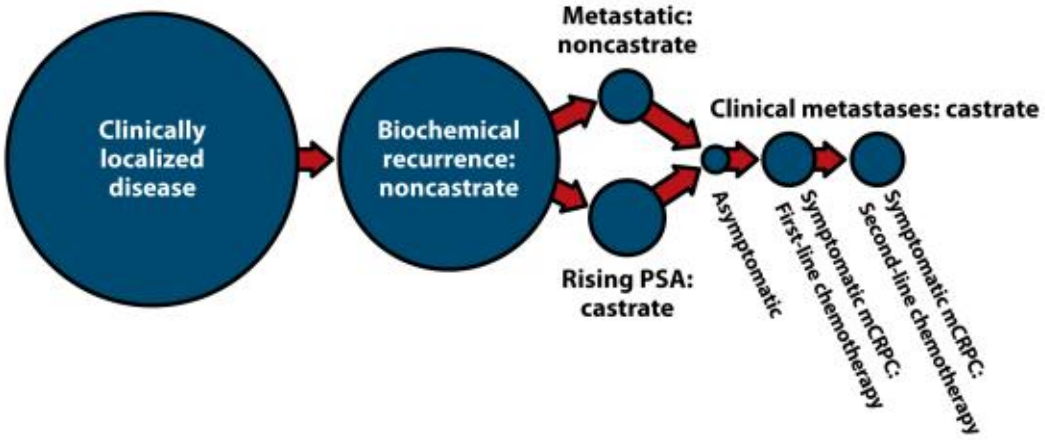

Figure 1-5. Proportional model of PCa states.

Reproduced with permission from publisher from Paller C, Management of Biochemically Recurrent Prostate Cancer After Local Therapy: Evolving Standards of Care and New

Directions. *Clin Adv Hematol Oncol.* 2013; 11(1), 14-23 [92]. The arrows in the figure represent disease progression after therapy.

Within 10 years post initial treatment, BCR affects 20-40% of patients treated with radical prostatectomy [93, 94] (~75,000 newly diagnosed PCa patients are treated with radical prostatectomy, which is ~30% of all those diagnosed [95]) and 30-50% of patients treated with radiation therapy [96] (~60,000 newly diagnosed patients are treated with radiation therapy, which is ~25% of all of those diagnosed [97]).

Progression of disease can lead to castration resistance, which means the PCa progresses in spite of ADT. This PCa can be non-metastatic (nmCRPC) or metastatic (mCRPC). nmCRPC is treated with drugs such as abiraterone or enzalutamide. Unfortunately, over 80% of patients with nmCRPC progress to mCRPC [98]. As of today, mCRPC is incurable and the goal of treatment is to extend life as long as possible, delay metastasis, and provide the best quality of life. mCRPC patients are commonly treated with abiraterone, anti-androgens, and chemotherapy [98, 99]. Other FDA approved options do exist, and many experimental therapeutics are being evaluated in clinical trials [100].

As PCa progresses aggressively, it may start to develop neuroendocrine-like features and eventually develop into neuroendocrine PCa (NEPC). NEPC is associated with advanced diseases and poor clinical outcome [101-103]. In NEPC, cells lose their granular structure, develop small cell neuroendocrine-like morphology, and become positive for neuroendocrine (NE) markers [104]. AR signaling significantly decreases or is completely lost in NEPC. PSA becomes an ineffective way of monitoring disease because PSA is controlled by the AR signaling pathway, and with the loss of AR expression, PSA

loses its ability to predict disease progression [105]. Approximately 25-30% of mCRPC have neuroendocrine phenotypes. It is believed that NEPC develops in response to ADT and/or targeting of the AR signaling pathways [106]. NEPC is treated with the chemotherapeutic cis-platin [107].

Although PCa is treatable for many patients, there is a clinical need for new therapeutics and ways to monitoring the disease. The clinical need exists for patients who develop resistance to anti-androgens and for those where it is difficult to delineate between malignant and indolent disease.

Imaging of Prostate Cancer

Imaging of PCa is used to detect and localize PCa. Imaging is helpful not only for detection but grading and staging of PCa as well. Currently, the main modes of imaging are ultrasound-based imaging, magnetic resonance-based imaging, computed tomography, and positron emission tomography [44].

Ultrasound Imaging: This is the oldest and most widely used imaging modality for PCa, pioneered in the 1980s. Transrectal ultrasonography (TRUS) mentioned earlier is well tolerated by patients and is inexpensive. TRUS can be used for guided biopsies and is considered to be the standard of care for PCa diagnosis. TRUS sensitivity is considered low. The appearances of cancer can overlap with benign lesions and the visualization of the capsule is poor. There are novel modalities such as contrast-enhanced modes to increase sensitivity [108]. Ultrasound imaging is approved for the following PCa related indication: an abnormal DRE, biopsy

guidance, evaluation of patient with known PCa, and follow-up of patients with PCa [109]. These indications were current as of 1991 and it does not appear that much has changed in terms of ultrasound imaging.

Magnetic Resonance Imaging (MRI): MRI in PCa is used mostly for intraprostatic disease detection and is useful for PCa staging and therapy guidance [110]. The recommended technique of MRI imaging in PCa is multi-parametric-MRI or mp-MRI. This method combines T2 weighted imaging for high contrast structural detail, and other functional MR imaging techniques [111]. A pre-biopsy mpMRI can identify the areas that are suspicious. mpMRI can also be used post-negative biopsy. Primarily, the mpMRI is used to determine the extent of the localized disease (without distant metastasis) to determine the proper treatment [112]. mpMRI limitations include: lack of sensitivity to differentiation BPH from PCa in the transition zones of the prostate, limited ability to differentiate between post-treatment change and local recurrence following treatment, and by inter-observer variability. MRI is not used for detection of metastasis [113].

Computed Tomography (CT) Scan: The CT scan uses x-rays to create a cross-section image of the body to determine if the PCa has spread into the lymph nodes. As mentioned earlier, CT scans are used for guiding IG-IMRT. The limitation of CT scans is their inability to detect architectural changes within normal size lymph nodes (lymph nodes that are not enlarged). The sensitivity is limited for detecting the microscopic lymph node metastases [114].

Bone Scan: Patients who are stratified as high risk (high PSA) would typically be recommended a bone scan. The bone scan can effectively detect bone metastasis. Technetium-99-methylenediphosphonate (99mTc-MDP) bone scintigraphy is used to find these distant bone lesions. The limitation of this technique is that it is only sensitive for bone lesions. 99mTc-MDP localizes along mineralization fronts and can accumulate due to tumor presence and due to other bone related issues. In the literature, sensitivity has been reported to be between 62-89%. However, due to its low specificity, in many cases the increase in its uptake cannot be characterized as a malignancy [115].

PET Imaging: CT scans, MRI, and bone scans are limiting because they can primarily detect nodal, local and bone disease. PET imaging is mostly used in relapsed disease. PET imaging is useful because it can target the tumor directly by being specific for either a surface marker or a tumor specific biological process. Traditionally, ^{18}F-fluorodeoxyglucose (FDG) can work really well in cancer where glucose uptake is high, but not in PCa because it primarily relies on fatty acid and fructose metabolism. ^{11}C-choline and ^{18}F-choline are tracers with limited use. Choline can be metabolized and internalized by choline kinase, which is a protein that is overexpressed in PCa. The choline tracers do not differentiate well between benign and malignant tumors or inflammatory conditions. Choline tracers are FDA approved for use in patients with recurrent disease. ^{18}F-fluiclovine has been recently approved by the FDA. ^{18}F-fluiclovine is an amino acid that can be taken

up by sodium-dependent amino acid transporters which are associated with aggressive tumors. Non-specificity has been reported as ^{18}F-fluiclovine can be taken up by inflamed areas and other malignancies. ^{18}-F-NaF is a sensitive bone metastasis detector but compared to^{99m}Tc, it is more expensive and has less clinically relevance due to lack of PET availability. ^{68}Gallium-prostate-specific membrane antigen (PSMA) is being investigated in clinical trials. PSMA is overexpressed in PCa and conjugated PSMA ligands have been developed. The previous ^{111}Indium-anti PSMA monoclonal antibody failed because it targeted an intracellular epitope, which caused binding to necrotic cells. PSMA ligands that are being developed now target a extracellular epitopes. ^{68}Ga-PSMA PET is not yet FDA approved but clinical studies indicate that it is better than conventional imaging where there is biochemical recurrence [116].

Vectors for Gene Therapy and Molecular Imaging

Gene therapy is the ability to make local modifications in the human genome. One of the most common techniques used for genetic alternation is recombinant DNA technology where a gene of interest (GOI) is inserted into a vector and delivered to target cells. This vector can be viral or plasmodial [117]. An ideal vector would be administered non-invasively, target only desired cells, and express a therapeutic amount of GOI or transgene. Gene therapy allows for the introduction of natural protein products and also enables production of proteins that are not typically found endogenously in the cells. Gene therapy can be applied to various diseases whether they are oncologic, infectious, or genetic [118]. Examples of how the GOI could function are [119]:

1. Replace a deficient gene or indirectly substitute for a loss of function gene that results in disease progression
2. Cause direct or indirect toxicity to “diseased” cells
3. Inhibit a gain-of-function pathway that is involved in disease progression

The GOI approach can be used to express genes that do not have a therapeutic function but can be detected by a signal the GOI generates or indirectly causes. A gene therapy approach can be used for molecular imaging by using reporter genes such as fluorescence proteins in the vectors as the GOI. Some of these reporter proteins are bi-modal and can work as both therapeutic and imaging reporters. The gene therapy approach used for molecular imaging is an emerging field called “molecular-genetic imaging” which allows for imaging of molecular-genetic processes rather than anatomy [120].

The inability to monitor gene expression is a limitation of gene therapy. A great use for molecular-genetic imaging is the possibility of using the reporter gene expression in conjunction with a therapeutic gene to assess gene therapy treatments. Molecular-genetic imaging can also be used as a stand-alone regimen to detect and monitor disease as any other clinically available imaging approach. The use of disease-specific promoters prevents reporter gene expression from occurring in unwanted locations. For example, a cancer-specific promoter can be used to express reporter genes in the cancer only and that same promoter can be used to express therapeutic genes. The reporter genes and therapeutic genes can be part of the same vector or the reporter gene can act as a therapeutic gene. Bi-modal protein such as herpes simplex 1 thymidine kinase (HSV1-TK) can be used for visualization and as a therapeutic because it converts non-toxic prodrugs such as ganciclovir into toxic compounds. Gene therapy vectors can also be evaluated using

reporter genes for their specificity and transcriptional efficiency by using the reporter gene as the GOI and later replacing the reporter gene with the therapeutic GOI. Using reporter genes for vector evaluation is a good way to determine if the vector is potent and specific to the target cells [121].

Plasmid

Plasmid DNA (pDNA) is a gene therapy tool that is applied in cancer, infectious, genetic, and acquired diseases [122-130]. Plasmids can be used to transiently express protein in cancer cells to induce an inflammatory response (plasmid vaccine) [131, 132] or cell death (targeted gene therapy). Targeting the plasmid can be accomplished by using disease-specific promoters upstream of the GOI [133]. Often times, the protein expressed performs its anti-cancer role after the administration of an activating agent. For example, the GOI causes toxicity indirectly by driving the expression of another toxic gene [134] or can be targeted for toxicity (by administering an otherwise non-toxic substrate that is converted into a toxic molecule only in cells expressing the GOI) [135]. As of October 2018, there are at least 62 active plasmid-based therapies in clinical trials around the world (according to clinicaltrials.gov).

Clinical Plasmid Therapy

As of October 2018, there are currently at least 20 plasmid DNA vaccines in phase II clinical trials that are active and 12 of them are for oncological diseases including neoplasia. Vaccines dominate the clinical plasmid therapy field, in part, because they have been studied longer in the clinical setting. There are various targeted gene therapy plasmids

being investigated for a variety of cancers. Interestingly, there are even investigations of a plasmid immunotherapy which consists of liposomal-non-coding DNA plasmid that is not considered gene therapy or a vaccine [136, 137].

Delivery

Plasmid delivery routes and methods have many variations in pre-clinical studies. Intratumoral, intraperitoneal, and subdermal routes are common examples of what is currently being practiced in clinical trials. Although intravenous route of delivery opens more doors for toxicity, there is one plasmid therapeutic being investigated that is neither a vaccine nor a targeted therapy because it is non-coding that has been administered intravenously [136].

Because plasmid DNA is negatively charged and suffers from a very short half-life in the cytoplasm, the amount of DNA that actually reaches the nucleus can be very low [138]. Nanoparticle delivery agents have been used clinically and pre-clinically as an alternative to naked DNA delivery. The most commonly used delivery agents are linear-polyethylenimine (l-PEI) [139] and cationic liposome [136]. Cationic liposomes and l-PEI have been used in clinical trials [137, 139, 140]. Limitations to l-PEI do exist, an important one being toxicity [141].

Production

Plasmid development is performed in bacteria and antibiotic resistance genes in the plasmid sequence are commonly used as a selection marker. For the purposes of translation to humans, the plasmid should be modified to reduce toxicity via bacteria-added attributes

and prevent the potential for antibiotic resistant bacteria in the patient. Current FDA guidelines do not prohibit the use of an antibiotic marker, but it is recommended to avoid the use of penicillin and beta-lactams in the production process [142].

Plasmid therapy has potential for gene therapy development and it has already been successful in clinical trials. Plasmids are commonly used as vaccines or targeted gene therapy and are even being developed as immunotherapies. Plasmids can be applied for molecular imaging in the same manner by making the GOI a reporter gene whose signal can be detected and quantified by an imaging technology [143], but this has not been verified in the clinical setting. Oncological applications of plasmids are extensive both for solid and hematological tumors. There are some advantages of using plasmids over a viral delivery of the gene, although the delivery is not as effective. For example, pDNA has a lower risk of integrating with the chromosomal DNA than a retrovirus [144]. Overall, pDNA poses a smaller risk because of improved safety over viral vectors. pDNA can also be delivered more than once, has a low risk of integration, and it's more cost-effective to construct and store. The disadvantages are the poor transfection efficiency and some risk of inflammation due to CpG motifs. Literature on systemic administration of plasmids in humans is limited. To the best of my knowledge, l-PEI coated plasmid has been administered to humans in at least one trial [139] and l-PEI has been administered in another trial with siRNA (NCT01435720).

Adenovirus

Like plasmids, adenoviruses (Ads) are used for gene therapy and vaccines. Ads are comprised of icosahedral protein capsid that encloses a linear duplex DNA genome of ~35 kilo basepairs. The Ads' genome encodes about 35 proteins. ~20 of these proteins are expressed in the early phase and allow the virus to control the cell to carry out the DNA replication process. The remainder of the proteins are expressed in the late phase and encode for the structural proteins [145]. Outside of their use in gene therapy, Ads found in our environment are known for causing cold-like symptoms [146].

Clinical Adenovirus Therapy

There are more than 400 gene therapy trials that have been or are being conducted with Ad vectors, most of them being for the treatment of cancer [145]. Ad vectors pose some advantages compared to other gene therapy methods. Ads are very well studied and can be grown into high titer stable stocks. Ads are highly effective at entering the cell compared to a plasmid with or without a delivery agent. The delivery of Ads is very effective in humans and this leads to higher expression of the GOI, which can make Ads very efficacious [147]. The Ad delivers a high levels of transgene expression for a short-term period because they do not integrate into the genome as lentiviruses do, which is ideal for diseases like cancer, but not as useful for genetic diseases where permanent gene alteration is required to see the benefits [148].

Ads are strongly immunogenic which poses some safety concerns, but the editing of the adenoviral genome allows for limiting some of the immunogenic response. There has been extensive experience with Ad vectors in various clinical applications so the safest

dosing and route of administration have already been well established [147]. Ad vectors are the most common vector used in clinical trials worldwide and account for ~20% of all of the gene therapy trials [149].

The toxicity is Ads' biggest red flag. Even with a lot of development of the Ad vectors for clinical applications, the interaction of the virions with macrophages in the blood, spleen, and liver is associated with acute toxicity [150]. Unfortunately, while Ads are very potent at getting the GOI expressed in the target, there still remains room for improvement when it comes to immunogenicity and hepatotoxicity. Ideally, it would be useful to develop Ads that can only enter target cells. Another issue Ads can run into in the clinic is the pre-immunity. Healthy individuals come across wild-type Ads and develop immunity. This hinders the use of Ads derived from common serotypes in these individuals [149].

Production

Most Ad vectors are modified versions of the Ad5 serotype. Ads can be replication deficient, replication competent, or conditionally-replicative, which means there is a lot of permissible control using Ads. The replication deficient Ads have essential genes *E1A* and *E1B* deleted and replaced by an expression cassette with a high activity and/or tissue/cancer specific promoter. The E1A proteins are essential for Ad replication because they induce the expression of ~20 delayed early genes. E1B proteins inhibit host cell apoptotic response to Ad infection [145].

The actual production of Ads can be a technically challenging and time consuming process. There are different cell lines that can be used such as HEK-293 cells for the

transfection of the Ad vector. Post-successful transfection, the cells make fully assembled virions. The process takes multiple rounds of amplification to obtain a therapeutic yield of viral particles and careful purification. Compared to the production of a plasmid, the Ad production is more labor intensive [149].

Ads can be engineered for cancer-specific expression of the GOI just like plasmids by using cancer-specific promoters. In the same manner, they can be utilized for molecular imaging just like pDNA. Ads, unlike pDNA, have been utilized for molecular-genetic imaging in the clinics already [151]. The difference between the two vectors is efficiency of delivery and off target effects. Although pDNA is safer, Ads provide a much more effective expression of the GOI because Ads are very effective at entering most cells. Both vectors still have room for improvement to achieve better specificity and less off-target effects.

Biomarkers

A biomarker refers to a category of medical signs which can be measured accurately and reproducibly to predict incidences of outcome or disease. Biomarkers by definition are objective, quantifiable characteristics of biological processes [152]. A biomarker can be measured by analyzing molecules such as DNA, RNA, protein, peptide, or biomolecule chemical modifications. Biomarker development involves initial discovery in basic studies, validation, and clinical development. The goal of the development is to stablish biomarker tests with clinical utility to inform clinical decision making and improve patient outcomes [153]. The clinical translation rate of biomarkers is very low, only 0.1% [154].

PSA is an example of a biomarker that was successful in clinical translation. There are various mechanisms which result in the presence of a biomarker due to a diseased state. For PSA, as stated earlier, this reason is that PCa cells express PSA and there is a disruption of layers between the prostate and blood vessels which causes leakage of PSA into the bloodstream. Other biomarkers can be overexpressed as a result of various cancer signaling pathways. If a protein becomes overexpressed in diseased cells, a common cause of that is the transcriptional regulation of the elevated protein. Though the levels of mRNA transcripts and protein levels may not always correlate, increased transcriptional output through promoter regulation can result in the elevated expression of genes in cancer cells [143].

Biomarkers can also be utilized for cancer imaging. Surface biomarkers in particular are useful targets for imaging disease because they can be targeted by antibodies, small molecules, or peptides [155]. Indirect mechanisms of imaging are also possible. Indirect means that the biomarker itself is not used as the target for imaging, but rather its promoter is used to express exogenous reporter genes. This technique is referred to as "molecular-genetic imaging." Molecular-genetic imaging can be accomplished through the use of viral and non-viral DNA vectors. The promoters incorporated in these vectors, in theory, would use the same transcriptional machinery as the endogenous promoters that result in biomarker expression. If the elevated biomarker expression is tumor-specific, then the biomarker-promoter is a good target for molecular-genetic imaging because it will be specific for those cells that are not expressing normal level of the biomarker [143].

Chapter II: Exploiting the transcriptional specificity of the alpha-methylacyl-CoA racemase *AMACR* promoter for the molecular imaging of prostate cancer

Chapter 1 is a first author manuscript with limited edits [156].

Overview

The metabolic protein α-methylacyl-CoA racemase (AMACR) is significantly overexpressed in prostate cancer compared to the normal prostate and other non-malignant tissue. Though an attractive target, there are no reports in the literature on leveraging the expression of AMACR for the molecular imaging of prostate cancer. Here, we used a molecular-genetic imaging strategy to exploit the transcriptional specificity of the AMACR promoter for the *in vivo* detection of prostate cancer using the reporter gene luciferase. We performed a stepwise truncation of the promoter and identified a 565 base pair minimal promoter for AMACR that retained both high activity and specificity. Following identification of the minimal promoter for AMACR, we used an advanced two-step transcriptional amplification system to maximize the promoter output. We showed that our optimized AMACR promoter can drive expression of luciferase for molecular imaging in subcutaneous xenograft models of androgen receptor-positive and androgen receptor-negative prostate cancer using a non-replicative adenovirus for gene delivery. Our results provide evidence that the AMACR promoter can be exploited to drive the cancer-specific expression of reporter genes and potentially even be incorporated into conditionally replicative adenoviruses for oncolytic therapy and other applications.

Introduction

The isomerase α-methylacyl-CoA racemase (AMACR) is most commonly known for its physiologic role in catalyzing the stereoconversion of the α-methyl proton of branched chained fatty acids undergoing β-oxidation in the mitochondria and peroxisomes [157, 158]. Deficiencies in AMACR protein or activity have been associated with several peroxisomal disorders that lead to neurological impairment due to accumulation of branched-chain fatty acids [159]. The effects of such deficiencies can be ameliorated by decreasing the intake of these lipids that come primarily from meat and dairy-based diets [160]. In the early 2000s, two research groups independently verified AMACR as a prostate cancer (PCa) biomarker based on its specific overexpression in malignant tissue compared to benign prostate tissue by immunohistochemistry (IHC) [161, 162]. Subsequent studies established that AMACR protein was also present in metastatic lesions - not only localized primary PCa - and its expression was independent of the androgen receptor (AR) signaling axis [163-165]. Over the years, AMACR has been established as a dependable biomarker of PCa with IHC analysis finding that AMACR expression in needles biopsies had a 97% sensitivity and 100% specificity for PCa detection [166]. Since its initial discovery in PCa, AMACR overexpression has been documented in a number of other cancers including colon, ovarian and breast [167].

The near-universal overexpression of AMACR in PCa has made it an attractive target for molecular imaging. Due to its overexpression in PCa compared to normal tissue, an AMACR imaging probe can potentially be used to non-invasively differentiate aggressive disease from indolent disease. A number of factors have hindered the

development of imaging probes for AMACR. Ideally, an AMACR imaging probe would be a small-molecule inhibitor of its enzymatic activity. There have been a number of studies that tried to develop assays for AMACR detection for high throughput screens of AMACR inhibitors but none of the inhibitors identified have moved toward clinical application [168-171]. Another complicating factor for a small-molecule imaging probe to be successful is that the probe will have to cross the cell membrane and possibly the membrane of an organelle to reach enzymatically active AMACR. A more favorable approach is a molecular-genetic imaging strategy where the transcriptional specificity of the AMACR promoter is harnessed to drive the expression of reporter genes for cancer detection. The DNA construct containing the promoter and reporter gene can be delivered by viral or non-viral means into the cell where transcription and translation of AMACR are occurring. The reporter genes can encode proteins for a number of imaging modalities including positron emission tomography, magnetic resonance, and bioluminescence imaging [172].

In this study, we detail the development of a molecular-genetic imaging technology for AMACR that can detect PCa *in vivo*. Initially, truncated versions of the full-length 2,295 base pair (bp) AMACR promoter were cloned and analyzed for transcriptional output using a luciferase assay in AR-negative and AR-positive PCa cell lines. From these experiments, we identified a 565 bp minimal AMACR promoter that was cancer-specific and possessed output equal to or greater than the full-length promoter. An advanced two-step transcriptional activation (A.TSTA) system was then used to enhance the output to the minimal AMACR promoter [173]. This system - placed downstream of the minimal AMACR promoter and upstream of luciferase - expresses a GAL4-VP16 fusion protein driven by the minimal promoter. The fusion protein binds GAL4 binding sites upstream of

the transcription initiation site that results in an increased transcription of luciferase. Using this system, the output of the minimal promoter was enhanced while still retaining specificity. The enhanced promoter system along with luciferase was then incorporated into a non-replicative adenovirus (Ad) vector. Ad vectors are an efficient natural gene delivery system and are well-researched for cancer gene therapy [174]. The highly efficient delivery of the non-replicative Ad allowed for the imaging of AR-positive and AR-negative PCa xenografts in vivo using bioluminescence. Our data provide proof-of-concept that the tissue-specificity of the AMACR promoter can be exploited for detecting PCa via reporter gene imaging. In the future, this strategy could even be applied to therapy by delivering suicide genes or using conditionally replicative Ad (CRAd) for oncolytic and radioviral therapy.

Results

AMACR expression in clinical samples and models of prostate cancer

At the protein level, AMACR has been reported in primary and metastatic PCa [161-164]. We confirmed these findings by staining sections from prostatectomy and metastatic lesion biopsies **(Figure 2-1A-D)**. As expected, no AMACR was present in healthy prostate tissue **(Figure 2-1A)**, but intense staining was observed in prostate adenocarcinoma **(Figure 2-1B)** and metastatic lesions acquired from liver and lymph node **(Figure 2-1 C-D)**. It has long been established that concordance between mRNA and protein levels in a cell or tissue is often low (~20%) [175]. Certain proteins are long–lived within the cell requiring infrequent transcription, thus while the protein may be present in the cell, the mRNA may not. For a molecular-genetic imaging strategy to be successful,

the tissue-specific promoter must be highly active with high transcriptional rates of the target gene. Though AMACR has been used as a biomarker for IHC for nearly two decades, little analysis of the gene at the transcriptional level has been reported. We analyzed RNA-seq data from three publicly available datasets for AMACR mRNA. In the TCGA [176] dataset comprised of primary PCa samples from 52 patients, we found that AMACR was highly up-regulated in PCa versus normal tissue from the same patient **(Figure 2-2A)**. Analysis of the Grasso [177] and Taylor [178] datasets found that AMACR was significantly overexpressed in primary and metastatic disease compared to normal tissue, however, no significant difference was observed between primary and metastatic disease **(Figure 2-1B).** Analysis of these datasets further supports the cancer-specificity of AMACR and its ubiquitous expression in both primary and metastatic disease. These data also document that significant transcript is present in PCa supporting the use of AMACR transcription machinery for molecular imaging detection of the disease.

The expression of AMACR at the protein and mRNA levels had previously been reported in LNCaP, PC3 and 22Rv1 cells and we confirmed those expression trends with our results [179-181]. To our knowledge, the expression of AMACR in MR42D cells had not been characterized prior in the literature. LNCaP cells were determined to have the most AMACR protein and mRNA by Western blot analysis and qPCR (**Figure 2-3A and Fig 2-3B).** The AMACR protein band in LNCaP cell line was found to be more intense that of the CaCo-2 cell line, a colon cancer cell line commonly used as a positive control for AMACR (**Figure 2-3A)**. The level of AMACR protein in the LNCaP-derived castration-resistant MR42D cells was similar to that of parental LNCaP cells, though mRNA levels differed (**Figure 2-3A and Fig 2-3B**). LNCaP cells are reliant on AR

signaling and produce prostate-specific antigen (PSA) whereas the MR42D cells are indifferent to AR signaling, possessing full-length AR, but producing no PSA [182, 183]. We also tested 22Rv1 cells, another castration-resistant model that expresses full-length AR and splice variants, and the highly metastatic AR-negative PC3 cells for AMACR expression [184]. The qPCR results (**Figure 2-3B**) indicated that 22Rv1 and PC3 cells may have some inhibition of AMACR protein at the translational level. This was speculated because the AMACR mRNA in 22Rv1 and PC3 was equal or greater than in MR42D, however, by Western blot (**Figure 2-3A)**, MR42D revealed more protein. As anticipated, no AMACR was detected at either the protein or mRNA level in prostate epithelial cells (PrEC) isolated from healthy prostate tissue and in the colon cancer cell line HT-29 (**Figure 2-3A and Figure 2-3B)**. We show that the mRNA levels in 22Rv1, PC3, and MR42D are similar while the protein expression in those cell lines differ. This may be due to translational regulation mechanisms which are outside of the promoter control. These results document that though protein levels may differ potentially due to, AMACR mRNA is widespread throughout PCa cell lines regardless of AR status.

Identification and optimization of a minimal promoter for maximum output

The full-length 2,295bp promoter was truncated in a stepwise fashion and the transcriptional efficiency of the truncated AMACR promoters was evaluated using a luciferase assay. The purpose of this assay was to identify a minimal promoter that had a transcriptional output similar to the full-length promoter. Truncations were performed from the 5' end of the full-length promoter and sites were picked randomly. All of the explored regulatory areas of the promoter based on previous literature search are in the 3' end and

remained untouched. According to Zhang et al., 43% of the population has a 20bp deletion that does not alter the promoter strength [185]. Based on sequencing results, the PBMC donor used for cloning was affected by the 20bp deletion. Quantitative analysis of the promoter truncations was performed on the PCa cell lines LNCaP, MR42D, PC3, and 22Rv1 were evaluated for transcriptional output with HT-29 cell line serving as a negative control for specificity. The cells were analyzed for luciferase expression 72 hours post-transfection. Several of the truncations, such as 1726bp and 1893bp, were found to produce a higher output than the full-length promoter (**Figure 2-4B-D**). The augmented activity of the 1726bp and 1893bp promoters was not universal across all cell lines as indicated by the results in LNCaP (**Figure 2-4A**). The 565bp promoter was selected as the minimal promoter for subsequent experiments because it exhibited an output equal to or greater than the full-length promoter and also retained its specificity with little activity in HT29 cells (**Figure 2-4E-F).**

Tissue-specific promoters such as AMACR often possess relatively weak transcriptional activity, especially when compared to strong viral promoters such as cytomegalovirus (CMV). As a result, this could potentially limit their utility *in vivo*. In order to enhance the transcriptional output of the AMACR minimal promoter without compromising its specificity for PCa, we opted to use a two-step transcriptional amplification (TSTA) system. This system was originally developed by Iyer *et al*. and later was further enhanced by Watanabe *et al*. to create an advanced TSTA (A.TSTA) system [173, 186]. The system is inserted downstream of the promoter and upstream of the gene of interest. An A.TSTA system was used with the AMACR minimal promoter to determine if transcriptional output could be enhanced. The A.TSTA element was inserted in the

AMACR 565bp *pGL3* vector and a luciferase assay was performed on 22Rv1, MR42D, and HT29 cells 72 hours post-transfection. The results documented that the output signal significantly increased in MR42D and 22Rv1 cells compared to the 565 bp promoter data but did not significantly affect HT-29 signal (**Figure 2-5A**). The results in **Figure 2-4 and Fig 2-5A** are on the same scale and the results in **Figure 2-5A** compare the additions of A.TSTA to the 565 bp promoter data shown in **Figure 2-4**. From these data, we can conclude that the addition of the A.TSTA to the minimal 565bp promoter construct increased transcriptional output without compromising the promoter specificity.

In vitro and *in vivo* Ad studies utilizing the AMACR minimal promoter

To further evaluate the strength of the AMACR minimal promoter, we used Ad to deliver the reporter construct into cells. Luciferase in the Ad genome was used as the reporter gene to assess the transcriptional efficiency of the promoter **(Figure 2-5B)**. In this study, only non-replicative Ad was used to assess promoter strength. For comparison, three viruses were constructed: a wild type Ad type 5 (Ad5) with the AMACR minimal promoter, an Ad with a chimeric fiber where the tail and shaft domains are Ad5 and the knob domain is of Ad3 (Ad5/3) with the AMACR minimal promoter, and Ad5/3 with the minimal promoter and A.TSTA. PC3, MR42D, and 22Rv1 cells were infected and analyzed for luciferase expression 48 hours post treatment (**Figure 2-5C**). We expected to see an increase in signal from cells infected with Ad5/3+AMACR 565bp compared to the Ad5+AMACR 565bp based the expanded tropism of Ad5/3. Our findings confirmed that the 5/3Ad was able to enter PC3 and MR42D cells better compared to Ad5, however, no significant difference in luciferase signal was observed when comparing the two Ads in the

22Rv1 cells. The addition of the A.TSTA increased the signal significantly in both PC3 and 22Rv1 cells. The infection with Ad5/3+AMACR 565bp+A.TSTA was shown to not be significant in MR42Ds due to high variability. Based on these results, PC3 and MR42D cells were chosen for *in vivo* xenograft models in the experiment that followed. In summary, (**Figure 2-5C**) demonstrated that gene delivery and expression can be improved by modifying the wild type Ad5 fiber to the chimeric Ad5/3 fiber and by adding the A.TSTA system downstream of the AMACR minimal promoter.

Next, we decided to investigate if the Ad5/3+AMACR 565bp+A.TSTA could drive the expression of luciferase *in vivo*. MR42D and PC3 cells were used to form subcutaneous tumors in nude mice. Once the tumors reached a volume of 50-100mm^3, they were injected with the virus via intratumoral administration and imaged at 72 hours and one week post-injection (**Figure 2-6)**. Both tumors were bioluminescent at 72 hours. PC3 tumors were observed to be more responsive to the Ad at 72 hours, while the MR42D signal was less intense at 72 hours compared to the PC3, the signal was stronger at the one week time point (data not shown), however. This observation suggests that there may be a slower transcriptional onset or less efficient entry to the cells in the MR42D model. The *in vivo* experiment documented that our transcriptional system using the AMACR promoter was powerful enough to have a detectable signal for at least a week after administration of the virus *in vivo*.

Discussion

The goal of this study was to develop a novel imaging strategy for the detection of PCa using the transcriptional specificity of the AMACR promoter to drive the expression

of the reporter gene luciferase. Detecting AMACR can potentially lead to decreased patient overtreatment and the associated co-morbidities and financial costs. Additionally, an AMACR imaging probe delivered intraprostatically could be employed for image-guided biopsy, surgery and focal therapy. Molecular imaging of PCa that exploits the AMACR promoter in this manner has never been investigated prior in the literature. This approach differs from a number of PCa-targeted agents because the promoter, and not the actual protein itself, was used for PCa detection [187]. At the protein level, the expression of AMACR has been identified in both primary and metastatic disease with little to no expression in healthy tissues. Our RNA-seq analysis confirmed the widespread cancer-specific expression of AMACR at the transcript level suggesting that our molecular-genetic imaging strategy can be employed to image both localized and metastatic disease. Another attribute making AMACR an attractive imaging target is that the transcription of the gene is not regulated by the AR. In one investigation, Luo *et al.* found that non-hormone refractory and hormone refractory metastases were strongly positive for AMACR by IHC [164]. Thus, unlike PSA or prostate-specific membrane antigen (PSMA) the level of AMACR expressed will not vary due to androgen deprivation therapy or treatment with second-generation making it a consistent target.

Though not affected by AR modulation, the precise elements that regulate AMACR expression are unknown across PCa cell lines. Previously, an extensive analysis of AMACR promoter activity in different PCa cell lines had not been performed. Chen *et al.* [188] inspired our promoter truncation experiment with their experiments to determine the promoter regulatory regions. Based on Chen *et al.* and Zhang *et al*. [185] who determined the CpG island on the 3’ end of the promoter controls gene expression in the colon, we

avoided deleting the 3' regulatory regions. The goal was to determine if there was a shorter, stronger promoter that can behave uniformly in the different PCa cell lines. Our data suggested that the promoter had regulatory sites in the upstream regions that are active in some cells, but activity was variable from cell type to cell type. The minimal 565bp promoter that we selected for our subsequent studies demonstrated stronger output than the full-length promoter in two PCa cell lines and the same output as the full length promoter in two other PCa cell lines. Unlike some of the other truncated promoters that had increased signal in the control cells, the 565bp promoter remained specific for PCa cells. In theory, a shorter promoter would be beneficial for future studies if using plasmid gene delivery as opposed to Ad. Plasmid size is important for delivery because there is a limitation to how much DNA mass can be delivered using polymer transfection reagents. Since delivery using *in vitro* transfection reagent is not as efficient as Ad infection, a shorter promoter would allow more copies of the plasmid delivered. For the purpose of this study, we chose the 565bp promoter because it had slightly higher transcriptional activity without losing specificity. Enhancing the transcription of the minimal promoter with the A.TSTA system worked especially well when Ad was used as the delivery method.

The efficiency of Ad gene delivery is very dependent on the viral ability to interact with cellular receptors. The wild type Ad5 binds to the coxsackie-Ad receptor (CAR) for entry via its knob domain on the Ad fiber. [189] A strategy in the adenoviral field is the use of chimeric fibers. A well-established method is to use the knob domain of Ad serotype 3, which enters cells independent of the CAR. A vector coding for the Ad3 knob, which binds CD46, was incorporated into the Ad5 genome by Krasnykh *et al*. to create a wild type Ad5 with the original tail and shaft domains of the fiber contain an Ad3 knob [190].

The Ad5/3 with its chimeric fiber expands the tropism of the virus and has been shown to enter cancer cells more efficiently [189]. Our results confirmed the improved targeting of the Ad5/3 in two of the cell lines, PC3 and MR42D. While MR42Ds have never been studied in the context of adenoviral therapy, our PC3 and 22Rv1 findings are consistent with previous literature that found 22Rv1s to be as sensitive to Ad11 as they are to Ad5 and PC3s to be more sensitive to Ad11 than Ad5 [191]. This is relevant because Ad11 binds CD46 for cell entry like Ad3, and therefore the comparison of infectivity between Ad5:Ad5/3 and Ad5:Ad11 should correlate.

While our preliminary results for a very advanced gene therapy approach are promising, there are some limitations to keep in mind. For the purposes of preclinical validation of the AMACR promoter, we used luciferase for PCa detection. If the AMACR promoter is to be pursued further, bioluminescence for PCa detection would have to be replaced with a clinically relevant modality such as positron emission tomography (PET). An example of a reporter gene that can be used for PET imaging is herpes simplex 1 thymidine kinase (HSV1-TK) [192]. HSV1-TK can also be used as a suicide gene for therapeutic purposes [135]. This approach may also have difficulty overcoming tumor heterogeneity and it will not have an effect on detecting necrotic tissue.

In addition to using this molecular-genetic imaging approach for differentiating aggressive PCa from benign disease, our technology can be developed further for therapeutic purposes. In this study, we used a non-replicative Ad to determine whether we can detect the PCa using the AMACR promoter. For therapy, suicide genes such as herpes simplex thymidine kinase or cytosine deaminase could be inserted into the promoter construct in place or adjacent to the reporter gene [135]. Additionally, a CRAd oncolytic

virus can benefit from our promoter system to treat PCa. In this scenario, CRAd replication can be guided by the cancer-specific AMACR promoter allowing for tissue-specific replication in the PCa leading to cancer cell death [193]. Our work provides strong evidence that there is value in using the AMACR promoter system in a CRAd and in and also for other Ad based strategies[174] for therapeutic applications.

Material and Methods

Immunohistochemistry

Immunohistochemistry was performed on formalin-fixed paraffin-embedded tissue sections using the rabbit anti-AMACR/p504S clone 13H4 antibody (Novus Bio). Unstained sections (4 μm) were de-paraffinized and rehydrated using standard methods. For antigen retrieval, slides were incubated in 6.0 pH buffer (Reveal Decloaking reagent from Biocare Medical) in a steamer for 30 min at 95-98°C. This was followed by a 20 min cool down period. A serum-free blocking solution (Sniper, Biocare Medical) was placed on sections for 30 min. Blocking solution was removed and slides were then incubated in primary antibody diluted in 10% blocking solution/90% TBST. The antibody was used according to the manufacturer's protocol. Patient biopsies for analysis were acquired using a University of Minnesota Human Subjects Division approved IRB protocol for tissue acquisition (IRB#1604M86 269) and with patient consent.

RNA-seq Analysis

The RNA-seq data from the TCGA was analyzed using a method previously described [194]. In short, the data were downloaded from dbGaP, study accession

phs000178.v9.v8 [176], yielding paired tumor/normal samples for 52 patients. Genes under 300 bp were removed from further analysis as these are not isolated effectively in standard RNA-seq library preps. Genes with low expression (those with less than 10 reads in half of the samples) were removed, and paired tumor and normal samples were analyzed for differential expression using edgeR.

Plasmids

For the plasmid promoter luciferase assay, a pGL3 Basic vector (Promega, E1751) was used as the backbone for cloning. For cloning the full-length promoter, peripheral blood mononuclear cell genomic DNA was used. Primers for the different length AMACR promoters can be found in the Table 2-1. The advanced two-step transcriptional amplification system was designed according to Watanabe *et al*. and synthesized by Genscript. An example of a plasmid map used can be found in the **Figure 2-7.**

Adenoviral Vectors

The vectors for adenoviral cloning were provided by the Davydova laboratory. Two adenoviral (Ad) vectors were used, a wild-type pAd5 and the chimeric pAd5/3. Cloning of the Ad vectors was done by homologous recombination with pShuttle vectors containing a firefly luciferase gene and the promoter based transcriptional system. Homologous recombination was performed in BJ5183 electrocompetent cells (Agilent). A total of three viruses were generated for this study (Ad5+AMACR 565 bp, Ad5/3+AMACR 565 bp, and Ad5/3+AMACR 565 bp+A.TSTA). Virus was generated based on Davydova *et al.* [195]. HEK-293T cells were used for viral productions. Cells were transfected with linearized

viral vectors (linearized by *PacI*) and delivered to cells using Qiagen Superfect transfection reagent. Cells were observed for the cytopathic effect to determine viral infection. The viruses were amplified and purified by a double cesium chloride density gradient ultracentrifugation and dialyzed in 10% glycerol in PBS. The adenoviral functional titer was determined by using an immunoassay kit from Cell Biolabs.

Cell Lines

The cell lines LNCaP, PC3, 22Rv1, HEK-293T and PrEC were purchased from the American Type Culture Collection (ATCC) and were maintained according to ATCC guidelines. MR42D cells were a gift from Dr. Amina Zoubeidi (Vancouver Prostate Center) and were cultured in 10 μM enzalutamide. HT-29 cells were a gift from Dr. Hiroshi Hiasa (Department of Pharmacology, University of Minnesota). All cell lines were verified by short-tandem repeat analysis and analyzed for mycoplasma contamination prior to our studies.

Western Blot

For protein quantification, 20 μg of protein (lysate) of each cell line were used to run on SDS-PAGE and transferred to a nitrocellulose membrane. The primary polyclonal rabbit AMACR antibody (Sigma, HPA020912) was used at 1:500 and was incubated overnight at 4°C. The blots were analyzed using a LICOR C-DiGit Blot Scanner.

Quantitative RT-qPCR

10^6 cells were used for RNA extraction using RNeasy kit (Qiagen). RNA to cDNA conversion was performed using the High capacity RNA to cDNA kit (Applied Biosystems). For gene quantification, Taqman RT-PCR was performed using the Taqman Universal PCR MasterMix (Applied Biosystems) and the following gene expression probes: AMACR –Hs01091292 and 18s ribosomal RNA Hs03928985 for a normalization control. A StepOnePlus Real-Time PCR system instrument (Applied Biosystems) was used for qPCR. Data was analyzed using a comparative Ct method were the fold change = $2^{-\Delta\Delta Ct}$).

Plasmid Luciferase Assay

10^4 cells/well were plated in 96 well plates the night before transfecting. Cells were transfected with 90 ng of the experimental plasmid DNA (pGL3 vector backbones) and 9 ng of control pRL-TK plasmid (Promega) with 0.24 µl of transfection reagent GeneJuice (Millipore) per well. Cells were analyzed 72 hours post-transfection. For analysis, cells were lysed using the passive lysis buffer from Promega. The Dual-Luciferase Reporter Assay System (Promega) was used to quantify luciferase activity. Each readout of the firefly luciferase (LUC) was normalized to its respective renilla luciferase control readout (REN). Results are reported as LUC/REN = Relative Luciferase Units (RLU).

Adenoviral Luciferase Assay

50,000 cells were plated in 24 wells plates with 500 ul of 5% FBS growth media. The next day cells were treated with 100vp/cell. Virus was prepared in 100ul of 5% FBS

growth media and added to the existing media in the wells. At 48 hours cells were lysed using 100 ul of passive lysis buffer from Promega and the luciferase activity was determined with the Luciferase Assay System (Promega). 40 ul of the lysate was taken for the luciferase assay. Luciferase readouts were normalized to the protein content as determined by the Coomassie Plus Protein Assay (ThermoFisher). 5 ul of the lysate was used for the protein assay.

In vivo Bioluminescence Detection

Animal work was done in agreement with our Institutional Animal Care and Use Committee (IACUC) protocol. PC3 and MR42D cells (10^6) were inoculated into the flanks of nude athymic mice (Envigo) of 3-4 weeks of age in a 1:1 dilution of Matrigel (Corning) to PBS. The tumors were allowed to grow for three weeks. The mice received single intratumoral injections of Ad5/3+AMACR565 BP+A.TSTA ($4x10^9$ vp in 50 μmL PBS). Images of *in vivo* expression of the luciferase were acquired at 72 hours and 1-week post injection of the virus. For image acquisition, mice were injected intraperitoneally with 150 mg/kg of D-Luciferin potassium salt (GoldBio) and imaged 10 minutes post-injection with the IVIS Spectrum (Caliper/Xenogen). Images were analyzed with Living Image 4.5 software. The min/max values of the signal were not constant for the two imaging timepoints as the signal was significantly lower at the 1-week time point.

Figures

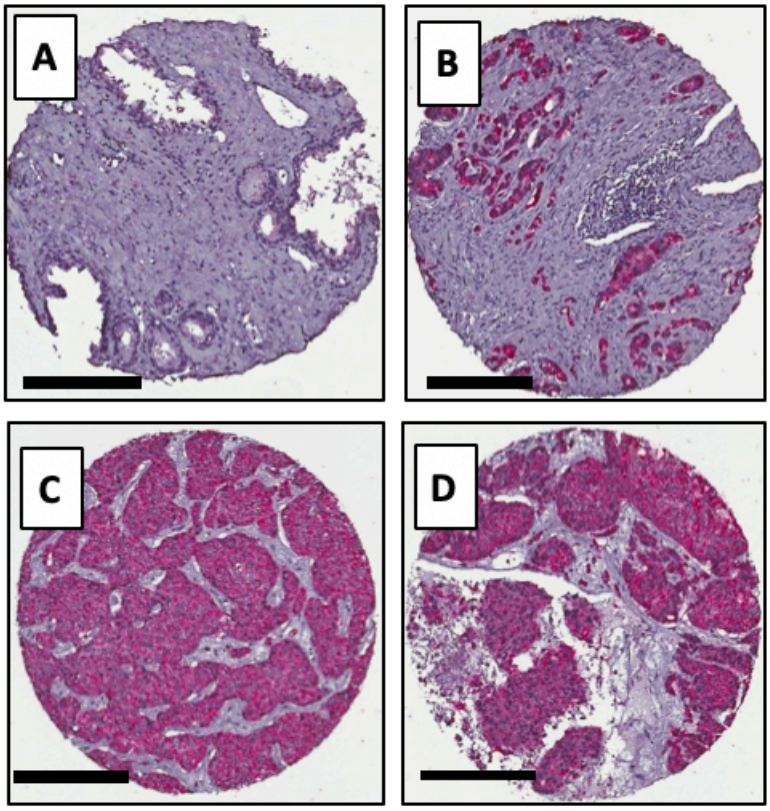

Figure 2-1. Clinical relevance of AMACR expression in primary and metastatic prostate cancer.

Immunohistochemical staining of AMACR in healthy prostate (**A**), prostate adenocarcinoma (**B**), liver metastasis (**C**) and adrenal metastasis (**D**). Scale bars (**A-D**), 200μm.

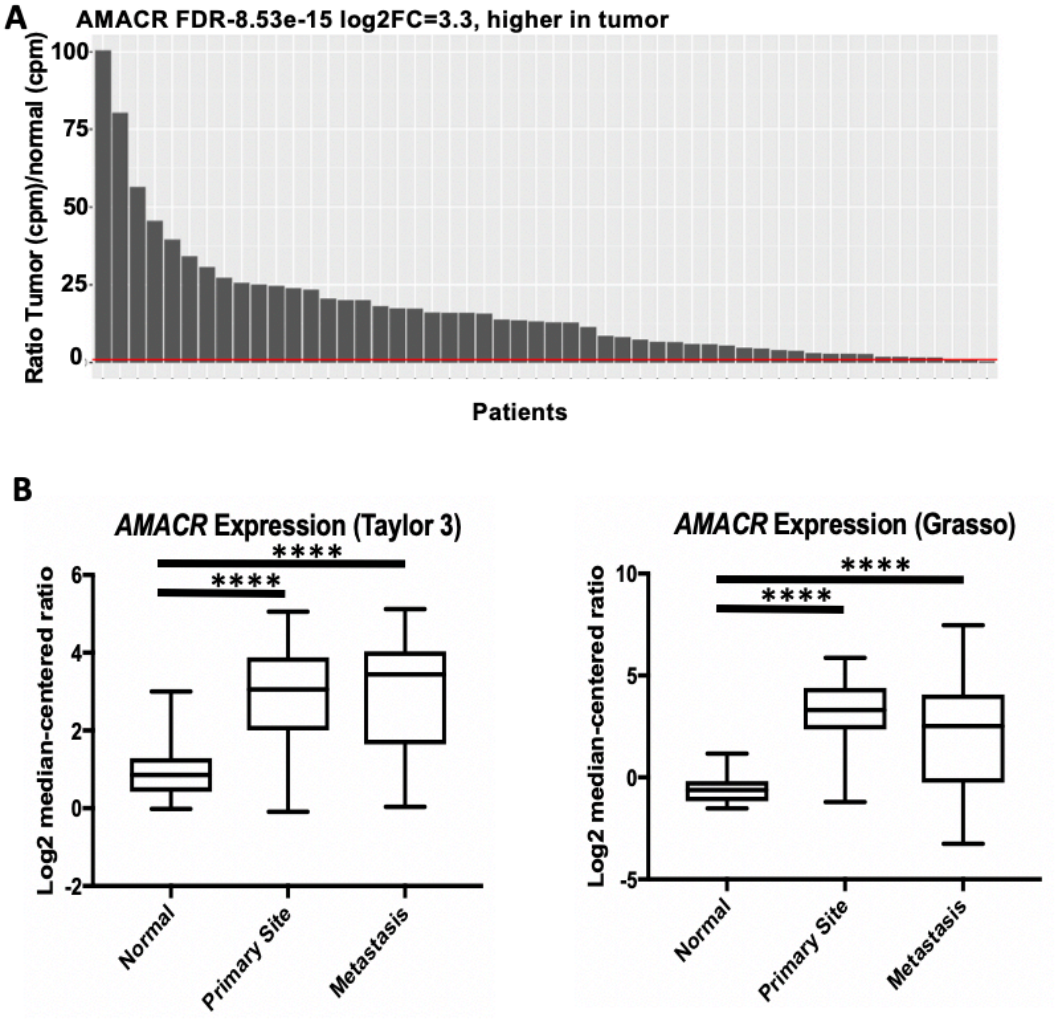

Figure 2-2 Analysis of AMACR in patient samples.

(A) Analysis of the TCGA RNA-seq data documenting that the AMACR expression is overexpressed in the PCa versus normal tissue (n=52). The red bar represents a ratio equal to 1 meaning AMACR expression in both PCa and normal tissue are the same. **(B)** Analysis of the AMACR expression in normal, primary and metastatic PCa from the Taylor and Grasso datasets. Significance was determined using the student t-test (**** $p<0.0001$).

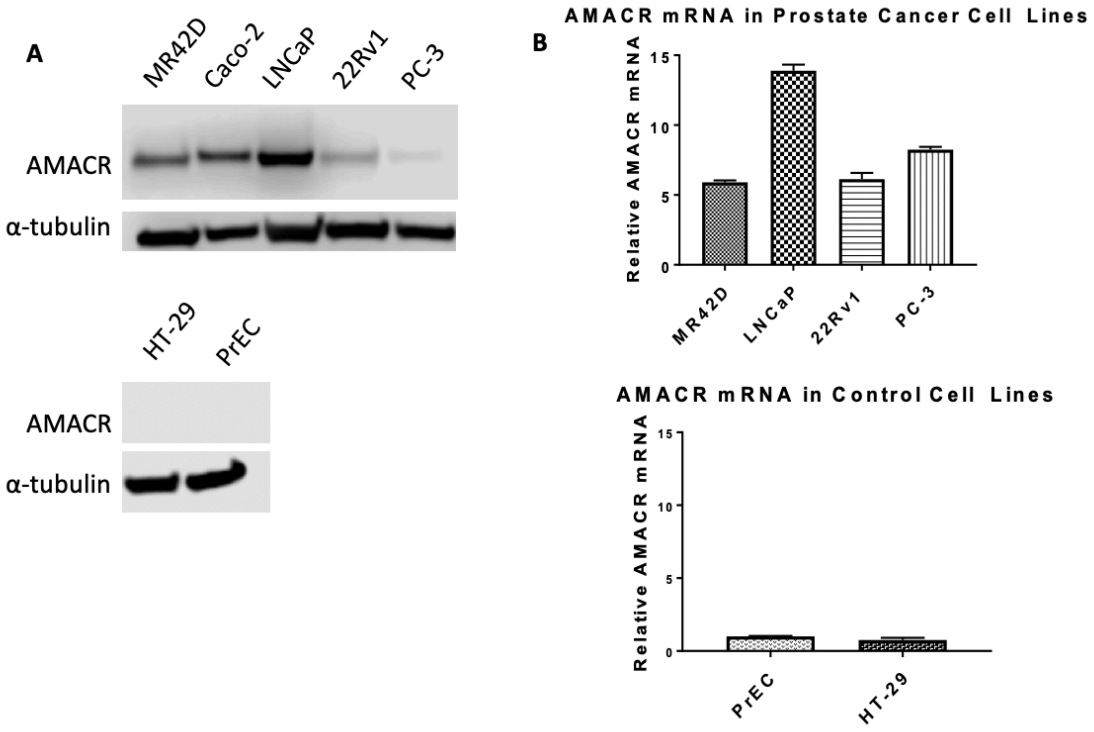

Figure 2-3. Overexpression of AMACR in prostate cancer cell line models.

(**A**) Western blot analysis of AMACR protein levels. *Top:* AMACR protein levels in four human PCa cell lines: MR42D, LNCaP, 22Rv1, PC-3, and the positive control colon cancer cell line Caco-2. *Bottom*: AMACR protein levels in prostate epithelial cells (PrEC) and colon cancer HT-29 cells. (**B**) Relative AMACR mRNA levels by qPCR normalized to reference gene 18S ribosomal RNA. *Top*: High AMACR mRNA levels in PCa cell lines. *Bottom*: Low AMACR mRNA levels in healthy PrEC and negative control HT-29 colon cancer cells.

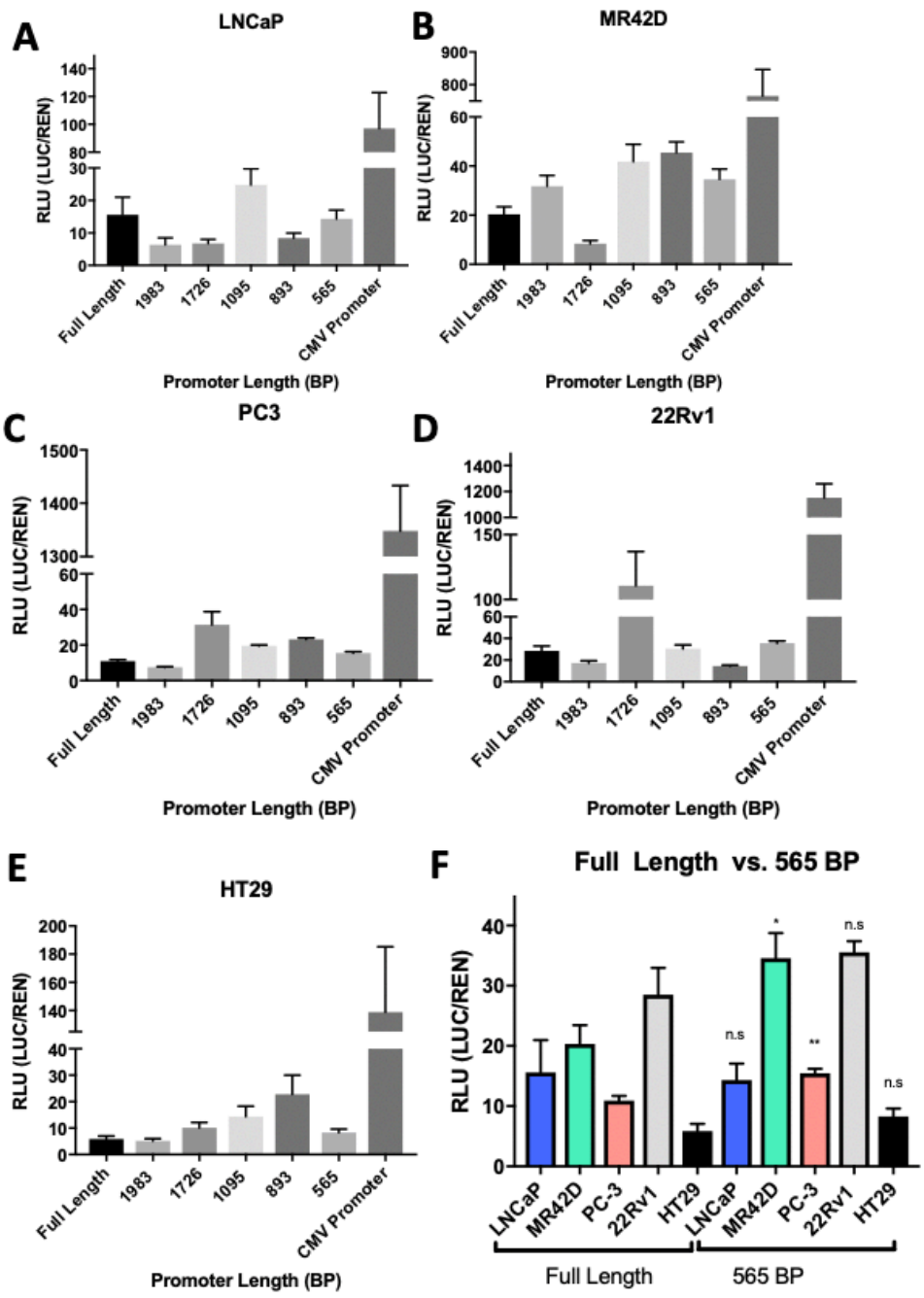

Figure 2-4. Truncated AMACR promoter analysis by the luciferase assay.

Transcriptional activity of the truncated AMACR promoters is represented in relative luciferase units (RLU). Luminescence was measure 72 hours post transfection of plasmid containing a promoter and firefly luciferase gene. Luminescence from the firefly luciferase

(LUC) driven by the AMACR promoter was normalized for transfection efficiency [co-transfection with pRL-TK which expresses renilla luciferase (REN)]. The full-length AMACR promoter and the constitutively-on CMV promoter are presented for comparison for each cell line. (**A-D**) AMACR promoter activity in PCa cells. (**E**) AMACR promoter activity in the low AMACR expressing colon cancer HT-29 cells. (**F**) A comparison of the full-length promoter activity in PCa cells and HT-29 cells to the 565bp truncated promoter. The 565bp promoter is shown to be equally powerful in LNCaP and 22Rv1 cells, more powerful in MR42D and PC-3 cells compared to the full-length promoter and did not show an increase in activity in the low AMACR expressing HT-29 cells. Results are presented as mean ± standard error of the mean (SEM) of n=6. Significance was determined using the student t-test (**** $p<0.0001$; *** $p<0.001$; ** $p<0.01$; * $p<0.05$).

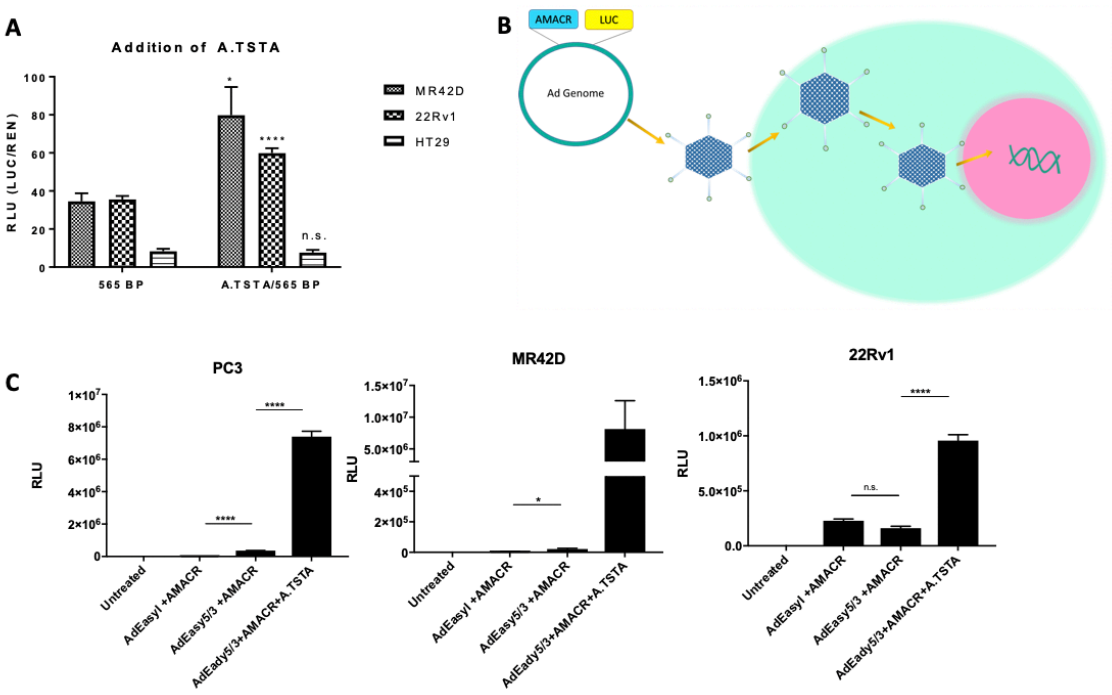

Figure 2-5. Addition of the advanced two-step transcriptional amplification system and assessment of promoter activity using adenoviral gene delivery in vitro.

(**A**) Luciferase signal 72-hour post transfection of plasmid containing the A.TSTA downstream of the AMACR 565bp promoter in PCa cells MR42D and 22Rv1, and colon cancer HT-29 cells. The 565 bp promoter data is from Figure 2-4 and placed here for comparison. Luminescence from the firefly luciferase (LUC) driven by the AMACR promoter was normalized for transfection efficiency [co-transfection with pRL-TK which expresses renilla luciferase (REN)]. (**B**) Adenovirus gene delivery to the cells. The promoter or promoter system is introduced to the Ad genome and a virus is constructed. Cells are infected with the virus and DNA is released into the nucleus for gene delivery. (**C**) Promoter activity expressed in RLU (luciferase signal normalized to total protein) 48 hours post-delivery of adenovirus containing firefly luciferase as the reporter gene. The activity of the 565bp promoter was analyzed using adenovirus serotype 5 (Ad5) and Ad

with a chimeric fiber with the knob domain of Ad3 in the Ad5 capsid (Ad5/3) for delivery. The addition of the A.TSTA was analyzed using only Ad5/3 for delivery. RLU is normalized to the protein concentration. Results are presented as mean ± standard error of the mean (SEM) of n=6 in **(A)** and n=3 in **(B).** Significance was determined using the student t-test (**** $p<0.0001$; *** $p<0.001$; ** $p<0.01$; *$p<0.05$, n.s.= not significant).

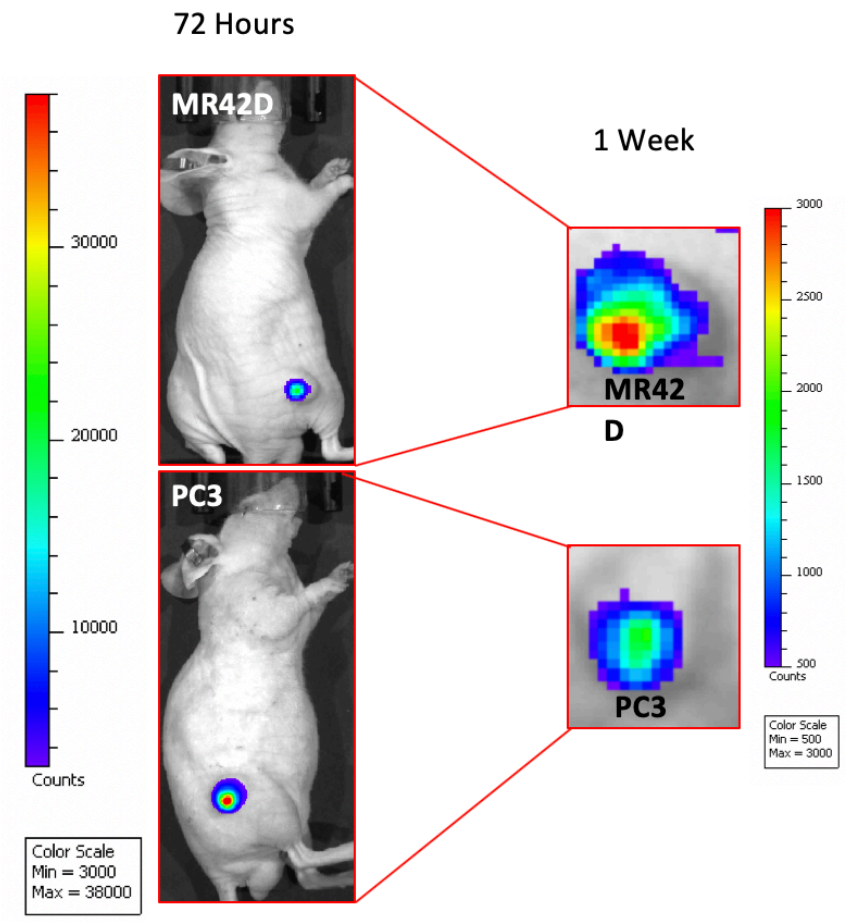

Figure 2-6. Ad5/3 gene delivery of luciferase guided by the AMACR 565bp promoter and the A.TSTA system.

Mice injected intratumorally with Ad5/3+AMACR 565bp+A.TSTA. The mice were injected with D-luciferin prior to imaging to detect AMACR promoter-driven expression. MR42D and PC3 subcutaneous xenografts in nude mice were used as the PCa models. Images were acquired at 72 hours (left) and at one week (right). The results presented are representative images of n = 3 mice. The signal was diminishing by the 1-week time point in both xenografts as demonstrated by the change in the minimum and maximum of the signal strength.

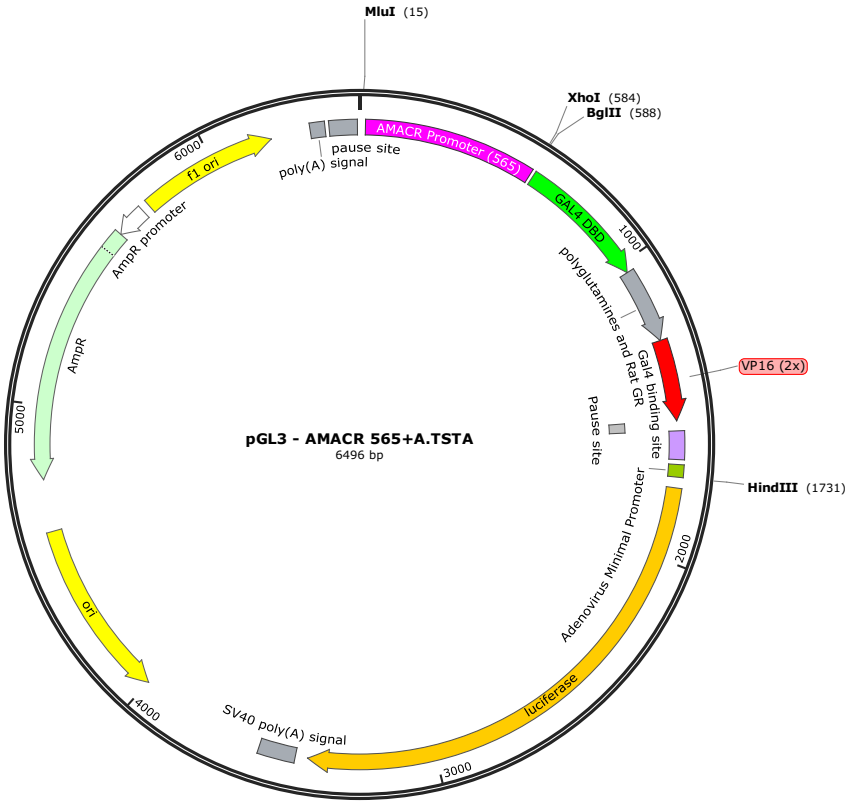

Figure 2-7. Example of experimental plasmid map.

The promoter was inserted using the MluI and XhoI while the A.TSTA was inserted using BglII and HindIII. The construct is designed according to Watanabe *et.al* with. Two VP2 domains instead of 1. The plasmid backbone used was pGL3 from Promega with the firefly luciferase reporter gene. More details on TSTA design can be found in Chapter 3 Methods.

Table 2-1. Primers for promoter truncation.

Primer	Sequence
Reverse (Rev63) – XhoI Cut Site	5' CGGCTCGAGCTGAAGGAAACTGAGCAG3'
Full Length (2295 BP) Forward - MluI Cut site	5' CGACGCGTCCTCAGAAGCATGTGA 3'
1983 Forward – MluI Cut site	5' GCAACGCGTGGGACTGCTGGATCATAT 3'
1726 Forward - MluI Cut site	5' GCAACGCGTTGTTGGCCATTTGTATGC 3'
1095 Forward - MluI Cut site	5' CGGACGCGTTCTGGTAGTG 3'
893 Forward - MluI Cut site	5' CGGACGCGTACTTGCTTGAG 3'
565 Forward - MluI Cut site	5' CGGACGCGTTCTGGTAGTG 3'
294 Forward- MluI Cut site	5' CCGACGCGTGTACAATAAAAGCG 3'

The table above provides detailed primers used for the truncation of the AMACR promoter. The same reverse primer was used do all the promoter cloning. The reverse primer, and full length forward primer were based on Chen *et al.* [188].

Chapter III: The molecular detection of lethal prostate cancer by PEG10 promoter-driven expression of reporter genes

Overview

Purpose: The retrotransposon-derived paternally expressed gene 10 (PEG10) protein is ordinarily expressed at high levels in the placenta. It was discovered recently that PEG10 isoforms promoted the progression of prostate cancer (PCa) to a highly lethal androgen receptor negative phenotype. PEG10 expression in castration resistant PCa (CRPC) has not been explored and a utility for the PEG10 overexpression has never been developed. Our study investigates the extent of PEG10 expression in PCa and develops the PEG10 promoter into a molecular-genetic imaging tool.

Experimental Design: To study PEG10 expression in castration resistant PCa, we analyzed patient microarray data, patient RNA seq data, patient biopsies, and patient derived xenografts. The PEG10 promoter was optimized for optimal transcription efficiency *in-vitro* and integrated into a reporter-plasmid to detect PCa *in-vivo*.

Results: Our investigations found that PEG10 is expressed in castration-resistant PCa. We subsequently developed a molecular genetic imaging strategy for the non-invasive imaging of highly lethal PCa by utilizing the cancer-specificity of the PEG10 promoter to drive the expression of reporter genes. By using this PEG10 promoter upstream of a reporter gene in a plasmid, we were able to detect PCa by fluorescence and positron emission tomography imaging after systemic administration of the plasmid in mice. Subcutaneous

CWR-R1 xenografts and CWR-R1 intratibial tumors were used as CRPC models to demonstrate the utility of our imaging system.

Conclusions: We show that PEG10 is more widely expressed in PCa than documented previously and that PEG10 expression occurs in CRPC. Because of its broad expression in aggressive forms of PCa, PEG10 can targeted for imaging using the transcriptional output of the PEG10 promoter. We developed a PEG10-biomarker driven imaging technology that has the potential to improve detection and monitoring of disease progression.

Introduction

Prostate cancer (PCa) is a prevailing disease affecting 1 in 9 men in the United States [196]. Once prostate cancer has metastasized to the bone and soft tissue, few effective treatment options exist. Androgen-deprivation therapy (ADT) is the clinical standard for the treatment of metastatic disease [197]. ADT suppresses the endogenous production of androgen by the testes leading to decreased signaling through the androgen receptor (AR). Signaling through the AR axis is required for the development and normal function of the adult prostate as well as the growth and survival of PCa cells [198]. Although initial response rates are high, all men will eventually fail ADT and develop castration-resistant prostate cancer (CRPC) [199]. Aberrant reactivation of the AR signaling axis, due to AR over-expression, constitutively active AR splice variants and the endogenous production of testosterone by the cancer cell, is a salient feature of CRPC [200]. The second-generation anti-androgens abiraterone and enzalutamide have recently demonstrated clinical advantages in CRPC patients treated with second-line hormonal

agents and docetaxel [201]. Resistance to these therapies inevitably occurs and many men develop a highly lethal subtype type of non-AR driven disease [202, 203]. Treatment options for this subtype are limited, consisting of taxanes and platinum agents [202]. Thus, there is an urgent need for the development of novel effective therapies to treat late-stage, drug resistant PCa.

The development of novel therapeutics, and the appropriate tailoring of existing therapies, is hindered by the inability to accurately quantify disease burden and patient response to therapy by molecular imaging [204]. The most commonly used imaging modality to assess disease burden, measure patient response to therapy and disease progression in men with PCa is the ^{99m}Tc methylene diphosphonate (^{99m}Tc-MDP) bone scan [205]. Though the bone scan is useful in measuring osseous metastases, a large percentage of men with late-stage disease now develop extensive visceral metastases for which no imaging gold standard exists [206]. The positron emission tomography (PET) tracer ^{18}F-fluorodeoxyglucose (^{18}F[FDG]) is commonly used in the clinic to image types of cancer that are dependent on glucose metabolism [207]. However, ^{18}F[FDG] has performed poorly for imaging PCa due to its unique metabolic properties that result in metastatic lesions with little avidity for glucose [207-209]. Other PET tracers such as ^{18}F-choline, radiolabeled PSMA ligands, and ^{18}F[NaF] are limited in the phenotypes of PCa they are able to detect [116]. More recently, the FDA approved a ^{18}F-labeled artificial amino acid derivative, ^{18}F-fluciclovine, for the imaging of recurrent PCa in patients with elevated PSA [210]. This tracer is still under investigation and has not been evaluated for imaging late-stage disease. Other imaging modalities such as magnetic resonance imaging and CT are limited in their application and tell nothing of the underlying biology of the

cancer cell [206]. Thus, there is no accurate modality currently available for imaging late-stage PCa.

One attractive imaging strategy that is non-invasive and allows for the detection of cancer with high specificity and low background is molecular-genetic imaging. Molecular-genetic imaging relies on the transcriptional mechanics of the disease rather than the targeting of a cell surface antigen or a metabolic protein [211]. In this strategy, the promoter of a cancer-specific gene is used to drive the expression of a reporter gene within the cancer cell. This promoter-reporter gene system is placed in a plasmid that is administered locally or systemically. Once the plasmid is delivered to the cancer cell, the cancer-specific promoter guides the expression of reporter genes such as herpes simplex 1 thymidine kinase (HSV1-TK) which can be detected via PET imaging after the administration of a radiolabeled nucleoside substrate [211]. Pre-clinical research using molecular-genetic imaging has previously been successful at detecting cancer models using cancer-specific promoters to drive reporter gene expression [212, 213]. Additionally, molecular genetic imaging can be further exploited for theranostic purposes by the expression of suicide genes such as cytosine deaminase[135]. Plasmid-based therapeutics and their delivery agents are currently in clinical trials which makes molecular-genetic imaging a translational tool [125, 212, 213].

Elevated paternally expressed gene 10 (PEG10) expression in PCa [214] has been reported and recently its upregulation was discovered in the transdifferentiation of AR-driven prostate adenocarcinoma to non-AR driven disease [215]. PEG10 is a retrotransposon-derived gene primarily expressed in the placenta and is crucial for embryonic development [216]. We investigated the expression of PEG10 in healthy

prostate tissue, primary adenocarcinoma, metastatic CRPC and AR-PCa. Our analysis discovered that PEG10 expression was not restricted to AR-disease but was also found in a subset of AR^+ CRPC including disease expressing AR splice variants. Harnessing the overexpression of PEG10, we used the transcriptional mechanisms of PEG10 to create a molecular-genetic imaging tool for the detection of these highly lethal PCa subtypes. The imaging strategy incorporated an optimized PEG10 promoter and a two-step transcriptional amplification element for enhanced output. Our final imaging construct allowed for the precise tumor detection in a CRPC subcutaneous xenograft model by PET/CT.

Results

Expression of PEG10 is prominent in metastatic disease and not adenocarcinoma.

Immunohistochemistry (IHC) analysis was performed on tissue microarrays (TMAs) of primary prostate adenocarcinoma. The antibody for IHC was validated using placenta as a positive control (**Figure 3-1**). No positive staining for PEG10 was observed in any of the primary prostate adenocarcinoma cores (0/120) even across a spectrum of high Gleason scores. (**Figure 3-2A**). Next, we analyzed publicly-available RNA-seq datasets [217-219] to quantify PEG10 expression between hormone naïve primary prostate tumors and metastasis (**Figure 3-2B**). These data documented a significant increase in PEG10 mRNA expression in CRPC metastases compared to primary tumors ($p<0.01$). We then analyzed a liver biopsy from a patient who demonstrated radiographic progression while on abiraterone in the presence of declining PSA. Here, strong PEG10 staining was observed in the liver biopsy while AR staining was completely absent (**Figure 3-2C**). The original biopsy from the prostate of this patient prior to surgery documented aggressive

Gleason 4 + 5 disease that was absent for PEG10 but positive for AR expression by IHC (**Figure 3-2D**).

Regulation of PEG10 by full length AR and AR variants.

Based on previous reports, the lack of AR expression in NEPC appeared to promote PEG10 expression [215]. In the CWR-R1-derivative cell line R1-AD1 [220], ChIP-seq analysis demonstrated that the wild type, androgen activated AR was bound to the PEG10 gene. Conversely, insignificant binding to the PEG10 gene was observed in ChIP-seq data from vehicle-treated R1-AD1 cells and in R1-D567 cells that only express the constitutively active AR variant, ARv567es (**Figure 3-3A**). We next used RT-PCR to test the androgen regulation of PEG10 mRNA in PCa cells treated with the synthetic androgen R1881 (**Figure 3-3B**). LNCaP cells, which express full-length wild-type AR, displayed an increase in PEG10 expression when grown in charcoal stripped serum (CSS). The addition of R1881 to the CSS media reduced the PEG10 expression in LNCaP cells back to baseline, indicating that active AR represses PEG10 expression. CWR-R1 cells, which express wild type AR and AR splice variants [221, 222] did not display R1881-mediated repression of PEG10 mRNA. Our data may be preliminary evidence that constitutive activity of AR variants expressed in CWR-R1 cells may be dominant over full-length AR in regulating PEG10 expression.

PEG10 expression is not confined to AR-negative PCa cells.

We discovered that cell lines previously reported to express elevated levels of PEG10 (DU145 and PC3) did not exhibit the highest expression levels out of the PCa cell

lines analyzed by qPCR (**Figure 3-4A**). The qPCR data found that AR^+ cell lines with a castration-resistant phenotype [223, 224] - CWR-R1, 22Rv1, and MR42D - had elevated PEG10 expression levels. Both CWR-R1 and 22Rv1 cells express AR splice variants in addition to full-length AR[221, 223] while MR42D cells express wild type AR but are indifferent to AR signaling [183]. The analysis of cell line PEG10 expression was also used to determine models and controls for studies of PEG10 promoter activity

IHC staining of PEG10 in a tissue microarray of LuCaP-series patient derived xenografts (PDXs) found strong straining in the PDXs representing AR-null neuroendocrine PCa (NEPC), including LuCaP 145.1 (**Figure 3-4B**). Strong staining was also observed in the AR splice variant-positive model LuCaP 86.2, while no staining for PEG10 was observed in the AR^+ adenocarcinoma model LuCaP 78. The IHC results of PDX staining for PEG10 support our hypothesis that there may be a path of alternative regulation of PEG10 expression by AR splice variants which results in elevated PEG10 expression. To test this directly, we investigated microarray data from CWR-R1 cells transfected with siRNA targeting AR exon 7, which ablates expression of full-length AR but not AR-V7, or CWR-R1 cells transfected with siRNA targeting AR exon 1, which ablates expression of both full-length AR and AR-V7 (**Figure 3-4C**). PEG10 expression was higher in CWR-R1 cells transfected with exon 1-targeted siRNA vs exon 7-targeted siRNA, indicating that AR-V7 may be activating PEG10 expression. Collectively, analysis of gene expression and IHC with PDX tissue support the hypothesis that lack of AR is not the only factor responsible for PEG10 upregulation and that AR-Vs may positively regulate PEG10 expression. To our knowledge, this is the first data demonstrating positive regulation of PEG10 expression by AR variants. Subsequently, a microarray of early

passage LuCaP PDX models was analyzed for PEG10 expression (**Figure 3-5A**). PEG10 was elevated in NEPC PDX models that are AR^- (**Figure 3-5B**, $p<0.0001$). However, based on the heatmap, it should be noted that some AR^+ PDXs did in fact exhibit elevated PEG10 which may be due to the presence of AR splice variants (LuCaP 86.2 and 147) [220, 225]. Aside from these individual examples, overall the PDX microarray did show a negative correlation between PEG10 and AR (Pearson's rho = -0.5242), supporting previous literature that wild-type AR does in fact play some role in downregulating PEG10 expression (**Figure 3-5C**).

PEG10 expression weakly correlates with downregulated AR in a patient microarray.

We next studied PEG10 in gene expression microarray data of 171 CRPC from 63 patients with metastatic CRPC [226] (**Figure 3-6A**). This gene expression microarray demonstrated evidence of large variability in PEG10 expression among tumors that are AR^+, NE^-. PEG10 expression was elevated in AR^+/NE^+ and AR^-/NE^+ tumors compared to the AR^+/NE^- tumor population (**Figure 3-6B**). This observation supports previous literature on PEG10 elevation in NEPC [215], but also shows that PEG10 expression can also be high in AR^+ tumors. AR^-/NE, which has been termed double-negative CRPC, displayed less PEG10 expression than NE^+ tumors. The mCRPC microarray revealed that in clinical samples, the negative correlation of PEG10 and AR was slightly weaker (**Figure 3-6C**) than in the LuCaP PDX models based on Pearson's correlation coefficient (Pearson's rho = -0.4217). The correlation between AR and PEG10 represented by Pearson's correlation coefficient supports that PEG10 expression correlates with AR downregulation but also

leaves room for our hypothesis that AR variants and/or other factors may play a role in regulating PEG10 expression.

ONECUT2 has a similar expression trend with PEG10.

ONECUT2 was recently identified as a regulator of lethal PCa by suppressing AR-dependent signaling [227, 228]. The recent literature documents that PEG10 expression in the 22Rv1 *in vivo* model decreased after inhibition of ONECUT2 and increased *in vitro* after ONECUT2 overexpression in LNCaP and C4-2 cells. In line with this, microarray data from CRPC patients demonstrated that elevation of ONECUT2 expression occurred in AR^{+}/NE^{+} and AR^{-}/NE^{+} tumor populations but not in double negative PCa (**Figure 3-7A**). The trend in expression was similar to that of PEG10. There was a positive correlation between PEG10 and ONECUT2 (**Figure 3-7B**) (Pearson's rho = 0.5292) and a negative correlation between AR and ONECUT2 (**Figure 3-7C**) (Pearson's rho = -0.4199). ONECUT2 expression in LuCaP PDX microarray was also elevated in NEPC compared to adenocarcinoma (**Figure 3-7D**).

PEG10 promoter is a powerful transcriptional tool.

After verifying PEG10 prominence in aggressive PCa, our goal was to use the elevated expression to create a powerful detection tool for PCa. Our strategy was to incorporate the transcriptional power of the PEG10 promoter in a molecular-genetic approach to image PCa. The promoter was first optimized to be more powerful than its intrinsic self. Two PEG10 promoter versions were cloned, a full length (~2 kb) promoter ($PEG10^{2KB}$) and a truncated ~1 kb promoter ($PEG10^{1KB}$) based on previous reports [229]

and placed into a pGL3-Basic vector (~4.8 kb) which has a luciferase reporter gene. The transcriptional efficiency of the two promoter variants was initially evaluated in AR^- cells with LNCaP as a control for known low PEG10 expression (**Figure 3-8A**). By luciferase assay, we discovered that the 1 kb promoter was significantly stronger than the full-length PEG10 promoter in the three cell lines. Equal mass of each construct was used for transfection. Because the 1 kb construct was ~15% smaller that the pGL3 vector with the 2 kb promoter, 15% more copies of the construct were delivered of $PEG10^{1KB}$ than $PEG10^{2KB}$. The 1 kb promoter resulted in more than 15% more luciferase signal, which proved that the 1 kb promoter was intrinsically more efficient in PCa cells and the results were not a result of more plasmid copies delivered. Our results were supported previous literature [229], where it was suggested that there must be repressor elements that exist in the 5' end of the promoter and those elements are eliminated in the $PEG10^{1KB}$ construct.

To further enhance activity of the truncated PEG10 promoter, we added a two-step transcriptional amplification (TSTA) element (**Figure 3-9**). There are various established versions of the TSTA in literature. In our study (**Figure 3-8B**), we tested the conventional-TSTA, which we called TSTA [186] and the advanced-TSTA (A.TSTA) [173]. Our designs used two VP-16 domains as described in the methods. The conventional TSTA contains a gene coding for the fusion protein of GAL4 binding domain and a VP16 activation domains from the herpes simplex virus 1 activator VP16 downstream of the promoter. Based on previous literature [230], we used two VP16 domains in the fusion protein in our plasmids. The fusion protein binds to an array of 5 GAL4 binding sites, which increases transcription of the reporter gene [186]. The A.TSTA contains additional

polyglutamines and rat glucocorticoid receptor in the fusion protein, increasing transcription even further [173].

Increased luciferase output was observed after the addition of both the TSTA to the 1 kb promoter (^{TSTA}PEG10^{1KB}) and A.TSTA ($^{A.TSTA}$PEG10^{1KB}) compared to the 1 kb promoter alone. Comparison of the two elements side by side showed that the transcriptional output for the $^{A.TSTA}$PEG10^{1KB} was significantly more powerful than the ^{TSTA}PEG10^{1KB} based on the luciferase activity results (**Figure 3-8B**). We then looked at AR^{+} CRPC models and compared the output of PEG10^{1KB}, ^{TSTA}PEG10^{1KB}, and $^{A.TSTA}$PEG10^{1KB} (**Figure 3-8C**) and found that universally the addition of A.TSTA increases the transcriptional power of the PEG10 promoter. It should be noted that the TSTA elements appear to have variable effects from cell line to cell line. An empty vector control was performed in all cell lines (**Figure 3-10**). Based on these data, $^{A.TSTA}$PEG10^{1KB} was the most powerful transcriptional tool developed. Interestingly, the HT-29 colon cancer cell line, exhibited increase signal with the addition of the TSTA elements even though their mRNA level resembles LNCaP (**Figure 3-8C**), it even appeared to actually decrease with TSTA element addition. The reason for this is not clear but the TSTA transcriptional regulatory mechanisms responsible must be different. The TSTA elements did appear to have variable effect in each cell line, but overall the effect was positive.

The luciferase gene in our construct was replaced with near-infrared fluorescence reporter protein 682 (iRFP682) which is excited at 663 nm and emits at 682 nm [231]. A transfection protocol similar to the one used in the luciferase assay was performed on CWR-R1, PC3, and LNCaP cells and the transcriptional output of the PEG10 promoter constructs was visualized via fluorescence cell imaging (**Figure 3-8E**). We found that the

PC3 cells appeared to have greater fluorescence intensity than the CWR-R1 even though CWR-R1 cells show higher levels of PEG10 mRNA. We attributed the lower expression of iRFP682 in CWR-R1 in this imaging experiment as a possible result of the transfection efficiency of the CWR-R1 cells with the transfection reagent used or different post-transcriptional regulations in the cell line that are beyond promoter control. These data documented that the $^{A.TSTA}PEG10^{1KB}$ promoter construct was powerful and it was selected for subsequent *in vivo* experiments.

PCa detection by optical imaging using the PEG10 promoter.

We evaluated our strategy for the near-infrared (NIR) imaging of PCa *in vivo* by detecting the reporter protein iRFP682 (**Figure 3-11**). Mice bearing subcutaneous CWR-R1 xenografts were injected systemically with either $^{A.TSTA}PEG10^{1KB}$ *iRFP682* plasmid or $^{TSTA}PEG10^{1KB}$ *iRFP682* plasmid using *in vivo*-jet PEI. The mice were imaged starting at 24 hours post-injection of the polymer-coated plasmid constructs. Images acquired using 675/720 nm excitation/emission. The images (**Figure 3-11A-B, Figure 3-12A**) of mice injected with the two plasmids demonstrated that the promoter alone was strong enough to drive expression levels of the fluorescent protein sufficient for detection. The addition of the A.TSTA to the plasmid resulted in significantly stronger signal compared to the promoter alone (**Figure 3-11C**) based on the two-way ANOVA analysis of region of interest (ROI) fluorescence intensity which indicated that the constructs were significantly different ($p=0.0374$). Bonferroni's post-hoc found the 72 hour time point to be significantly different between the two mouse groups. An identical ROI measurement was drawn around each tumor for consistency since tumor sizes varied from mouse to mouse for the

acquisition of these measurements. In a separate experiment, mice were injected with the $^{A.TSTA}$PEG10^{1KB} *iRFP682* and tumors were excised at 96 hours post-injection. In a separate injection of the $^{A.TSTA}$PEG10^{1KB} *iRFP682* plasmid-polymer complex, *ex vivo* visualization of the tumors documented high expression of the iRFP682 protein (**Figure 3-11D**).

We normalized the radiant efficiency min/max values to the $^{A.TSTA}$PEG10^{1KB} *iRFP682* construct, however, we showed that the promoter alone can be sufficient to detect the tumor as the min/max values are slightly lower (**Figure 3-12B**). It is important to note that background fluorescence exists in the mice even on the special low-fluorescence diet (alfalfa free) the mice were fed (**Figure 3-13A**). The background signal in untreated mice can be visualized in the bladders, gut/stomach, as well as some upper-body regions. After injection of $^{A.TSTA}$PEG10^{1KB} *iRFP682,* there is a visible increase in background in the gut/stomach regions (**Figure 3-13B**). Because the PEG10 is not expressed in these organs in mice, we do not necessarily attribute the elevation in fluorescence signal to the promoter activity although we cannot eliminate that as a possibility. The reason behind the fluorescence in the gut/stomach regions may be an off-target effect, however, to the best of our knowledge, fluorescence reporter constructs through systemic delivery have not been previously explored in literature and we therefore are not able to offer a precise explanation. The background signal can be considered negligible when the s.c. xenograft is imaged *ex vivo* (**Figure 3-13C**).

We used subcutaneous (s.c.) HT-29 xenografts for a low-control because they had low PEG10 mRNA levels and appeared to not have an increase in signal with the addition of A.TSTA in the luciferase assay (**Figure 3-8D**). Mice were imaged at 24, 48, and 72 hours post construct injection (**Figure 3-14A-B**). When normalized to the same min/max

values as CWR-R1 (**Figure 3-11A-B**), HT-29 did not show any visible signal. The xenografts were verified for low expression of PEG10 by IHC (**Figure 3-15**).

To demonstrate that this gene therapy imaging approach is applicable for metastasis detection, we repeated our fluorescence imaging studies in an intratibial (i.t.) PCa model that mimics bone metastasis [232]. The i.t. model was developed by injecting CWR-R1 cells into one of tibia of each mouse. Three weeks post tumor inoculation, the mice were injected with the $^{A.TSTA}$PEG10^{1KB} *iRFP682* plasmid and imaged at 25, 48, and 72 hours (**Figure 3-16A**). Compared to the healthy legs, there was visual signal apparent at the tibia of the i.t. CWR-R1 legs. We compared the signal of the healthy legs of each mouse to the i.t. legs by using same-size ROIs around the tibias (**Figure 3-16B**). The i.t. legs had significantly more near-infrared fluorescence due to the construct as determined by two-way ANOVA ($p=0.0234$). Bonferroni's post-hoc analysis indicated significant difference at the 48 and 72 hour time points.

PCa detection by PET/CT imaging via the PEG10 promoter.

Encouraged by our NIR imaging results, we decided to use our transcriptional technology to detect PCa *in vivo* using the clinically relevant imaging modality PET/CT. To develop a PET/CT imaging strategy, we opted to use herpes simplex virus 1 thymidine kinase (HSV1-TK) as the reporter gene. HSV1-TK works by phosphorylating radiolabeled pyrimidine nucleoside derivatives such as 5-[^{124}I]iodo-2'-fluoro-2'-deoxy-1-β-D-arabino-5-iodouracil (^{124}I-FIAU) [192]. ^{124}I-FIAU is a poor substrate for mammalian thymidine kinase; however, cells expressing HSV1-TK can phosphorylate and trap high levels of the radiolabeled nucleoside substrate (**Figure 3-17A**) [233]. Using HSV1-TK as the reporter

gene, we were able image subcutaneous CWR-R1 xenografts 72 hours post-injection of $^{A.TSTA}$PEG10^{1KB} *HSV1-TK* plasmid construct with ^{124}I-FIAU. To control for off-target expression of HSV1-TK and localization of ^{124}I-FIAU, non-tumor bearing mice were injected with $^{A.TSTA}$PEG10^{1KB} *HSV-TK* plasmid construct (**Figure 3-18**). Off-target localization of free ^{124}I from deiodated FIAU was seen as anticipated in the thyroid (Ty) due to the glands involvement in the metabolism of iodine and in the bladder (B) due to iodine excretion in the urine [234, 235]. Both Ty and B signal can be seen in a representative image of a non-tumor bearing mouse as visualized in the 2-D (**Figure 3-18Aa**) and 3-D reconstructed images (**Figure 3-18Ab**). The mice in the CWR-R1 xenograft group exhibited the same non-specific uptake in the Ty and B, as documented in the 2-D (**Figure 3-18Ba**) and 3-D reconstructed images of a representative mouse (**Figure 3-18Bb**). To confirm that the signal in the tumor was the result of *HSV1-TK* expression, s.c. tumors were analyzed by qPCR and IHC. Both HSV1-TK and PEG10 were detected (**Figure 3-17B-C**).

The CWR-R1 s.c. model was verified by PET/CT imaging. Mice with i.t. CWR-R1 tumors (5 weeks post-inoculation) in the tibia were injected with $^{A.TSTA}$PEG10^{1KB} *HSV1-TK*. Mice were injected with ^{124}I-FIAU forty-eight hours post DNA injection and imaged the next day. Signal at the tumor legs was clearly visible inside the tibia while no signal was present at the site of the healthy tibia in 2-D analysis (**Figure 3-19A**). 3-D reconstruction was performed and slicing of the legs had to be done because the PET signal was inside the bone (**Figure 3-19B**).

In the s.c. PET experiment not much signal was visible in the gastrointestinal tract and liver, the site of FIAU metabolism [212, 235], but in the IT experiment significant

signal was also seen in the liver and gastrointestinal tract (full body image not shown). We injected 250 uCi in the IT experiment vs 150 uCi in the subcutaneous experiment, so the increase of ^{124}I-FIAU dose may be responsible for the difference in gastrointestinal signal.

Discussion

The goal of this study was to greater understand PEG10 expression in PCa and develop a method for detecting aggressive subtypes of PCa by exploiting the disease-specific expression of PEG10. The expression of PEG10 in PCa was previously only documented in NEPC (23). By analyzing PCa models and clinical specimens, we found that PEG10 is expressed in CRPC (cell lines, PDXs, microarray) in addition to AR-NEPC. Previous research hypothesized that PEG10 expression was strongly associated with the absence of AR [215]. We found a negative correlation between the expression of AR and PEG10 in the LuCaP PDX models and mCRPC patient microarray analysis. Analysis of the AR variant expressing cell lines proposes that AR splice variants may play a role in PEG10 expression. Our data gives a very preliminary introduction that there may be an association between AR variants and PEG10. Recent findings have shown that ONECUT2 acts as a suppressor of AR activity, a survival factor, and a driver of a NE differentiation in PCa. We explored the trends of PEG10, AR, and ONECUT2 expression by microarray analysis. Our analysis showed a negative correlation between AR and ONECUT2, a positive correlation between ONECUT2 and PEG10, and elevated ONECUT2 in NE^+ PCa. The data supports published findings that ONECUT2 indirectly regulates PEG10 through suppression of AR or directly regulates PEG10 by binding to its promoter [227, 228]. The

recent report results [227, 228] elucidated that PEG10 is a marker of NE differentiation that is present in highly lethal disease subtypes.

By harnessing the transcriptional specificity of the PEG10 promoter, we were able to develop a molecular genetic strategy for detecting CRPC by molecular imaging. Tissue-specific promoters are often weak when compared to constitutively active viral promoters such as CMV. In the past, TSTA has been used to improve the output of inherently weak tissue-specific promoters [186]. Based on our results, the PEG10 promoter by itself was not a weak promoter and can achieve strong PCa specific expression. Though the promoter is sufficient on its own, the A.TSTA element significantly improved signal in multiple *in vitro*. Although there were a few times when the A.TSTA did not add significant improvement, in the majority of the cell lines and assays, the A.TSTA did contribute to significant increase in gene transcription. We managed to optimize a stronger promoter than its intrinsic version without compromising specificity or toxicity, thus creating a powerful imaging tool that detects PCa for a greater duration of time compared to other reported promoter-guided imaging technologies in the literature [212, 213]. In this study, we used our optimized PEG10 promoter to drive the expression of reporter genes for optical and nuclear imaging (iRFP682 and HSV1-TK). Our PEG10 molecular imaging approach was sensitive enough to detect small bone lesions in the intratibial bone metastasis model of CRPC using the CWR-R1 cell line. The ability to detect bone lesions is significant because there is currently no reliable imaging agent available in the clinics to detect such tumors. The promoter could be used alone or with the A.TSTA enhancement. The A.TSTA showed variable enhancement, but since human tumors are heterogenous, we would not expect the construct to work equally across all cells. Overall, the PEG10

promoter shows promise of utility across a variety of different PCa models. To the best of our knowledge, no form of two step transcriptional amplification systems have be used in clinical trials, so for clinical translation the promoter alone would be the best candidate since we have shown it is sufficient for signal generation. In the future, this strategy can be employed for theranostic purposes by the expression of suicide genes such as cytosine deaminase and radioviral therapy using conditionally replicative viruses.

Most of the molecular genetic imaging studies reported in the literature relied on using Ad delivery of the reporter constructs rather than the systemic injection of a polymer-coated plasmid as in our study. Previously, the promoters of PCa-specific genes such as probasin [236] and PSA [237, 238] were used to drive tissue-specific expression of reporter genes by molecule genetic imaging. Studies using the PSA promoter also [237, 238] utilized the TSTA elements to enhance transcription within the adenovirus, similarly to our previous work on using the promoter of the metabolic protein a-methylacyl CoA racemase promoter to detect PCa *in vivo* [156]. Though recombinant viruses have been widely used as vectors for gene delivery, a number of issues exist when using viruses in this capacity including difficulty in production, poor reproducibility, immunogenicity, insertional mutagenesis into the human genome and poor bioavailability. The imaging technology that we developed in this study has potential for clinical translation. While the use of the PEG10 promoter for molecular imaging is novel, plasmid therapeutics in humans and the use of cationic reagents for plasmid delivery are not. The l-PEI reagent used in this study is under investigation in a clinical trial for plasmid delivery in France [124] and Israel [124]. Non-complexed DNA is also in clinical trials without a transfection reagent for the treatment of pancreatic [239] and ovarian cancers [129]. A plasmid CRPC vaccine applied by

intradermal injection in the United States has also done well in a clinical trial [131] and there are a number of PCa plasmid vaccines currently being investigated in clinical trials. Plasmid gene therapy has seen success in the cancer field and our PEG10-based technology has the potential for clinical development. We believe the limiting factor in plasmid-based agents is the delivery agents and delivery route. l-PEI is known to cause toxicity, and we observed some of that in our mice after systemic administration [240] but we were successful at decreasing toxicity by increasing the total volume of administration.

Our findings that PEG10 expression was present in AR- and AR splice variant PCa underscores the utility of PEG10 detection in disease management and drug development. Effective therapies do not exist for AR- and AR splice variant driven PCa. The ability to monitor patient response to therapy radiographically is critical to the development of new agents to combat these lethal forms of the disease. We have shown that the PEG10 promoter can be used as a detection tool in an expression vector. The promoter has transcriptional power alone or can be enhanced with A.TSTA, which may increase transcription. The molecular genetic detection of PCa using the PEG10 promoter by PET has the potential to be developed into an effective imaging tool. We acknowledge that this study is the first of its kind where the PEG10 promoter is applied as an imaging tool and that more investigation of PEG10's regulation by AR variants must be performed in order to further validate the hypothesis.

Materials and Methods

Immunohistochemistry

IHC was performed on formalin-fixed paraffin-embedded tissue sections using (1:500) rabbit anti- PEG10 (Novus NBP2-13749) and (1:100) rabbit anti-androgen receptor SP107 (Sigma). Unstained sections (4 μm) were de-paraffinized and rehydrated using standard methods. For antigen retrieval, slides were incubated in 6.0 pH buffer (Reveal Decloaking reagent, Biocare Medical) in a steamer for 30 min at 95–98°C, followed by a 20 min cool down period. A serum-free blocking solution (Sniper, Biocare Medical) was placed on sections for 30 min. Blocking solution was removed and slides were incubated in primary antibody diluted in 10% blocking solution/90% TBST. The antibody was used according to the manufacturer's protocol.

CHiP-Seq

CHiP-Seq data were obtained based on previous literature [220].

RNA-Seq

RNA-Seq FPKM values in **Figure 3-2B** were obtained using the methods described in [219].

Tissue Microarrays

PEG10 IHC analysis was performed on a 120 Case High Grade Race Disparity tissue microarray (TMA) constructed from African American and Caucasian patients and on a LuCaP patient-derived xenograft tissue TMA acquired from the Prostate Cancer

Biorepository Network (PCBN). The liver biopsy analyzed for PEG10 staining was acquired using a University of Minnesota Human Subjects Division approved IRB protocol for tissue acquisition (IRB#1604M86269) and with patient consent.

DNA Microarray

Expression values in **Figure 3-4C** were obtained using the publicly available expression profiling by array GSE41784. Microarray data was extracted from previously published studies of a set of metastatic tumors from men with castration resistant prostate cancer (**Figure 3-5**) [226] and patient-derived xenograft (PDX) models of prostate cancer (**Figure 3-6**) [241]. Both datasets are available in the Gene Expression Omnibus under accessions GSE77930 and GSE93809.

Cell Lines

Prostate cancer cell lines 22Rv1, DU145, PC3, LNCaP were obtained from the American Type Culture Collection (ATCC) and were maintained according to ATCC guidelines. MR42D cells were a gift from Dr. Amina Zoubeidi (Vancouver Prostate Center) and maintained with 10uM enzalutamide. CWR-R1 cells were a gift from Dr. Scott Dehm (University of Minnesota). HT-29 cells were a gift from Dr. Hiroshi Hiasa (University of Minnesota). All cell lines were verified by short-tandem repeat analysis and analyzed for mycoplasma contamination prior to our studies.

R1881 Treatment of CWR-R1 and LNCaP Cells

10^6 cells per well were plated in 6-well plates in full growth media and incubated overnight. Media was then changed to 10% CSS-DMEM and cells were incubated for 24 hours. Control cells were kept in FBS. Cells were then treated with the following: Control: Full growth (FBS) media/DMSO, CSS: 10% CSS media/DMSO, CSS+R1881: 10% CSS Media/ 10 nM R1881 in DMSO. Cells were incubated for 24 hours and the same treatment was re-applied after 24 hours. The total incubation in R1881 was 48 hours after which cells were collected for RNA extraction.

Quantitative RT-QPCR

RNA was extracted from 10^6 cells with a RNeasy kit (Qiagen). RNA was converted to cDNA using the High Capacity RNA to cDNA kit (Applied Biosystems). Taqman RT-PCR was performed using the Taqman Universal PCR Master Mix (Applied Biosystems) and the following Taqman Gene Expression probes: PEG10; Hs00248288_s1, 18S5 ribosomal RNA; Hs03928985 for a normalization control, and a custom HSV1-TK probe (**Figure 3-17B**) [242]. Taqman probe in the supplemental was PEG10; Hs01122880. qPCR was performed on a StepOnePlus Real-Time PCR system instrument (Applied Biosystems). Data was analyzed using the comparative Ct method (fold change = $2^{-\Delta\Delta Ct}$) [243].

Plasmids

A pGL3 Basic vector (Promega, E1751) was used as the backbone for all of the cloning. Primers for the full length PEG10 promoter cloning from PBMC cDNA and truncated 1KB promoter were based on previous literature (**Table 3-1**) [229]. MluI and

XhoI were the cut sites used for the promoter insertion. The conventional single construct two-step transcriptional amplification was designed according to previous literature and synthesized by Genscript[173, 186, 244]. The TSTA element was designed head-to-tail or "unidirectional". The system can be used head-to-head or head-to-tail (bidirectional) according to patent US7527942B2. Both orientations have been tested in literature. Our GAL4-VP16 fusion protein consisted of GAL4 amino acids 1-147 and two consecutive VP16 domains, amino acids 413-456. Some literature uses VP16 amino acids 413-454. We used amino acids 413-456 based on literature that states that single most crucial aspect VP16 is located between residues 429 and 456[244]. A linker was used to fuse the two proteins (PEFLQPGGS). A pause site of 33 base pairs was placed downstream of the consecutive GAL4-VP16(x2) sequences [245] (no linker was used between the consecutive VP16 sequences) followed by five GAL4 DNA binding sites (cggagtactgtcctccg) each separated by two base pairs (ag) [246]. An adenovirus minimal promoter was placed 16 bp after the last GAL4 binding site (23 bp from GAL4 binding site to TATA box). The advanced two-step transcriptional amplification system was designed according to previous literature and synthesized by Genscript [173]. Our A. TSTA is identical to our TSTA other than the addition of polyglutamines and rat glucocorticoid receptor protein between the GAL4 binding domain and VP16 sequences. A map of the PEG10 1KB promoter with the A.TSTA can be found in **Figure 3-20.** BglII and HindIII were used as the insert cut sites for the TSTA elements. To the best of our knowledge, this particular system may be unique due to our approach of combining the polyglutamines and rat glucocorticoid receptor and using two VP16 domains rather than one VP16 domain like in the original advanced TSTA.

For fluorescence studies, the firefly luciferase encoding gene in pGL3 basic was replaced with a near-infrared protein 682 (*iRFP682*). piRFP682-N1 was a gift from Vladislav Verkhusha (Addgene plasmid # 45459). For *in vivo* PET studies, the Luc gene was replaced with HSV1-TK (cloned from pLV-SFFV-HSVTK, Imanis Life Sciences, DNA1052). Correct insertion of DNA fragments was verified by Sanger sequencing and gel restriction analysis.

Luciferase Assays

On day 1, cells were plated in 96 well plates (10^4 cell/ well). On day 2, cells were transfected with 90 ng of experimental plasmid DNA and 9 ng of control pRL-TK per well with 0.24µl GeneJuice (Millipore). 72 hours post-transfection (or day 5), cells were lysed using the passive lysis buffer from Promega. Luciferase activity was quantified using the Dual-Luciferase Reporter Assay System (Promega). Each experimental firefly luciferase output (LUC) was normalized to its respective renilla luciferase (REN) control output. Relative luciferase units (RLU) are LUC/REN.

***In vitro* iRFP Imaging**

On day 1, 10^4 cells were plated in a 96 well plate. On day 2, cells were transfected with plasmids containing the iRPF682 gene. 90 ng of DNA and 0.24µl of GeneJuice (Millipore) were used for the transfection. Cells were incubated for 72 hours and visualized on the Odyssey Infrared imaging system (LI-COR) using the 700nm channel.

Xenograft Models

3-4 week old hsd:athymic mice were purchased from Envigo. For each mouse, 10^6 CWR-R1 or HT-29 cells were suspended in 200µl of a 1:1 mixture of Matrigel (Corning) and 1X PBS. The cells were implanted s.c. into the flanks of the mice using a 25 gauge needle. The tumors were allowed to grow until visible with the naked eye to start imaging experiments.

CWR-R1 Intratibial Model

3-4 week old hsd:athymic mice were purchased from Envigo. $2.5x10^5$ of CWR-R1 cells in 1X PBS were injected into the tibia of one leg. Tumors were allowed to form for three weeks before near-infrared imaging. The same tumors were used for PET imaging 5 weeks post intratibial injections.

Systemic In-Vivo DNA Delivery

Plasmid DNA was prepared with EndoFree Plasmid Kit (Qiagen). Endotoxin level was ensured as <0.1EU/ug DNA. For the delivery of the plasmids in-vivo, low molecular weight l-PEI-based cationic polymer, in vivo-jetPEI™ (Polyplus-transfection) was used as gene delivery reagent for tail vein IV administration. A ratio of 6 was used for nitrogen to phosphate (N/P=6) was used for all injections. 40 ug of plasmid DNA and 4.8µl of 150 mM in vivo-jet PEI™ were combined according to the manufacturer's instructions to form the DNA polyplex in a total volume of 400µl for each mouse. Acute toxicity was observed initially when 200µl was used as the final volume for each systemic tail vein injection. Increasing the volume to 400µl decreased the acute toxicity (only 1 mouse was found with

acute toxicity out of all of the experiments presented in this work). Plasmid DNA/PEI complex was delivered using a 26 gauge needle.

In-Vivo Fluorescence Imaging

Mice were imaged with the IVIS Spectrum (Caliper/Xenogen) at the University of Minnesota – University Imaging Center. Mice were placed on special low fluorescence diet, TC.97184 (Envigo). For each imaging session, mice were under a 2.0% isoflurane/oxygen mixture. For the filters, 675nm/720nm were used. Living Image 4.5 software was used for image acquisition and analysis. For ROI analysis, a circle of the same size was used on all mice and placed in regions of high fluorescence in each tumor.

PET-CT imaging and data analysis

For subcutaneous CWR-R1 model: On day 1, mice were injected with the plasmid/PEI complexes (40 ug DNA). 72 hours post DNA delivery, ^{124}I-FIAU (purchased from 3D imaging, Arkansas) was injected into the mice via IV (150 uCi per animal). For intratibial CWR-R1 model: On day 1, mice were injected with the plasmid/PEI complexes. 48 hours post DNA delivery, ^{124}I-FIAU (purchased from 3D imaging, Arkansas) was injected into the mice via IV (250 uCi per animal). 24 hours post isotope injection, the animals were imaged using Siemens Inveon microPET/CT at the University of Minnesota – University Imaging Center. Acquisition time was 40 minutes. Animals were kept under 2% isoflurane/oxygen mixture throughout the duration of the scan. For the 2D image analysis, Inveon Research Software was used. AMIRA was used for 3D reconstruction.

Statistical Analysis

Data analysis was performed on GraphPad Prism 7 (GraphPad Software Inc.). qPCR results were analyzed in Excel. Statistical significance was determined using the unpaired two-tailed Student's t-test, unpaired two-tailed Welch's t-test where the variances are shown to be different via F-test, one-way ANOVA, or two-way ANOVA. Only two-tailed tests were used. Results are depicted as mean+SEM unless stated otherwise. All p values of <0.05, <0.01, <0.001, and <0.0001were considered significant. Pearson's correlation coefficient was used to determine correlation between genes (Pearson's rho). The symbols used to represent the p values were : ns ($p>0.05$), * ($p\leq0.05$), **($p\leq0.01$), ***($p\leq0.001$), ****($p\leq0.0001$). The test used in each statistical analysis is specified in the figure legend.

Figures

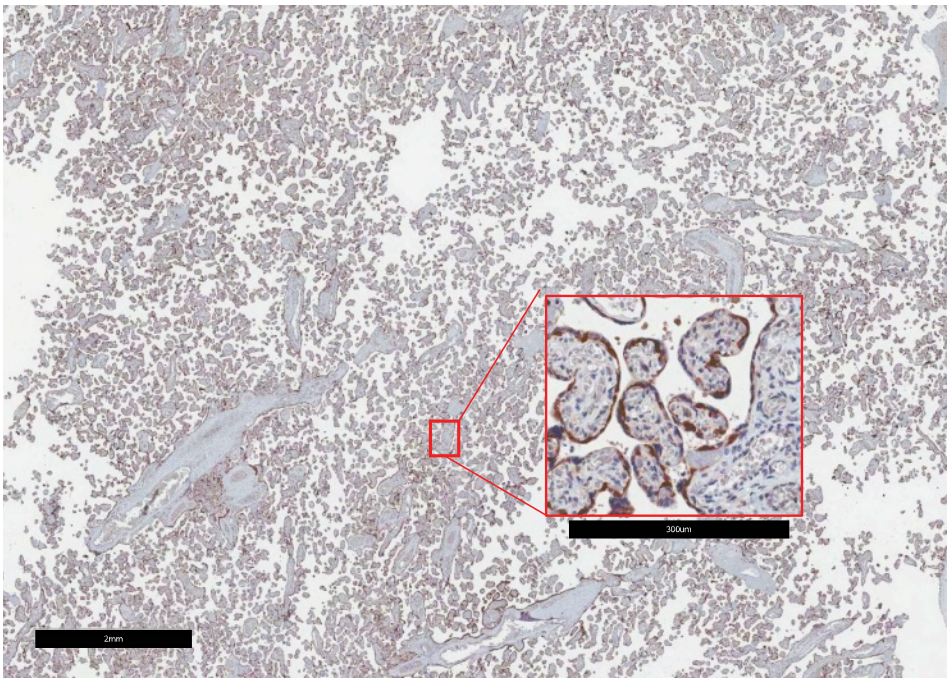

Figure 3-1. PEG10 staining in human placenta.

Positive control for PEG10 expression. The placenta is the known to be abundant in PEG10 expression.

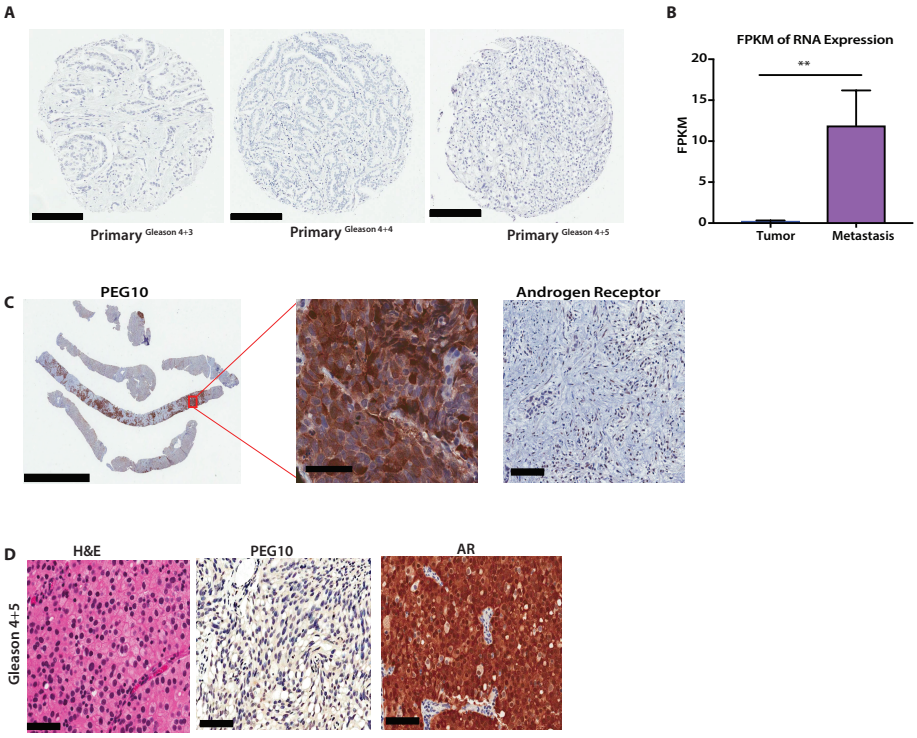

Figure 3-2. PEG10 expression in primary PCa tumors versus metastasis.

(**A**) IHC staining for PEG10 in primary PCa tumors graded Gleason 4+3, 4+4, and 4+5. Scale bars represent 200µm. (**B**) RNA-seq analysis of PEG10 expression in primary tumor versus metastasis. Multiple raw FASTQ RNA-seq datasets were obtained via DbGAP and aligned and transcripts quantified via a uniform pipeline, enabling cross-experimental comparisons. Data is reported as FPKM. Significance was determined by unpaired two-tailed Welch's t-test after a significant F-test and Grubb's outlier test were used in (**C**) PEG10 IHC staining in a case study of a patient with AR^- liver metastasis. Scale bars represent 4 mm, 60µm, and 100µm left to right. (**D**) IHC staining of PEG10 in a case study of patient with AR^+ adenocarcinoma graded Gleason 4+5. Scale bars represent 60µm. (** $p<0.01$). Results are expressed in mean+standard error of the mean (SEM). (**** $p<0.0001$; *** $p<0.001$; ** $p<0.01$; * $p<0.05$, n.s. = not significant).

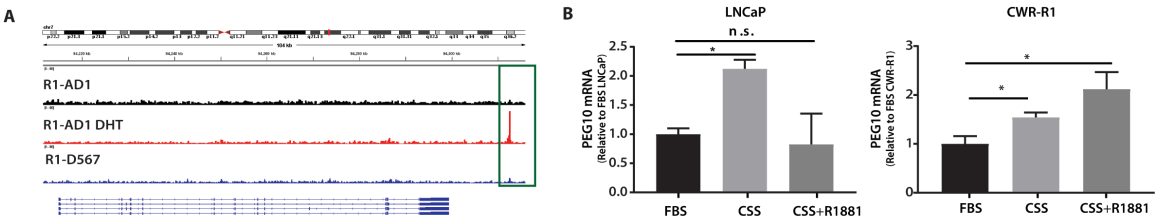

Figure 3-3. AR variants interact with PEG10.

(**A**) CHiP-seq analysis of the AR binding to PEG10. All cells were pretreated with CSS. The full-length AR-expressing R1-AD1 cells were treated with DHT for AR activation and AR variant-expressing R1-567 cells were treated with vehicle. (**B**) PEG10 expression in LNCaP and CWR-R1 cells after treatment with CSS or CSS+R1881. The PEG10 expression for each cell line was normalized relative to their corresponding FBS controls. Significance was determined by two-tailed Student's t-test (n=3). (**** $p<0.0001$; *** $p<0.001$; ** $p<0.01$; * $p<0.05$, n.s. = not significant). Results in (B) are expressed in mean+standard error of the mean (SEM).

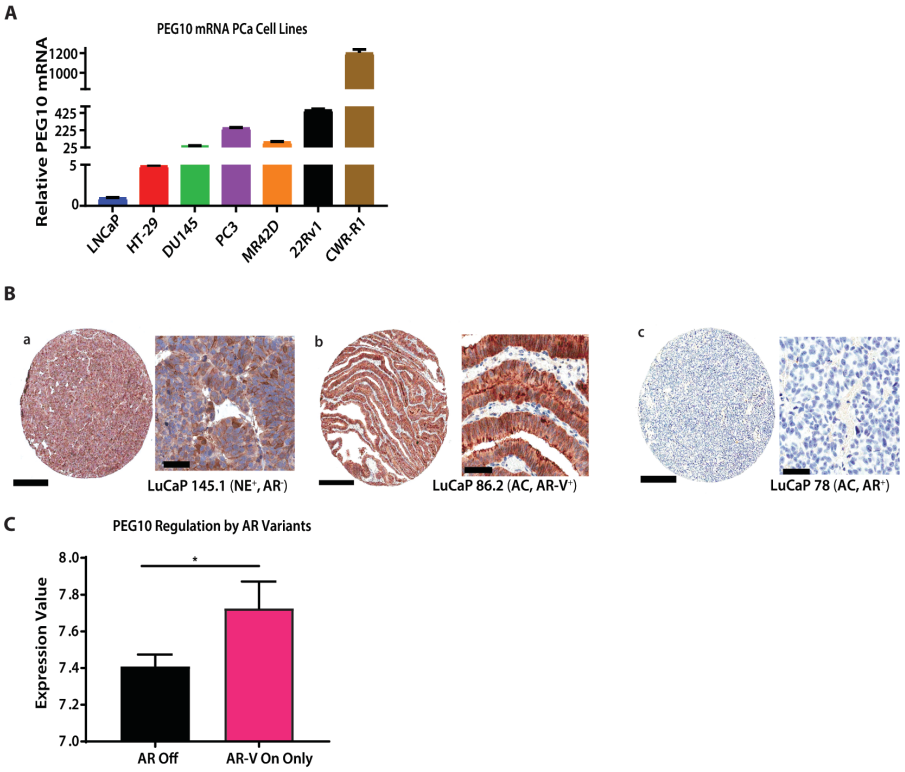

Figure 3-4. PEG10 is elevated in the presence of AR variants.

(**A**) PEG10 mRNA in PCa cell lines expressed relative to housekeeping gene 18S5. (**B**) PEG10 staining in LuCaP PCa PDXs where (**Ba**) is LuCaP 145.1, a model of NE^+, AR^- PCa, (**Bb**) is LuCaP 86.2, an adenocarcinoma (AC) PCa model, $AR\text{-}V7^+$, and (**Dc**) LuCaP 78, an AC model with only wild-type AR expression. Scale bars represent 300µm in full image and 60µm in magnified (**C**) AR regulation of PEG10 expression in R1-AD1 cells. PEG10 expression levels are represented as an expression value of RNA analyzed by Illumina Beadchips. AR-Off cells were treated with siRNA targeting AR exon 1. AR-V On Only cells were treated with siRNA targeting AR exon 7. Significance was determined using the unpaired two-tailed Student's t-test (n=3). (**** $p<0.0001$; *** $p<0.001$; ** $p<0.01$; * $p<0.05$, n.s. = not significant). Results in (C) are expressed in mean+standard error of the mean (SEM).

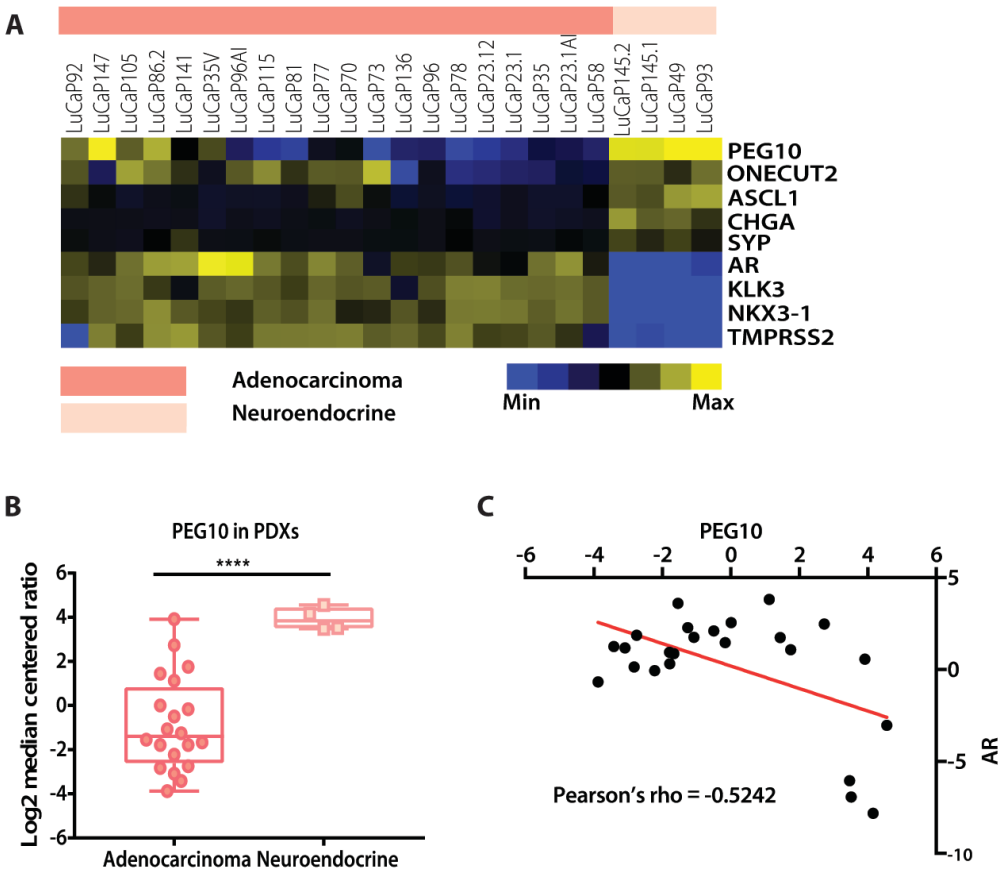

Figure 3-5. PEG10 analysis of LuCaP patient derived xenografts.

(**A**) PEG10 and ONECUT2 expression represented in a microarray heatmap of early passage LuCaP PDXs microarray. The samples are sorted by the adenocarcinoma or NE status. (**B**) Microarray PEG10 expression represented as log2 median centered ratio in adenocarcinoma and NE PDXs presented microarray (A). Significance was determined using Welch's unpaired- t-test after using an F-test and Grubb's test. (**C**) Negative correlation of PEG10 and AR in LuCaP microarray in (A). Pearson's correlation test, p=0.0085. Colored red line represents linear regression. (**** p<0.0001; *** p<0.001; ** p<0.01; * p<0.05, n.s. = not significant). Results in (B) are expressed minimum to maximum with all points shown.

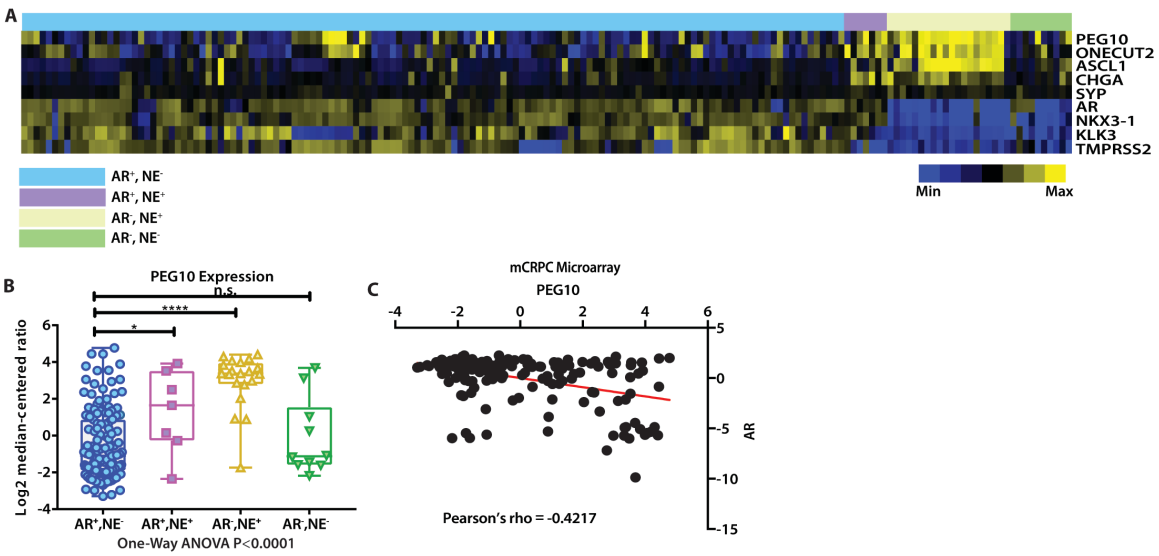

Figure 3-6. PEG10 analysis of patient microarray.

(**A**) Negative correlation of PEG10 and AR in LuCaP microarray in (F). Pearson's correlation test, p=0.0085. Colored red line represents linear regression. (**I**) PEG10 and ONECUT2 expression represented in a CRPC microarray (n=171 tumors from 63 men). Samples are sorted by the AR and NE status. (**B**) PEG10 expression represented as log2 median centered ratio in patient tumor samples represented in microarray (A) sorted by the AR and NE status. Significance was determined by one-way ANOVA with Dunnett's post-test. (**C**) Negative correlation between PEG10 and AR in CRPC microarray. Pearson's correlation test, p<0.0001. Colored red line represents linear regression. (**** p<0.0001; *** p<0.001; ** p<0.01; * p<0.05, n.s. = not significant). Results in (B) are expressed minimum to maximum with all points shown.

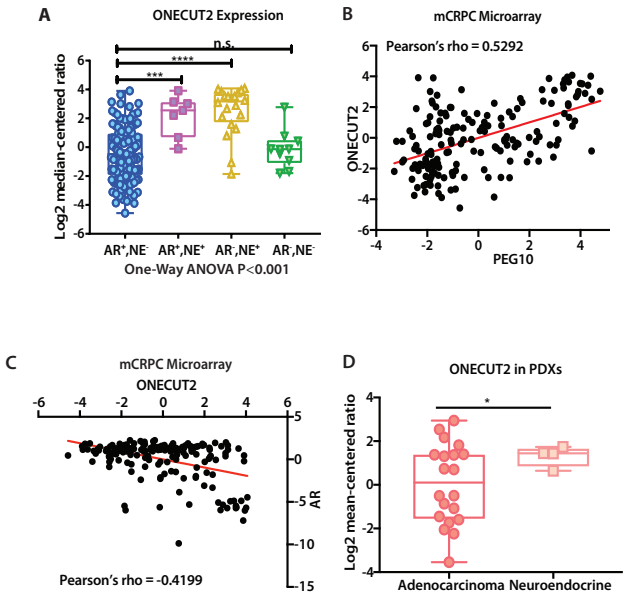

Figure 3-7. ONECUT2 correlates with PEG10 expression patterns.

(**A**) ONECUT2 expression represented as log2 median centered ratio in the CRPC microarray (heat map represented in **Figure 3-6A**) sorted by AR and NE status. Significance was determined by one-way ANOVA with Dunnett's post-test (**B**) Positive correlation between PEG10 and ONECUT2 in patient microarray (**Figure 3-6**). Pearson's correlation test, P<0.0001. (**C**) Negative correlation between ONECUT2 and AR in mCRPC microarray (**Figure 3-6**). Pearson's correlation test, P<0.0001. Colored blue line represents linear regression. (**D**) ONECUT2 expression represented as log2 median centered ratio in adenocarcinoma and NE PDXs presented microarray (**Figure 3-5**). Significance was determined using Welch's unpaired- t-test after using an F-test and Grubb's test Colored red line represents linear regression. Significance in A was determined using the unpaired two-tailed (**** p<0.0001; *** p<0.001; ** p<0.01; * p<0.05, n.s. = not significant). Results in (A,D) are expressed minimum to maximum with all points shown.

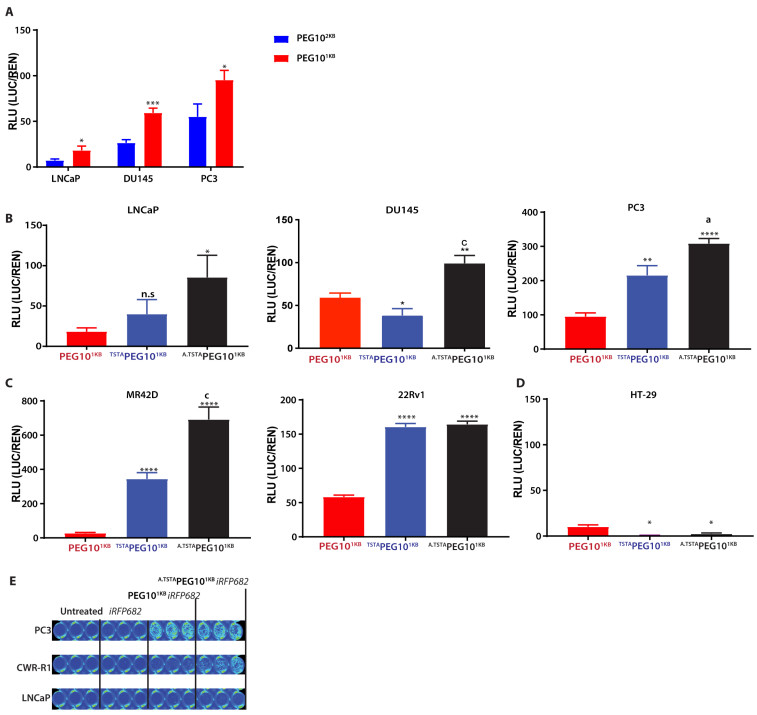

Figure 3-8. Transcriptional analysis of the PEG10 promoter.

(**A**) Luciferase activity in relative luciferase units (RLU) of the full length PEG10 promoter ($PEG10^{2KB}$) and the truncated 1KB promoter ($PEG10^{1KB}$) in LNCaP, DU145 and PC3. (**B**) Comparison of the luciferase activity of $PEG10^{1KB}$ promoter with $^{TSTA}PEG10^{1KB}$ and $^{A.TSTA}PEG10^{1KB}$ in LNCaP, DU145, PC3. (**C**) Comparison of the luciferase activity of $PEG10^{1KB}$ promoter with $^{TSTA}PEG10^{1KB}$ and $^{A.TSTA}PEG10^{1KB}$ in CRPC cell lines MR42D and 22Rv1. (**E**) Near-infrared detection of the iRFP682 in cells transfected with various constructs. *iRFP682* is a construct with no promoter. Significance was determined using the unpaired two-tailed Student's t-test (**** $p<0.0001$; *** $p<0.001$; ** $p<0.01$; * $p<0.05$, n.s. = not significant were used to indicate significance between $PEG10^{2KB}$ and $PEG10^{1KB}$, $PEG10^{1KB}$ and $^{TSTA}PEG10^{1KB}$, $PEG10^{1KB}$ and $^{A.TSTA}PEG10^{1KB}$. **a** $p<0.05$ and **c** $p<0.001$ were used to represent significance comparing $^{TSTA}PEG10^{1KB}$ and $^{A.TSTA}PEG10^{1KB}$). Results are expressed in mean+ SEM.

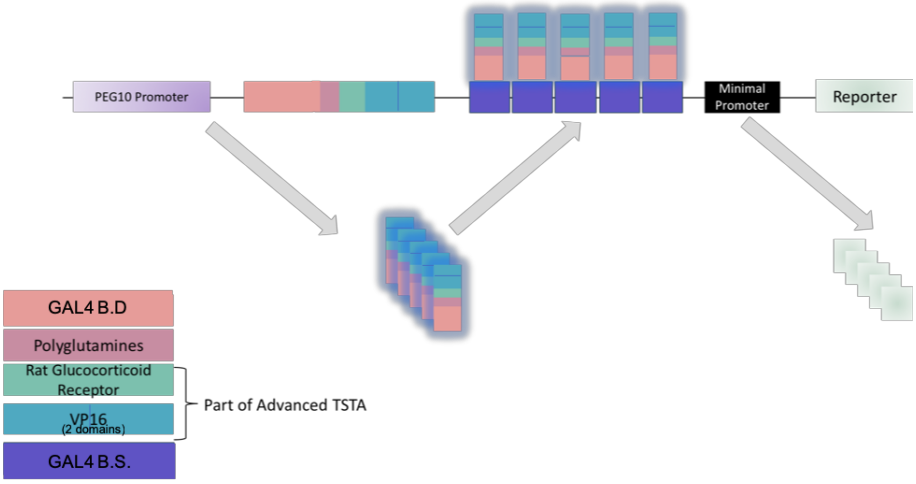

Figure 3-9. TSTA Schematic.

The PEG10 promoter drives the expression of a fusion protein. In conventional TSTA the fusion protein consists of GAL4 binding domain (B.D.) and VP16. The advanced TSTA has the added element of polyglutamines and rat glucocorticoid receptor. The fusion protein is then transcribed and translated after which it binds to the the GAL4 DNA binding sites (B.S.), upstream of a minimal promoter, resulting in the transcription of the gene.

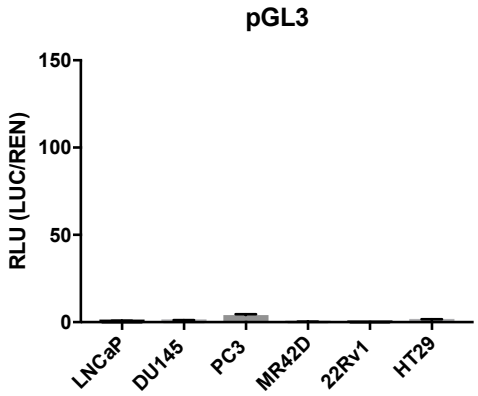

Figure 3-10. Luciferase expression in empty pGL3 vector.

Luciferase expression in cells treated with an empty pGL3 vector was low (no promoter).

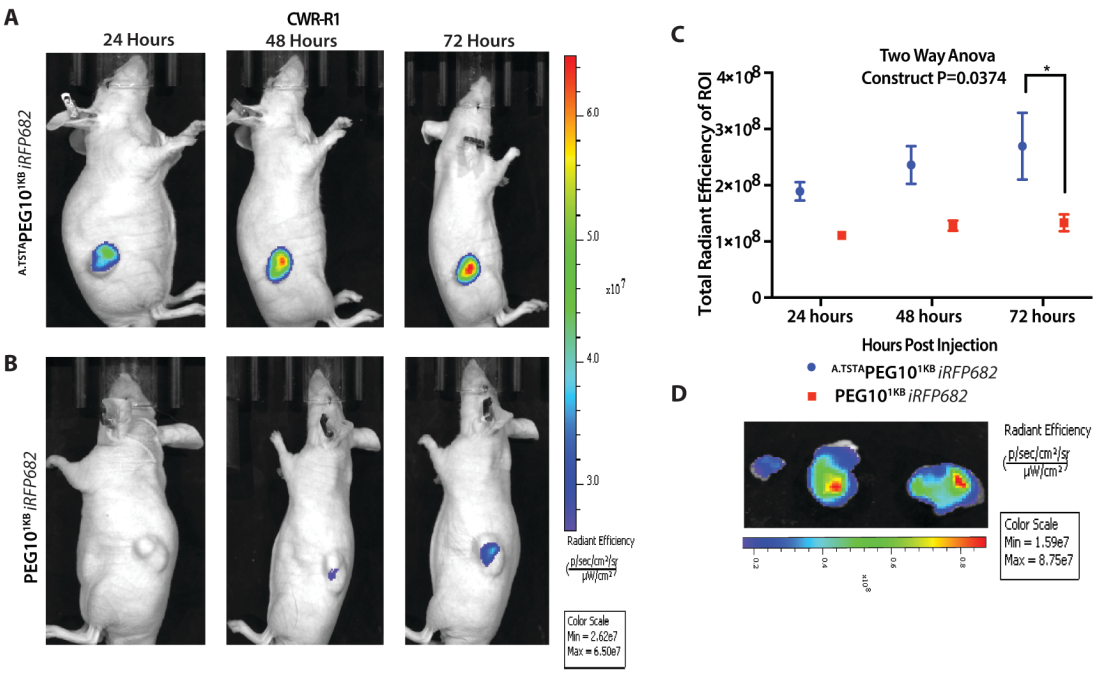

Figure 3-11. ***In vivo*** **near-infrared fluorescence molecular imaging with PEG10 promoter guided expression of iRFP682 in subcutaneous CWR-R1 model.**

Representative images of mice with CWR-R1 s.c. xenografts injected with (**A**) $^{A.TSTA}$PEG10^{1KB} *iRFP682* (n=3) and (**B**) PEG10^{1KB} *iRFP682* (n=4) across different time points post injection. (**C**) Region of interest (ROI) signal presented in mean ± SEM. Significance was determined using by matching two-way ANOVA (construct p=0.0374) with Bonferroni's post-test (* $p<0.05$). (**D**) Tumors excised from mice injected with $^{A.TSTA}$PEG10^{1KB} *iRFP682* 72 hours post intravenous administration (n = 3).

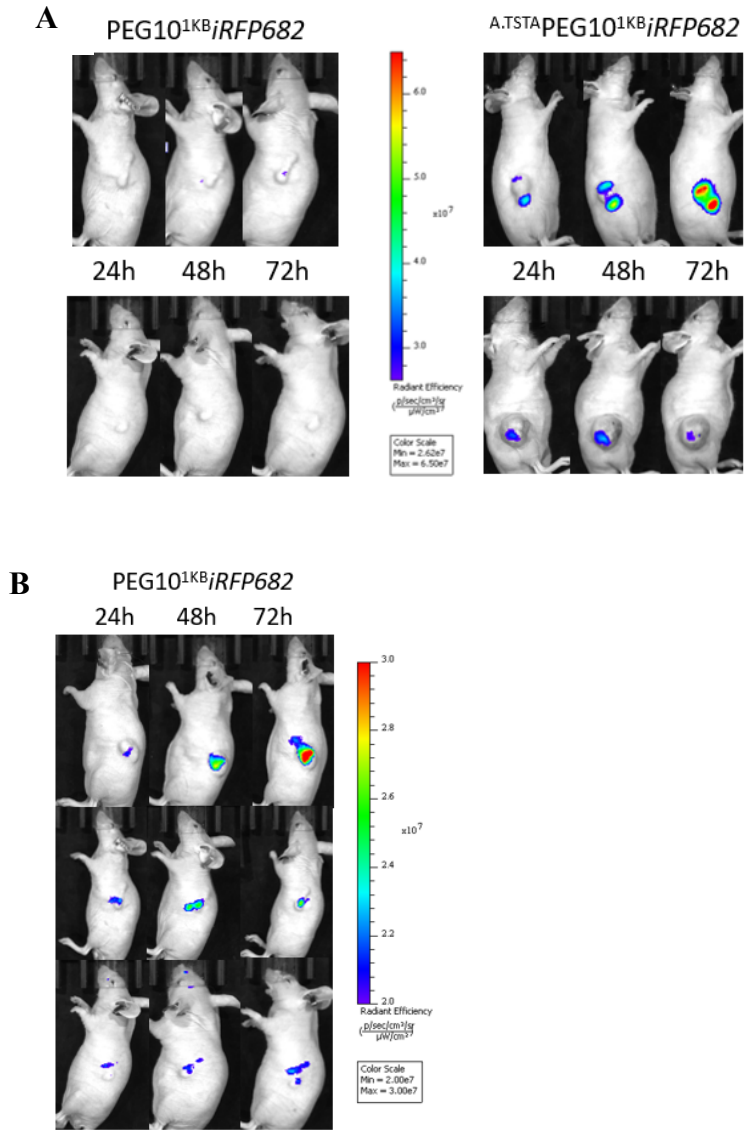

Figure 3-12. Near-infrared imaging with PEG10^{1KB} and *iRFP682*. $^{A.TSTA}$PEG10^{1KB} *iRFP682* with different normalization.

(A) Mice from **Figure 3-11**. (B) Mice injected with PEG10^{1KB} *iRFP682* from **Figure 3-11A** and **Figure 3-11B** using lower minimum and maximum values for the radiant efficiency.

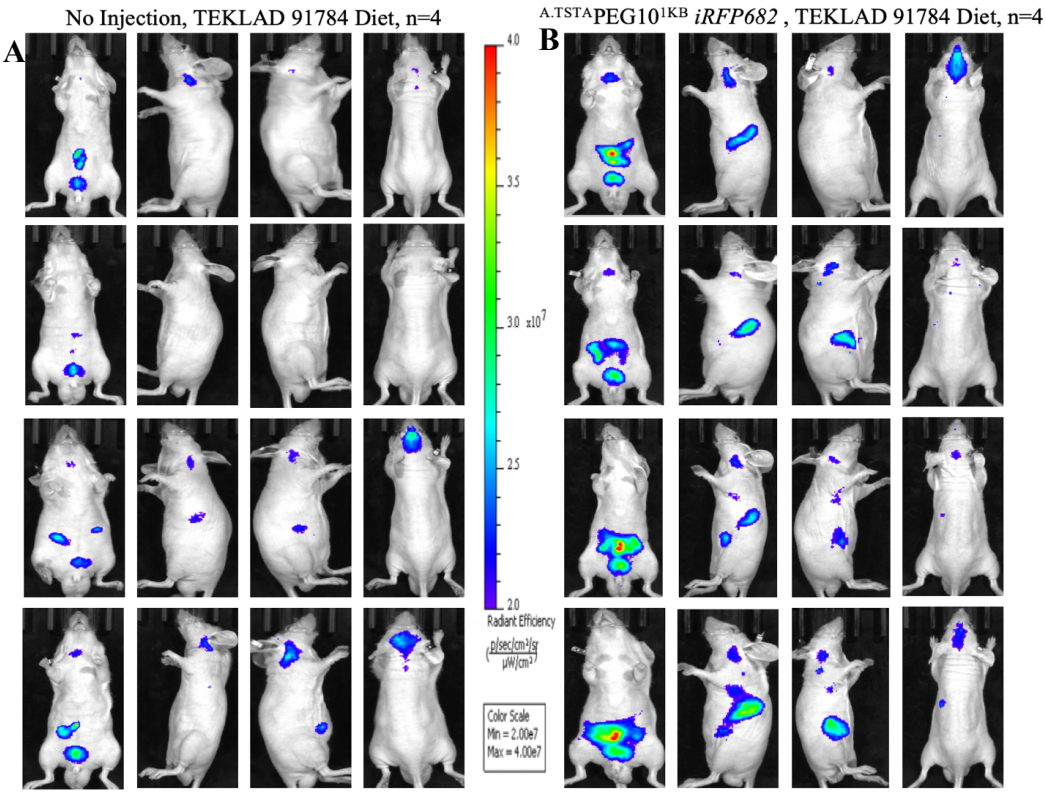

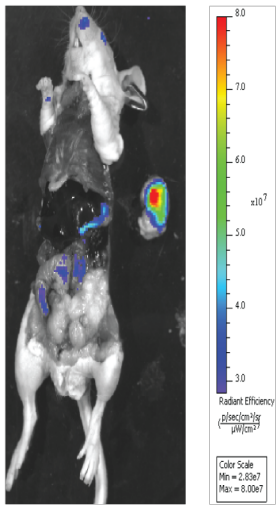

Figure 3-13. Negative *in vivo* controls for near-infrared imaging.

(A) Control mice not injected with anything on a TEKLAD 91784 diet. A variability in background signal in the gut, stomach, bladder, throat region, and skull region. (B) A tumorless mouse injected with $^{A.TSTA}PEG10^{1KB}$ *iRFP682*. An increase in signal can be seen in the stomach and gut area. (C) A representative image (n=3) of a mouse with a CWR-R1 tumor injected with $^{A.TSTA}PEG10^{1KB}$ *iRFP682.* and cut open 96 hours post intravenous injection of the DNA. There is slight fluorescence in the stomach and gut.

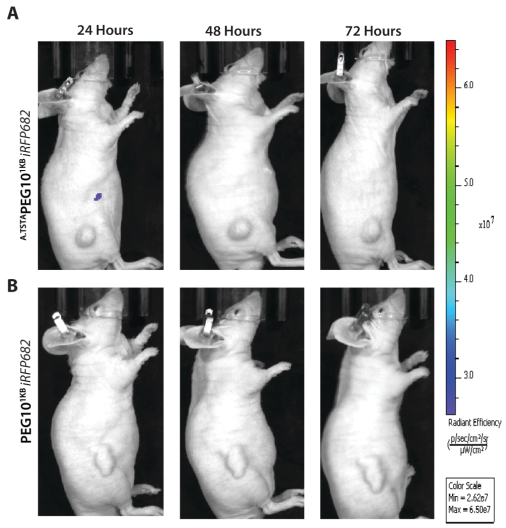

Figure 3-14. *In vivo* near-infrared fluorescence molecular imaging with PEG10 promoter guided expression of iRFP682 in negative control HT-29 subcutaneous xenografts.

Representative images of mice with HT-29 s.c. xenografts injected with (**A**) $^{A.TSTA}$PEG10^{1KB} *iRFP682* (n=4) and (**B**) PEG10^{1KB} *iRFP682* (n=4) across different time points post injection.

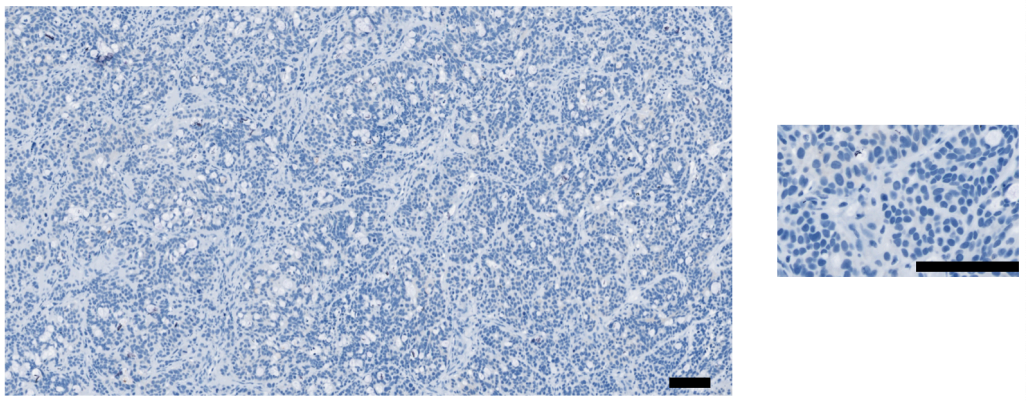

Figure 3-15. PEG10 expression by IHC in HT-29 xenografts.

Representative image of HT-29 xenografts (n=4) stained for PEG10 by IHC. Size bars represent 100um.

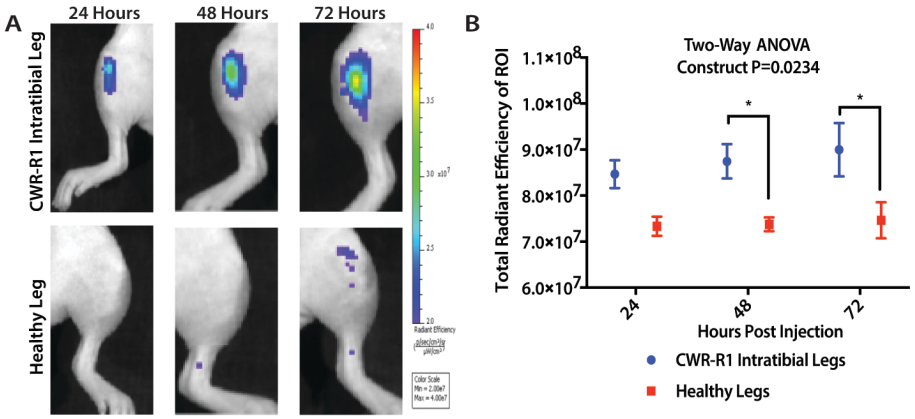

Figure 3-16. *In vivo* near-infrared fluorescence molecular imaging with PEG10 promoter guided expression of iRFP682 in CWR-R1 intratibial model.

(**A**) Representative image of mice with intratibial tumors in one of the tibia injected with $^{A.TSTA}PEG10^{1KB}$ (n=4) across different time points post injection. (**B**) Region of interest (ROI) signal presented in mean ± SEM of the SWR-R1 intratibial legs and healthy legs. Significance was determined using by matching two-way ANOVA (construct p=0.0234) with Bonferroni's post-test (* $p<0.05$).

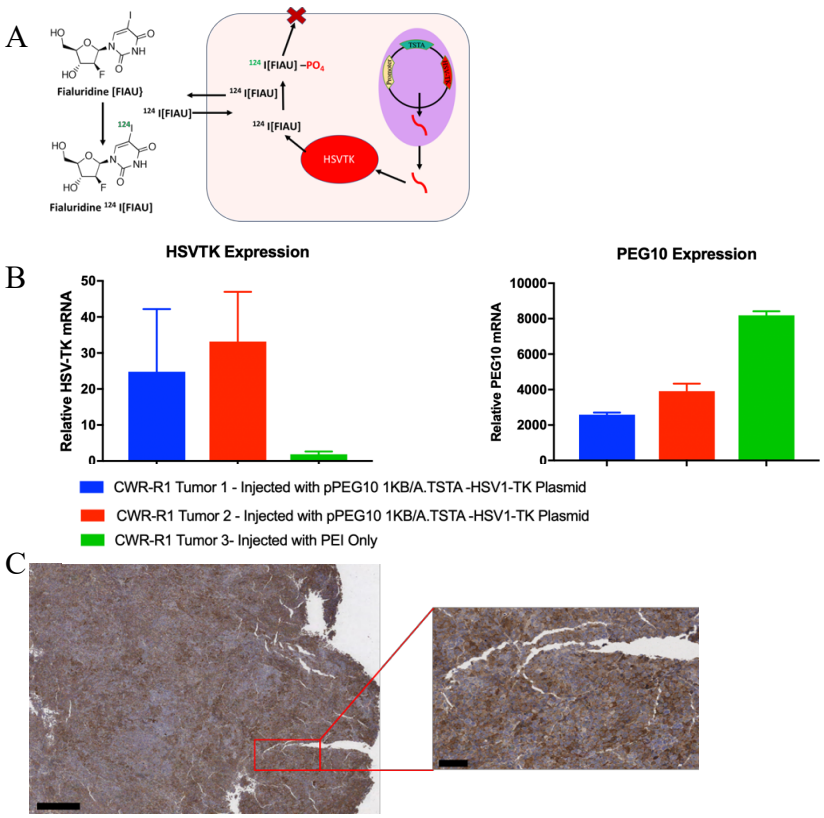

Figure 3-17. HSV-TK and PEG10 expression in CWR-R1 tumors.

(A) Schematic of ^{124}I[FIAU] entrapment. (B) *HSV-TK* expression was analyzed in tumors of 2 mice that were injected with $^{A.TSTA}$PEG10^{1KB} *HSV-TK* and in a tumor of a negative control mouse that was injected in vivo-jetPEI only. HSV1-TK Taqman Gene expression samples were custom made based on previous literature. PEG10 expression in the corresponding tumors was also analyzed. Three pieces of tumor from each mouse were used for mRNA extraction and run in three technical replicates. Statistical analysis was not performed because n=3 mice were not used. Variability was seen in HV1-TK expression between tumor pieces. We hypothesis this to be due to the amount of stromal tissue found in the different pieces. (C) Expression of PEG10 protein in CWR-R1 xenografts was confirmed using immunohistochemistry (n=2). The size bar in the image on the left is 582 um, the size bar on the right is 96um.

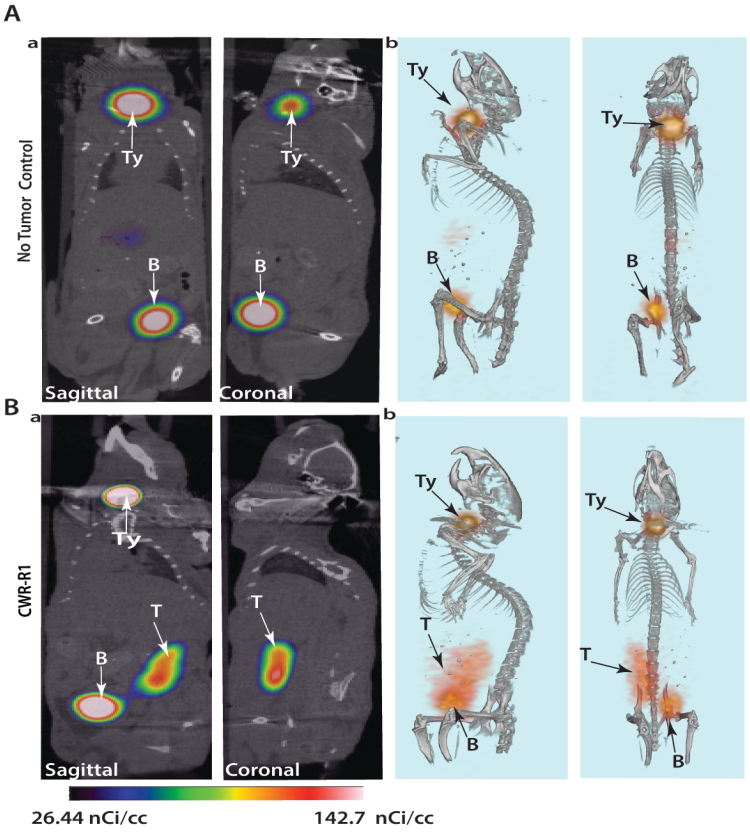

Figure 3-18. ***In vivo*** **PET/CT imaging with PEG10 promoter guided expression of HSV1-TK of subcutaneous CWR-R1 model.**

(**A**) Control tumor-less mice injected with $^{A.TSTA}$PEG10^{1KB} *HSV1-TK* and imaged 24 hours post injection with ^{124}I-FIAU (n=3) where (**Aa**) Representative 2D images and (**Ab**) Representative 3D images. (**B**) Mice with CWR-R1 subcutaneous tumors injected with $^{A.TSTA}$PEG10^{1KB} *HSV1-TK* (n=3) and imaged 24 hours post injection with ^{124}I-FIAU where (**Ba**) Representative 2D images and (**Bb**) Representative 3D images. Ty= thyroid, B= bladder, T= tumor.

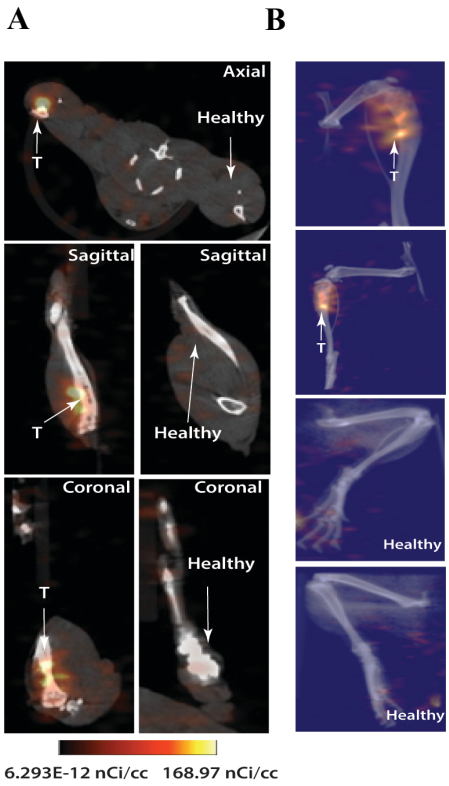

Figure 3-19. ***In vivo*** **PET/CT imaging with PEG10 promoter guided expression of HSV1-TK of intratibial CWR-R1 model.**

Intratibial CWR-R1 mice injected with $^{A.TSTA}$PEG10^{1KB} *HSV1-TK* (n=3) and imaged 24 hours post injection with ^{124}I-FIAU where (**A**) are representative 2D images and (**B**) are representative 3D images. T= tumor.

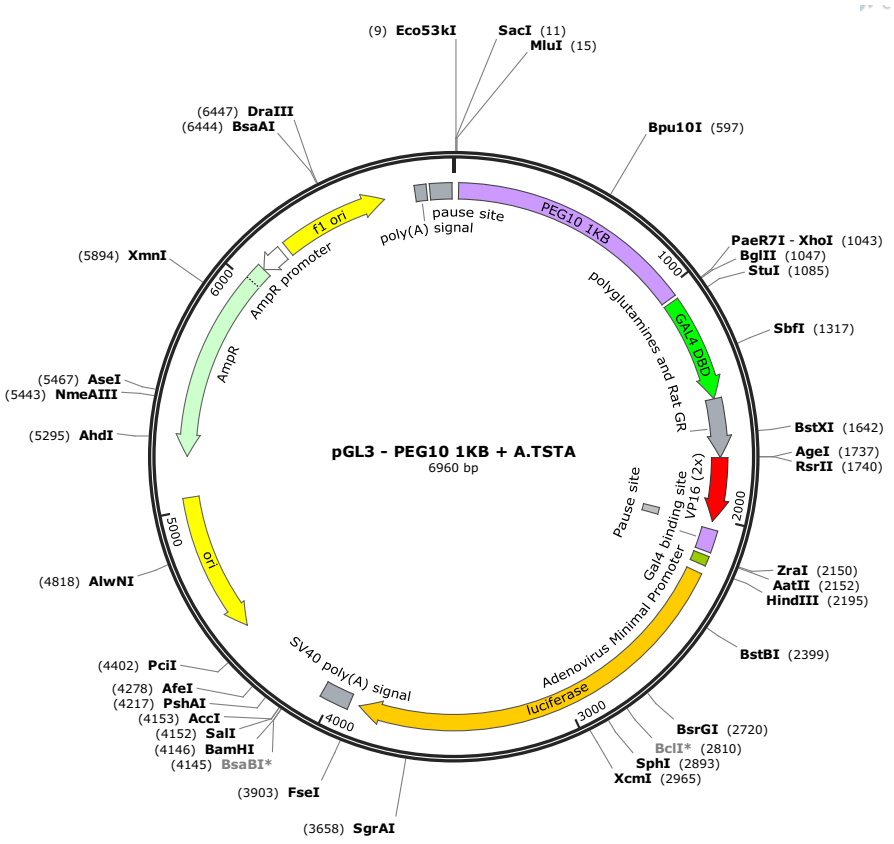

Figure 3-20. Plasmid map of $^{A.TSTA}PEG10^{1KB}$ in pGL3-Basic.

The A.TSTA consists of: PEG10 promoter, a fusion protein (GAL4, polyglutamines, rat glucocorticoid receptor, two consecutive VP16 activation domains), a pause site, five GAL4 DNA binding sites, and an adenovirus minimal promoter upstream of the luciferase reporter gene.

Table 3-1. Primers for PEG10 promoter cloning.

Reverse Primer (XhoI)	5'- ACGTGCTCGAG**CCGAAGTTGAAGCGCGTGT**-3′
Full Length ~2KB Forward Primer (MluI)	5'-TCGAACGCGT**AATTTGACAGCGGTCACCAG**-3'
~1KB Promoter Forward Primer (MluI)	5'-TCGAACGCGT**TCTGGCCTCCAGCCGG** -3'

Primers were based on previous literature [229]. The target sequence was between -1941 and +19 positions based on their transcription start site results. The same reverse primer was used for both promoters. The truncation happened at the 5' end of the promoter. The lengths of the promoters are rounded. The cut sites are underlined and the promoter sequences are bolded.

Bibliography

1. Prevention, C.f.D.C.a. *Prostate Cancer Statistics*. 2018 June 10th, 2019]; Available from: https://www.cdc.gov/cancer/prostate/statistics/index.htm.
2. Society, A.C. Facts and Figures 2019, American Cancer Society: Atlanta, GA.
3. Eggener, S.E., A.S. Cifu, and C. Nabhan, *Prostate Cancer Screening.* JAMA, 2015. **314**(8): p. 825-6.
4. Publishing, H.H. *PSA: Prostate-Specific Antigen, Persisting Scientific Ambiguities*. 2009 June 10, 2019]; Available from: https://www.health.harvard.edu/newsletter_article/PSA-Prostate-Specific-Antigen-Persisting-Scientific-Ambiguities.
5. Aaron, L., O.E. Franco, and S.W. Hayward, *Review of Prostate Anatomy and Embryology and the Etiology of Benign Prostatic Hyperplasia.* Urol Clin North Am, 2016. **43**(3): p. 279-88.
6. Datta, K., et al., *Mechanism of lymph node metastasis in prostate cancer.* Future Oncol, 2010. **6**(5): p. 823-36.
7. McNeal, J.E., *Anatomy of the prostate: an historical survey of divergent views.* Prostate, 1980. **1**(1): p. 3-13.
8. McNeal, J.E., *Normal histology of the prostate.* Am J Surg Pathol, 1988. **12**(8): p. 619-33.
9. Arnold, J.T. and J.T. Isaacs, *Mechanisms involved in the progression of androgen-independent prostate cancers: it is not only the cancer cell's fault.* Endocr Relat Cancer, 2002. **9**(1): p. 61-73.
10. Rybak, A.P., R.G. Bristow, and A. Kapoor, *Prostate cancer stem cells: deciphering the origins and pathways involved in prostate tumorigenesis and aggression.* Oncotarget, 2015. **6**(4): p. 1900-19.
11. Society, A.C. *Survival Rates for Prostate Cancer*. 2019 June 10, 2019]; Available from: https://www.cancer.org/cancer/prostate-cancer/detection-diagnosis-staging/survival-rates.html.
12. Institute, N.C., *Cancer Stat Facts: Prostate Cancer*. 2019: SEER.
13. Bubendorf, L., et al., *Metastatic patterns of prostate cancer: an autopsy study of 1,589 patients.* Hum Pathol, 2000. **31**(5): p. 578-83.
14. Zeliadt, S.B., et al., *Biopsy follow-up of prostate-specific antigen tests.* Am J Prev Med, 2012. **42**(1): p. 37-43.
15. Tsodikov, A., et al., *Reconciling the Effects of Screening on Prostate Cancer Mortality in the ERSPC and PLCO Trials.* Ann Intern Med, 2017. **167**(7): p. 449-455.
16. Care, I.f.Q.a.E.i.H., *What is low-risk prostate cancer and how is it treated?* 2018, InformedHealth.org [Internet]: Cologne, Germany.
17. Efstathiou, J.A., et al., *Prostate-specific antigen-based serial screening may decrease prostate cancer-specific mortality.* Urology, 2006. **68**(2): p. 342-7.

18. Kettering, M.S. *Prostate Cancer Screening Guidelines*. June 11, 2019]; Available from: https://www.mskcc.org/cancer-care/types/prostate/screening/screening-guidelines-prostate.
19. Leitzmann, M.F. and S. Rohrmann, *Risk factors for the onset of prostatic cancer: age, location, and behavioral correlates.* Clin Epidemiol, 2012. **4**: p. 1-11.
20. Mistry, S., et al., Can Urol Assoc J, 2009. **3**(3): p. 205-210.
21. Odedina, F.T., et al., *Prostate cancer disparities in Black men of African descent: a comparative literature review of prostate cancer burden among Black men in the United States, Caribbean, United Kingdom, and West Africa.* Infect Agent Cancer, 2009. **4 Suppl 1**: p. S2.
22. Chen, Y.C., et al., *Family history of prostate and breast cancer and the risk of prostate cancer in the PSA era.* Prostate, 2008. **68**(14): p. 1582-91.
23. Wolf, A.M., et al., *American Cancer Society guideline for the early detection of prostate cancer: update 2010.* CA Cancer J Clin, 2010. **60**(2): p. 70-98.
24. Nicotera, T.M., et al., *Regulation of PSA secretion and survival signaling by calcium-independent phopholipase A(2)beta in prostate cancer cells.* Prostate, 2009. **69**(12): p. 1270-80.
25. Balk, S.P., Y.J. Ko, and G.J. Bubley, *Biology of prostate-specific antigen.* J Clin Oncol, 2003. **21**(2): p. 383-91.
26. Pezaro, C., H.H. Woo, and I.D. Davis, *Prostate cancer: measuring PSA.* Intern Med J, 2014. **44**(5): p. 433-40.
27. Institute, N.C. *Prostate-Specific Antigen (PSA) Test*. 2017 June 10, 2019]; Available from: https://www.cancer.gov/types/prostate/psa-fact-sheet.
28. Pentyala, S., et al., *Prostate cancer markers: An update.* Biomed Rep, 2016. **4**(3): p. 263-268.
29. Thompson, I.M., et al., *Prevalence of prostate cancer among men with a prostate-specific antigen level < or =4.0 ng per milliliter.* N Engl J Med, 2004. **350**(22): p. 2239-46.
30. Gleason, D.F., *Classification of prostatic carcinomas.* Cancer Chemother Rep, 1966. **50**(3): p. 125-8.
31. Carter, H.B., *Differentiation of lethal and non lethal prostate cancer: PSA and PSA isoforms and kinetics.* Asian J Androl, 2012. **14**(3): p. 355-60.
32. Singh, R., et al., *Repeating the measurement of prostate-specific antigen in symptomatic men can avoid unnecessary prostatic biopsy.* BJU Int, 2003. **92**(9): p. 932-5.
33. Neuhaus, J. and B. Yang, *Liquid Biopsy Potential Biomarkers in Prostate Cancer.* Diagnostics (Basel), 2018. **8**(4).
34. Garisto, J.D. and L. Klotz, *Active Surveillance for Prostate Cancer: How to Do It Right.* Oncology (Williston Park), 2017. **31**(5): p. 333-40, 345.
35. Mahal, B.A., et al., *Use of Active Surveillance or Watchful Waiting for Low-Risk Prostate Cancer and Management Trends Across Risk Groups in the United States, 2010-2015.* JAMA, 2019.
36. Artibani, W., et al., *Management of Biochemical Recurrence after Primary Curative Treatment for Prostate Cancer: A Review.* Urol Int, 2018. **100**(3): p. 251-262.

37. Lee, D.K., et al., *Progression of prostate cancer despite an extremely low serum level of prostate-specific antigen.* Korean J Urol, 2010. **51**(5): p. 358-61.
38. Mahal, B.A., et al., *Association of very low prostate-specific antigen levels with increased cancer-specific death in men with high-grade prostate cancer.* Cancer, 2016. **122**(1): p. 78-83.
39. Leibovici, D., et al., *Prostate cancer progression in the presence of undetectable or low serum prostate-specific antigen level.* Cancer, 2007. **109**(2): p. 198-204.
40. William K. Oh, M., Mark Hurwitz, MD, Anthony V. D'Amico, MD, Jerome P. Richie, MD, and Philip W. Kantoff, MD., *Biology of Prostate Cancer*, in *Holland-Frei Cancer Medicine*, P.R. Kufe DW, Weichselbaum RR, Editor. 2003, BC Decker: Hamilton (ON).
41. Nazir, B., *Pain during transrectal ultrasound-guided prostate biopsy and the role of periprostatic nerve block: what radiologists should know.* Korean J Radiol, 2014. **15**(5): p. 543-53.
42. Chen, N. and Q. Zhou, *The evolving Gleason grading system.* Chin J Cancer Res, 2016. **28**(1): p. 58-64.
43. National Cancer Institute, S.T.M. *Prostate Cancer - Morphology & Grade*. June 12, 2019]; Available from: https://training.seer.cancer.gov/prostate/abstract-code-stage/morphology.html.
44. Sarkar, S. and S. Das, *A Review of Imaging Methods for Prostate Cancer Detection.* Biomed Eng Comput Biol, 2016. **7**(Suppl 1): p. 1-15.
45. Society, A.C. *Prostate Cancer Stages*. 2017 June 17, 2019]; Available from: https://www.cancer.org/cancer/prostate-cancer/detection-diagnosis-staging/staging.html.
46. Cancer, A.J.C., *Prostate Cancer Staging*. 2010.
47. Lepor, H., *Selecting candidates for radical prostatectomy.* Rev Urol, 2000. **2**(3): p. 182-9.
48. Center, M.S.K.C. June 17, 2019]; Radical Prostatectomy for Prostate Cancer]. Available from: https://www.mskcc.org/cancer-care/types/prostate/treatment/radical-prostatectomy.
49. Chao, M.W., et al., *Brachytherapy: state-of-the-art radiotherapy in prostate cancer.* BJU Int, 2015. **116 Suppl 3**: p. 80-8.
50. Society, A.C. *Radiation Therapy for Prostate Cancer* . 2016 June 17, 2019]; Available from: https://www.cancer.org/cancer/prostate-cancer/treating/radiation-therapy.html.
51. Stish, B.J., et al., *Low dose rate prostate brachytherapy.* Transl Androl Urol, 2018. **7**(3): p. 341-356.
52. King, C.R., *LDR vs. HDR brachytherapy for localized prostate cancer: the view from radiobiological models.* Brachytherapy, 2002. **1**(4): p. 219-26.
53. Center, M.S.K.C. *Radiation Therapy for Prostate Cancer* . June 17, 2019]; Available from: https://www.mskcc.org/cancer-care/types/prostate/treatment/radiation-therapy.
54. Fischer-Valuck, B.W., Y.J. Rao, and J.M. Michalski, *Intensity-modulated radiotherapy for prostate cancer.* Transl Androl Urol, 2018. **7**(3): p. 297-307.

55. Center, M.S.K.C. *Image-Guided, Intensity-Modulated Radiation Therapy (IG-IMRT) to the Prostate*
Share
. 2018 June 17, 2019]; Available from: https://www.mskcc.org/cancer-care/patient-education/intensity-modulated-radiation-therapy-prostate.
56. Hoshina, R.M., et al., *A Literature Review of Proton Beam Therapy for Prostate Cancer in Japan.* J Clin Med, 2019. **8**(1).
57. Sheets, N.C., et al., *Intensity-modulated radiation therapy, proton therapy, or conformal radiation therapy and morbidity and disease control in localized prostate cancer.* JAMA, 2012. **307**(15): p. 1611-20.
58. Yu, J.B., et al., *Stereotactic body radiation therapy versus intensity-modulated radiation therapy for prostate cancer: comparison of toxicity.* J Clin Oncol, 2014. **32**(12): p. 1195-201.
59. Kothari, G., et al., *Stereotactic Body Radiotherapy for Primary Prostate Cancer.* Technol Cancer Res Treat, 2018. **17**: p. 1533033818789633.
60. Marshall, S. and S. Taneja, *Focal therapy for prostate cancer: The current status.* Prostate Int, 2015. **3**(2): p. 35-41.
61. Center, M.S.K.C. *Focal Therapies for Prostate Cancer*
. June 17, 2019]; Available from: https://www.mskcc.org/cancer-care/types/prostate/treatment/focal-therapies.
62. Ashrafi, A.N., et al., *Focal therapy for prostate cancer: concepts and future directions.* Curr Opin Urol, 2018. **28**(6): p. 536-543.
63. Center, M.S.K.C. *Systemic Therapies*. June 17, 2019]; Available from: https://www.mskcc.org/cancer-care/types/prostate/treatment/systemic-therapies.
64. Lonergan, P.E. and D.J. Tindall, *Androgen receptor signaling in prostate cancer development and progression.* J Carcinog, 2011. **10**: p. 20.
65. Society, A.C. *Hormone Therapy for Prostate Cancer*. 2018 June 17, 2019]; Available from: https://www.cancer.org/cancer/prostate-cancer/treating/hormone-therapy.html.
66. Crawford, E.D., et al., *Androgen-targeted therapy in men with prostate cancer: evolving practice and future considerations.* Prostate Cancer and Prostatic Diseases, 2019. **22**(1): p. 24-38.
67. Lepor, H. and N.D. Shore, *LHRH Agonists for the Treatment of Prostate Cancer: 2012.* Rev Urol, 2012. **14**(1-2): p. 1-12.
68. Fraietta, R., D.S. Zylberstejn, and S.C. Esteves, *Hypogonadotropic hypogonadism revisited.* Clinics (Sao Paulo), 2013. **68 Suppl 1**: p. 81-8.
69. Thompson, I.M., *Flare Associated with LHRH-Agonist Therapy.* Rev Urol, 2001. **3 Suppl 3**: p. S10-4.
70. Crawford, E.D. and A.H. Hou, *The role of LHRH antagonists in the treatment of prostate cancer.* Oncology (Williston Park), 2009. **23**(7): p. 626-30.
71. Alex, A.B., S.K. Pal, and N. Agarwal, *CYP17 inhibitors in prostate cancer: latest evidence and clinical potential.* Ther Adv Med Oncol, 2016. **8**(4): p. 267-75.
72. de Bono, J.S., et al., *Abiraterone and increased survival in metastatic prostate cancer.* N Engl J Med, 2011. **364**(21): p. 1995-2005.

73. Auchus, R.J., et al., *Use of prednisone with abiraterone acetate in metastatic castration-resistant prostate cancer.* Oncologist, 2014. **19**(12): p. 1231-40.
74. Schalken, J. and J.M. Fitzpatrick, *Enzalutamide: targeting the androgen signalling pathway in metastatic castration-resistant prostate cancer.* BJU Int, 2016. **117**(2): p. 215-25.
75. Ito, Y. and M.D. Sadar, *Enzalutamide and blocking androgen receptor in advanced prostate cancer: lessons learnt from the history of drug development of antiandrogens.* Res Rep Urol, 2018. **10**: p. 23-32.
76. Masiello, D., et al., *Bicalutamide functions as an androgen receptor antagonist by assembly of a transcriptionally inactive receptor.* J Biol Chem, 2002. **277**(29): p. 26321-6.
77. Shore, N.D., et al., *Efficacy and safety of enzalutamide versus bicalutamide for patients with metastatic prostate cancer (TERRAIN): a randomised, double-blind, phase 2 study.* Lancet Oncol, 2016. **17**(2): p. 153-163.
78. Fizazi, K., et al., *Darolutamide in Nonmetastatic, Castration-Resistant Prostate Cancer.* N Engl J Med, 2019. **380**(13): p. 1235-1246.
79. Institute, N.C. *FDA Approves Apalutamide for Some Men with Prostate Cancer*. 2018 June 17, 2019]; Available from: https://www.cancer.gov/news-events/cancer-currents-blog/2018/apalutamide-fda-nonmetastatic-prostate.
80. Teply, B.A. and R.J. Hauke, *Chemotherapy options in castration-resistant prostate cancer.* Indian J Urol, 2016. **32**(4): p. 262-270.
81. Pienta, K.J., *Preclinical mechanisms of action of docetaxel and docetaxel combinations in prostate cancer.* Semin Oncol, 2001. **28**(4 Suppl 15): p. 3-7.
82. Fujita, K. and N. Nonomura, *Role of Androgen Receptor in Prostate Cancer: A Review.* World J Mens Health, 2018.
83. Vasaitis, T.S., R.D. Bruno, and V.C. Njar, *CYP17 inhibitors for prostate cancer therapy.* J Steroid Biochem Mol Biol, 2011. **125**(1-2): p. 23-31.
84. Karl K. Kwok, E.C.V., James N. Gibson, *Antineoplastic drugs*, in *Pharmacology and Therapeutics for Dentistry*. 2017, Elsevier. p. 530-562.
85. Koivisto, P., et al., *Androgen receptor gene amplification: a possible molecular mechanism for androgen deprivation therapy failure in prostate cancer.* Cancer Res, 1997. **57**(2): p. 314-9.
86. Linja, M.J., et al., *Amplification and overexpression of androgen receptor gene in hormone-refractory prostate cancer.* Cancer Res, 2001. **61**(9): p. 3550-5.
87. Gregory, C.W., et al., *Androgen receptor stabilization in recurrent prostate cancer is associated with hypersensitivity to low androgen.* Cancer Res, 2001. **61**(7): p. 2892-8.
88. Hu, R., S.R. Denmeade, and J. Luo, *Molecular processes leading to aberrant androgen receptor signaling and castration resistance in prostate cancer.* Expert Rev Endocrinol Metab, 2010. **5**(5): p. 753-764.
89. Eisermann, K., et al., *Androgen receptor gene mutation, rearrangement, polymorphism.* Transl Androl Urol, 2013. **2**(3): p. 137-147.
90. Korpal, M., et al., *An F876L mutation in androgen receptor confers genetic and phenotypic resistance to MDV3100 (enzalutamide).* Cancer Discov, 2013. **3**(9): p. 1030-43.

91. Chandrasekar, T., et al., *Mechanisms of resistance in castration-resistant prostate cancer (CRPC).* Transl Androl Urol, 2015. **4**(3): p. 365-80.
92. Paller, C.J. and E.S. Antonarakis, *Management of biochemically recurrent prostate cancer after local therapy: evolving standards of care and new directions.* Clin Adv Hematol Oncol, 2013. **11**(1): p. 14-23.
93. Roehl, K.A., et al., *Cancer progression and survival rates following anatomical radical retropubic prostatectomy in 3,478 consecutive patients: long-term results.* J Urol, 2004. **172**(3): p. 910-4.
94. Freedland, S.J., et al., *Risk of prostate cancer-specific mortality following biochemical recurrence after radical prostatectomy.* JAMA, 2005. **294**(4): p. 433-9.
95. Burkhardt, J.H., et al., *Comparing the costs of radiation therapy and radical prostatectomy for the initial treatment of early-stage prostate cancer.* J Clin Oncol, 2002. **20**(12): p. 2869-75.
96. Kupelian, P.A., et al., *Use of different definitions of biochemical failure after external beam radiotherapy changes conclusions about relative treatment efficacy for localized prostate cancer.* Urology, 2006. **68**(3): p. 593-8.
97. Shipley, W.U., et al., *Radiation therapy for clinically localized prostate cancer: a multi-institutional pooled analysis.* JAMA, 1999. **281**(17): p. 1598-604.
98. Albala, D.M., *Imaging and treatment recommendations in patients with castrate-resistant prostate cancer.* Rev Urol, 2017. **19**(3): p. 200-202.
99. Sumanasuriya, S. and J. De Bono, *Treatment of Advanced Prostate Cancer-A Review of Current Therapies and Future Promise.* Cold Spring Harb Perspect Med, 2018. **8**(6).
100. Ritch, C. and M. Cookson, *Recent trends in the management of advanced prostate cancer.* F1000Res, 2018. **7**.
101. Santoni, M., et al., *Neuroendocrine differentiation in prostate cancer: novel morphological insights and future therapeutic perspectives.* Biochim Biophys Acta, 2014. **1846**(2): p. 630-7.
102. Grigore, A.D., E. Ben-Jacob, and M.C. Farach-Carson, *Prostate cancer and neuroendocrine differentiation: more neuronal, less endocrine?* Front Oncol, 2015. **5**: p. 37.
103. Gupta, K. and S. Gupta, *Neuroendocrine differentiation in prostate cancer: key epigenetic players.* Transl Cancer Res, 2017. **6**(Suppl 1): p. S104-S108.
104. Ather, M.H., et al., *Correlation of three immunohistochemically detected markers of neuroendocrine differentiation with clinical predictors of disease progression in prostate cancer.* BMC Urol, 2008. **8**: p. 21.
105. Beltran, H., et al., *Molecular characterization of neuroendocrine prostate cancer and identification of new drug targets.* Cancer Discov, 2011. **1**(6): p. 487-95.
106. Komiya, A., et al., *The prognostic significance of loss of the androgen receptor and neuroendocrine differentiation in prostate biopsy specimens among castration-resistant prostate cancer patients.* Mol Clin Oncol, 2013. **1**(2): p. 257-262.
107. Humeniuk, M.S., et al., *Platinum sensitivity in metastatic prostate cancer: does histology matter?* Prostate Cancer Prostatic Dis, 2018. **21**(1): p. 92-99.

108. Harvey, C.J., et al., *Applications of transrectal ultrasound in prostate cancer.* Br J Radiol, 2012. **85 Spec No 1**: p. S3-17.
109. Rifkin, M.D., *Ultrasound of the prostate--applications and indications.* Schweiz Med Wochenschr, 1991. **121**(9): p. 282-91.
110. Pat F. Fulgham, M.D.B.R., MD; Jonathan N. Rubenstein, MD; Samir S. Taneja, MD; Peter R. Carroll, MD; Peter A. Pinto, MD; Marc A. Bjurlin, DO, MSc; Scott Eggener, MD. *MRI of the Prostate, Standard Operating Procedure (SOP)*. 2019 July 12, 2019]; Available from: https://www.auanet.org/guidelines/mri-of-the-prostate-sop.
111. Ghai, S. and M.A. Haider, *Multiparametric-MRI in diagnosis of prostate cancer.* Indian J Urol, 2015. **31**(3): p. 194-201.
112. Pedler, K., et al., *The current status of MRI in prostate cancer.* Aust Fam Physician, 2015. **44**(4): p. 225-30.
113. Ludwig, D.R., et al., *Imaging in Prostate Cancer: Magnetic Resonance Imaging and Beyond.* Mo Med, 2018. **115**(2): p. 135-141.
114. Taneja, S.S., *Imaging in the diagnosis and management of prostate cancer.* Rev Urol, 2004. **6**(3): p. 101-13.
115. Tombal, B. and F. Lecouvet, *Modern Detection of Prostate Cancer's Bone Metastasis: Is the Bone Scan Era Over?* Adv Urol, 2012. **2012**: p. 893193.
116. Wallitt, K.L., et al., *Clinical PET Imaging in Prostate Cancer.* Radiographics, 2017. **37**(5): p. 1512-1536.
117. Goncalves, G.A.R. and R.M.A. Paiva, *Gene therapy: advances, challenges and perspectives.* Einstein (Sao Paulo), 2017. **15**(3): p. 369-375.
118. Dickler, H.B. and E. Collier, *Gene therapy in the treatment of disease.* Journal of Allergy and Clinical Immunology, 1994. **94**(6): p. 942-951.
119. Shah, K., et al., *Molecular imaging of gene therapy for cancer.* Gene Ther, 2004. **11**(15): p. 1175-87.
120. Blasberg, R.G. and J.G. Tjuvajev, *Molecular-genetic imaging: current and future perspectives.* J Clin Invest, 2003. **111**(11): p. 1620-9.
121. Kang, J.H. and J.K. Chung, *Molecular-genetic imaging based on reporter gene expression.* J Nucl Med, 2008. **49 Suppl 2**: p. 164S-79S.
122. Cocco, E., et al., *Dual-Targeting Nanoparticles for In Vivo Delivery of Suicide Genes to Chemotherapy-Resistant Ovarian Cancer Cells.* Mol Cancer Ther, 2017. **16**(2): p. 323-333.
123. Barve, M., et al., *Phase 1 Trial of Bi-shRNA STMN1 BIV in Refractory Cancer.* Mol Ther, 2015. **23**(6): p. 1123-1130.
124. Buscail, L., et al., *First-in-man phase 1 clinical trial of gene therapy for advanced pancreatic cancer: safety, biodistribution, and preliminary clinical findings.* Mol Ther, 2015. **23**(4): p. 779-89.
125. Gofrit, O.N., et al., *DNA based therapy with diphtheria toxin-A BC-819: a phase 2b marker lesion trial in patients with intermediate risk nonmuscle invasive bladder cancer.* J Urol, 2014. **191**(6): p. 1697-702.
126. He, Z.Y., et al., *Ovarian cancer treatment with a tumor-targeting and gene expression-controllable lipoplex.* Sci Rep, 2016. **6**: p. 23764.

127. Kim, H., et al., *Gene therapy using plasmid DNA-encoded anti-HER2 antibody for cancers that overexpress HER2.* Cancer Gene Ther, 2016. **23**(10): p. 341-347.
128. Lampreht Tratar, U., et al., *Gene Electrotransfer of Plasmid-Encoding IL-12 Recruits the M1 Macrophages and Antigen-Presenting Cells Inducing the Eradication of Aggressive B16F10 Murine Melanoma.* Mediators Inflamm, 2017. **2017**: p. 5285890.
129. Lavie, O., et al., *A phase 1/2a, dose-escalation, safety, pharmacokinetic, and preliminary efficacy study of intraperitoneal administration of BC-819 (H19-DTA) in subjects with recurrent ovarian/peritoneal cancer.* Arch Gynecol Obstet, 2017. **295**(3): p. 751-761.
130. Lara, A.R., O.T. Ramirez, and M. Wunderlich, *Plasmid DNA production for therapeutic applications.* Methods Mol Biol, 2012. **824**: p. 271-303.
131. McNeel, D.G., et al., *Real-time immune monitoring to guide plasmid DNA vaccination schedule targeting prostatic acid phosphatase in patients with castration-resistant prostate cancer.* Clin Cancer Res, 2014. **20**(14): p. 3692-704.
132. Norell, H., et al., *Vaccination with a plasmid DNA encoding HER-2/neu together with low doses of GM-CSF and IL-2 in patients with metastatic breast carcinoma: a pilot clinical trial.* J Transl Med, 2010. **8**: p. 53.
133. Zheng, C. and B.J. Baum, *Evaluation of promoters for use in tissue-specific gene delivery.* Methods Mol Biol, 2008. **434**: p. 205-19.
134. Sidi, A.A., et al., *Phase I/II marker lesion study of intravesical BC-819 DNA plasmid in H19 over expressing superficial bladder cancer refractory to bacillus Calmette-Guerin.* J Urol, 2008. **180**(6): p. 2379-83.
135. Zarogoulidis, P., et al., *Suicide Gene Therapy for Cancer - Current Strategies.* J Genet Syndr Gene Ther, 2013. **4**.
136. Fairman, J., K.H. Liu, and S. Menne, *Prevention of liver tumor formation in woodchucks with established hepatocellular carcinoma by treatment with cationic liposome-DNA complexes.* BMC Cancer, 2017. **17**(1): p. 172.
137. Keasey, N., et al., *A non-coding cationic lipid DNA complex produces lasting anti-leukemic effects.* Cancer Biol Ther, 2010. **10**(6): p. 625-31.
138. Suschak, J.J., J.A. Williams, and C.S. Schmaljohn, *Advancements in DNA vaccine vectors, non-mechanical delivery methods, and molecular adjuvants to increase immunogenicity.* Hum Vaccin Immunother, 2017. **13**(12): p. 2837-2848.
139. Meleshko, A.N., et al., *Phase I clinical trial of idiotypic DNA vaccine administered as a complex with polyethylenimine to patients with B-cell lymphoma.* Hum Vaccin Immunother, 2017. **13**(6): p. 1-6.
140. Amit, D. and A. Hochberg, *Development of targeted therapy for bladder cancer mediated by a double promoter plasmid expressing diphtheria toxin under the control of H19 and IGF2-P4 regulatory sequences.* J Transl Med, 2010. **8**: p. 134.
141. Zakeri, A., et al., *Polyethylenimine-based nanocarriers in co-delivery of drug and gene: a developing horizon.* Nano Rev Exp, 2018. **9**(1): p. 1488497.
142. Schmeer, M., T. Buchholz, and M. Schleef, *Plasmid DNA Manufacturing for Indirect and Direct Clinical Applications.* Hum Gene Ther, 2017. **28**(10): p. 856-861.

143. Bhang, H.E. and M.G. Pomper, *Cancer imaging: Gene transcription-based imaging and therapeutic systems.* Int J Biochem Cell Biol, 2012. **44**(5): p. 684-9.
144. Nichols, W.W., et al., *Potential DNA vaccine integration into host cell genome.* Ann N Y Acad Sci, 1995. **772**: p. 30-9.
145. Wold, W.S. and K. Toth, *Adenovirus vectors for gene therapy, vaccination and cancer gene therapy.* Curr Gene Ther, 2013. **13**(6): p. 421-33.
146. Khanal, S., P. Ghimire, and A.S. Dhamoon, *The Repertoire of Adenovirus in Human Disease: The Innocuous to the Deadly.* Biomedicines, 2018. **6**(1).
147. Crystal, R.G., *Adenovirus: the first effective in vivo gene delivery vector.* Hum Gene Ther, 2014. **25**(1): p. 3-11.
148. Harui, A., et al., *Frequency and stability of chromosomal integration of adenovirus vectors.* J Virol, 1999. **73**(7): p. 6141-6.
149. Lee, C.S., et al., *Adenovirus-Mediated Gene Delivery: Potential Applications for Gene and Cell-Based Therapies in the New Era of Personalized Medicine.* Genes Dis, 2017. **4**(2): p. 43-63.
150. Jonsson, F. and F. Kreppel, *Barriers to systemic application of virus-based vectors in gene therapy: lessons from adenovirus type 5.* Virus Genes, 2017. **53**(5): p. 692-699.
151. Barton, K.N., et al., *Phase I study of noninvasive imaging of adenovirus-mediated gene expression in the human prostate.* Mol Ther, 2008. **16**(10): p. 1761-9.
152. Strimbu, K. and J.A. Tavel, *What are biomarkers?* Curr Opin HIV AIDS, 2010. **5**(6): p. 463-6.
153. Goossens, N., et al., *Cancer biomarker discovery and validation.* Transl Cancer Res, 2015. **4**(3): p. 256-269.
154. Poste, G., *Bring on the biomarkers.* Nature, 2011. **469**(7329): p. 156-7.
155. Bernsen, M.R., et al., *Biomarkers in preclinical cancer imaging.* Eur J Nucl Med Mol Imaging, 2015. **42**(4): p. 579-96.
156. Shapovalova, M., et al., *Exploiting the transcriptional specificity of the alpha-methylacyl-CoA racemase AMACR promoter for the molecular imaging of prostate cancer.* Oncotarget, 2018. **9**(94): p. 36693-36704.
157. Autio, K.J., et al., *Role of AMACR (alpha-methylacyl-CoA racemase) and MFE-1 (peroxisomal multifunctional enzyme-1) in bile acid synthesis in mice.* Biochem J, 2014. **461**(1): p. 125-35.
158. Daugherty, S.E., et al., *Polymorphic variants in alpha-methylacyl-CoA racemase and prostate cancer.* Prostate, 2007. **67**(14): p. 1487-97.
159. Dick, D., R. Horvath, and P.F. Chinnery, *AMACR mutations cause late-onset autosomal recessive cerebellar ataxia.* Neurology, 2011. **76**(20): p. 1768-70.
160. Lloyd, M.D., et al., *Alpha-methylacyl-CoA racemase--an 'obscure' metabolic enzyme takes centre stage.* FEBS J, 2008. **275**(6): p. 1089-102.
161. Jiang, Z., et al., *P504S: a new molecular marker for the detection of prostate carcinoma.* Am J Surg Pathol, 2001. **25**(11): p. 1397-404.
162. Walsh, P.C., *Alpha-methylacyl-CoA racemase: a new molecular marker for prostate cancer.* J Urol, 2002. **168**(4 Pt 1): p. 1635.
163. Rubin, M.A., et al., *alpha-Methylacyl coenzyme A racemase as a tissue biomarker for prostate cancer.* JAMA, 2002. **287**(13): p. 1662-70.

164. Luo, J., et al., *Alpha-methylacyl-CoA racemase: a new molecular marker for prostate cancer.* Cancer Res, 2002. **62**(8): p. 2220-6.
165. Zha, S., et al., *Alpha-methylacyl-CoA racemase as an androgen-independent growth modifier in prostate cancer.* Cancer Res, 2003. **63**(21): p. 7365-76.
166. Hessels, D. and J.A. Schalken, *Urinary biomarkers for prostate cancer: a review.* Asian J Androl, 2013. **15**(3): p. 333-9.
167. Zhou, M., et al., *Alpha-Methylacyl-CoA racemase: a novel tumor marker over-expressed in several human cancers and their precursor lesions.* Am J Surg Pathol, 2002. **26**(7): p. 926-31.
168. Yevglevskis, M., et al., *A novel colorimetric assay for alpha-methylacyl-CoA racemase 1A (AMACR; P504S) utilizing the elimination of 2,4-dinitrophenolate.* Chem Commun (Camb), 2017. **53**(37): p. 5087-5090.
169. Zeng, Y., et al., *Horseradish peroxidase and aptamer dual-functionalized nanoprobe for the amplification detection of alpha-methylacyl-CoA racemase.* Anal Chim Acta, 2015. **899**: p. 100-5.
170. Yang, D.K., et al., *Selection of aptamers for fluorescent detection of alpha-methylacyl-CoA racemase by single-bead SELEX.* Biosens Bioelectron, 2014. **62**: p. 106-12.
171. Wilson, B.A., et al., *High-throughput screen identifies novel inhibitors of cancer biomarker alpha-methylacyl coenzyme A racemase (AMACR/P504S).* Mol Cancer Ther, 2011. **10**(5): p. 825-38.
172. Niu, G. and X. Chen, *Molecular imaging with activatable reporter systems.* Theranostics, 2012. **2**(4): p. 413-23.
173. Watanabe, M., et al., *Advanced two-step transcriptional amplification as a novel method for cancer-specific gene expression and imaging.* Oncol Rep, 2011. **26**(4): p. 769-75.
174. Sharma, A., et al., *Adenoviral vector-based strategies for cancer therapy.* Curr Drug ther, 2009. **4**(2): p. 117-138.
175. Maier, T., M. Guell, and L. Serrano, *Correlation of mRNA and protein in complex biological samples.* FEBS Lett, 2009. **583**(24): p. 3966-73.
176. Cancer Genome Atlas Research, N., *The Molecular Taxonomy of Primary Prostate Cancer.* Cell, 2015. **163**(4): p. 1011-25.
177. Grasso, C.S., et al., *The mutational landscape of lethal castration-resistant prostate cancer.* Nature, 2012. **487**(7406): p. 239-43.
178. Taylor, B.S., et al., *Integrative genomic profiling of human prostate cancer.* Cancer Cell, 2010. **18**(1): p. 11-22.
179. Honma, I., et al., *Aberrant expression and potency as a cancer immunotherapy target of alpha-methylacyl-coenzyme A racemase in prostate cancer.* J Transl Med, 2009. **7**: p. 103.
180. Yocum, A.K., et al., *Development of selected reaction monitoring-MS methodology to measure peptide biomarkers in prostate cancer.* Proteomics, 2010. **10**(19): p. 3506-14.
181. Gumulec, J., et al., *Evaluation of alpha-methylacyl-CoA racemase, metallothionein and prostate specific antigen as prostate cancer prognostic markers.* Neoplasma, 2012. **59**(2): p. 191-201.

182. Horoszewicz, J.S., et al., *LNCaP model of human prostatic carcinoma.* Cancer Res, 1983. **43**(4): p. 1809-18.
183. Bishop, J.L., et al., *PD-L1 is highly expressed in Enzalutamide resistant prostate cancer.* Oncotarget, 2015. **6**(1): p. 234-42.
184. Cunningham, D. and Z. You, *In vitro and in vivo model systems used in prostate cancer research.* J Biol Methods, 2015. **2**(1).
185. Zhang, X., et al., *Deletion hotspots in AMACR promoter CpG island are cis-regulatory elements controlling the gene expression in the colon.* PLoS Genet, 2009. **5**(1): p. e1000334.
186. Iyer, M., et al., *Two-step transcriptional amplification as a method for imaging reporter gene expression using weak promoters.* Proc Natl Acad Sci U S A, 2001. **98**(25): p. 14595-600.
187. Ceci, F., et al., *New aspects of molecular imaging in prostate cancer.* Methods, 2017. **130**: p. 36-41.
188. Chen, W., et al., *Molecular cloning and preliminary analysis of the human alpha-methylacyl-CoA racemase promoter.* Mol Biol Rep, 2009. **36**(3): p. 423-30.
189. Davydova, J., et al., *Infectivity-enhanced cyclooxygenase-2-based conditionally replicative adenoviruses for esophageal adenocarcinoma treatment.* Cancer Res, 2004. **64**(12): p. 4319-27.
190. Krasnykh, V.N., et al., *Generation of recombinant adenovirus vectors with modified fibers for altering viral tropism.* J Virol, 1996. **70**(10): p. 6839-46.
191. Wong, H.H., et al., *Modification of the early gene enhancer-promoter improves the oncolytic potency of adenovirus 11.* Mol Ther, 2012. **20**(2): p. 306-16.
192. Yaghoubi, S.S. and S.S. Gambhir, *PET imaging of herpes simplex virus type 1 thymidine kinase (HSV1-tk) or mutant HSV1-sr39tk reporter gene expression in mice and humans using [18F]FHBG.* Nat Protoc, 2006. **1**(6): p. 3069-75.
193. Jounaidi, Y., J.C. Doloff, and D.J. Waxman, *Conditionally replicating adenoviruses for cancer treatment.* Curr Cancer Drug Targets, 2007. **7**(3): p. 285-301.
194. Van Etten, J.L., et al., *Targeting a Single Alternative Polyadenylation Site Coordinately Blocks Expression of Androgen Receptor mRNA Splice Variants in Prostate Cancer.* Cancer Res, 2017. **77**(19): p. 5228-5235.
195. Davydova, J. and M. Yamamoto, *Oncolytic adenoviruses: design, generation, and experimental procedures.* Curr Protoc Hum Genet, 2013. **Chapter 12**: p. Unit 12 14.
196. Siegel, R.L., K.D. Miller, and A. Jemal, *Cancer statistics, 2018.* CA Cancer J Clin, 2018. **68**(1): p. 7-30.
197. Sharifi, N., J.L. Gulley, and W.L. Dahut, *Androgen deprivation therapy for prostate cancer.* JAMA, 2005. **294**(2): p. 238-44.
198. Bluemn, E.G. and P.S. Nelson, *The androgen/androgen receptor axis in prostate cancer.* Curr Opin Oncol, 2012. **24**(3): p. 251-7.
199. Sharifi, N., *Mechanisms of Androgen Receptor Activation in Castration-Resistant Prostate Cancer.* Endocrinology, 2013. **154**(11): p. 4010-4017.
200. D. Crona, Y.W., *Androgen Receptor-Dependent and -Independent Mechanisms Involved in Prostate Cancer Therapy Resistance.* Cancers, 2017. **9**(67).

201. Ammannagari, N. and S. George, *Anti-androgen therapies for prostate cancer: A focused review*. Vol. 11. 2014. 15-19.
202. Vlachostergios, P.J., L. Puca, and H. Beltran, *Emerging Variants of Castration-Resistant Prostate Cancer.* Curr Oncol Rep, 2017. **19**(5): p. 32.
203. Beltran, H., et al., *Aggressive variants of castration-resistant prostate cancer.* Clin Cancer Res, 2014. **20**(11): p. 2846-50.
204. Kelloff, G.J., et al., *Challenges in clinical prostate cancer: role of imaging.* AJR Am J Roentgenol, 2009. **192**(6): p. 1455-70.
205. Langsteger, W., et al., *(18)F-NaF-PET/CT and (99m)Tc-MDP Bone Scintigraphy in the Detection of Bone Metastases in Prostate Cancer.* Semin Nucl Med, 2016. **46**(6): p. 491-501.
206. Lindenberg, M.L., et al., *Imaging Locally Advanced, Recurrent, and Metastatic Prostate Cancer: A Review.* JAMA Oncol, 2017. **3**(10): p. 1415-1422.
207. Zhu, A., D. Lee, and H. Shim, *Metabolic positron emission tomography imaging in cancer detection and therapy response.* Semin Oncol, 2011. **38**(1): p. 55-69.
208. Phelps, M.E., *Positron emission tomography provides molecular imaging of biological processes.* Proc Natl Acad Sci U S A, 2000. **97**(16): p. 9226-33.
209. Liu, Y., L.S. Zuckier, and N.V. Ghesani, *Dominant uptake of fatty acid over glucose by prostate cells: a potential new diagnostic and therapeutic approach.* Anticancer Res, 2010. **30**(2): p. 369-74.
210. Parent, E.E. and D.M. Schuster, *Update on (18)F-Fluciclovine PET for Prostate Cancer Imaging.* J Nucl Med, 2018. **59**(5): p. 733-739.
211. Minn, I., et al., *Molecular-genetic imaging of cancer.* Adv Cancer Res, 2014. **124**: p. 131-69.
212. Bhatnagar, A., et al., *AEG-1 promoter-mediated imaging of prostate cancer.* Cancer Res, 2014. **74**(20): p. 5772-81.
213. Bhang, H.E., et al., *Tumor-specific imaging through progression elevated gene-3 promoter-driven gene expression.* Nat Med, 2011. **17**(1): p. 123-9.
214. Li, C.M., et al., *PEG10 is a c-MYC target gene in cancer cells.* Cancer Res, 2006. **66**(2): p. 665-72.
215. Akamatsu, S., et al., *The Placental Gene PEG10 Promotes Progression of Neuroendocrine Prostate Cancer.* Cell Rep, 2015. **12**(6): p. 922-36.
216. Ono, R., et al., *Deletion of Peg10, an imprinted gene acquired from a retrotransposon, causes early embryonic lethality.* Nat Genet, 2006. **38**(1): p. 101-6.
217. Pflueger, D., et al., *Discovery of non-ETS gene fusions in human prostate cancer using next-generation RNA sequencing.* Genome Res, 2011. **21**(1): p. 56-67.
218. Robinson, D., et al., *Integrative Clinical Genomics of Advanced Prostate Cancer.* Cell, 2015. **162**(2): p. 454.
219. Bhanvadia, R.R., et al., *MEIS1 and MEIS2 Expression and Prostate Cancer Progression: A Role For HOXB13 Binding Partners in Metastatic Disease.* Clin Cancer Res, 2018. **24**(15): p. 3668-3680.
220. Nyquist, M.D., et al., *TALEN-engineered AR gene rearrangements reveal endocrine uncoupling of androgen receptor in prostate cancer.* Proc Natl Acad Sci U S A, 2013. **110**(43): p. 17492-7.

221. Wadosky, K.M. and S. Koochekpour, *Androgen receptor splice variants and prostate cancer: From bench to bedside.* Oncotarget, 2017. **8**(11): p. 18550-18576.
222. Guo, Z., et al., *A novel androgen receptor splice variant is up-regulated during prostate cancer progression and promotes androgen depletion-resistant growth.* Cancer Res, 2009. **69**(6): p. 2305-13.
223. Li, Y., et al., *Androgen receptor splice variants mediate enzalutamide resistance in castration-resistant prostate cancer cell lines.* Cancer Res, 2013. **73**(2): p. 483-9.
224. Luk, I.S., et al., *BIRC6 Targeting as Potential Therapy for Advanced, Enzalutamide-Resistant Prostate Cancer.* Clin Cancer Res, 2017. **23**(6): p. 1542-1551.
225. Kohli, M., et al., *Androgen Receptor Variant AR-V9 Is Coexpressed with AR-V7 in Prostate Cancer Metastases and Predicts Abiraterone Resistance.* Clin Cancer Res, 2017. **23**(16): p. 4704-4715.
226. Kumar, A., et al., *Substantial interindividual and limited intraindividual genomic diversity among tumors from men with metastatic prostate cancer.* Nat Med, 2016. **22**(4): p. 369-78.
227. Rotinen, M., et al., *ONECUT2 is a targetable master regulator of lethal prostate cancer that suppresses the androgen axis.* Nat Med, 2018. **24**(12): p. 1887-1898.
228. Guo, H., et al., *ONECUT2 is a driver of neuroendocrine prostate cancer.* Nat Commun, 2019. **10**(1): p. 278.
229. Lux, H., et al., *Genetic and molecular analyses of PEG10 reveal new aspects of genomic organization, transcription and translation.* PLoS One, 2010. **5**(1): p. e8686.
230. Zhang, L., et al., *Molecular engineering of a two-step transcription amplification (TSTA) system for transgene delivery in prostate cancer.* Mol Ther, 2002. **5**(3): p. 223-32.
231. Shcherbakova, D.M. and V.V. Verkhusha, *Near-infrared fluorescent proteins for multicolor in vivo imaging.* Nat Methods, 2013. **10**(8): p. 751-4.
232. Corey, E., et al., *Establishment and characterization of osseous prostate cancer models: intra-tibial injection of human prostate cancer cells.* Prostate, 2002. **52**(1): p. 20-33.
233. Yaghoubi, S.S. and S.S. Gambhir, *Measuring herpes simplex virus thymidine kinase reporter gene expression in vitro.* Nat Protoc, 2006. **1**(4): p. 2137-42.
234. Mahajan, S. and C.R. Divgi, *The role of iodine-124 positron emission tomography in molecular imaging.* Clinical and Translational Imaging, 2016. **4**(4): p. 297-306.
235. Bettegowda, C., et al., *Imaging bacterial infections with radiolabeled 1-(2'-deoxy-2'-fluoro-beta-D-arabinofuranosyl)-5-iodouracil.* Proc Natl Acad Sci U S A, 2005. **102**(4): p. 1145-50.
236. Trujillo, M.A., et al., *A probasin promoter, conditionally replicating adenovirus that expresses the sodium iodide symporter (NIS) for radiovirotherapy of prostate cancer.* Gene Ther, 2010. **17**(11): p. 1325-32.

237. Jiang, Z.K., et al., *Androgen-independent molecular imaging vectors to detect castration-resistant and metastatic prostate cancer.* Cancer Res, 2011. **71**(19): p. 6250-60.
238. Burton, J.B., et al., *Adenovirus-mediated gene expression imaging to directly detect sentinel lymph node metastasis of prostate cancer.* Nat Med, 2008. **14**(8): p. 882-8.
239. Hanna, N., et al., *Phase 1/2a, dose-escalation, safety, pharmacokinetic and preliminary efficacy study of intratumoral administration of BC-819 in patients with unresectable pancreatic cancer.* Cancer Gene Ther, 2012. **19**(6): p. 374-81.
240. Chollet, P., et al., *Side-effects of a systemic injection of linear polyethylenimine-DNA complexes.* J Gene Med, 2002. **4**(1): p. 84-91.
241. Nguyen, H.M., et al., *LuCaP Prostate Cancer Patient-Derived Xenografts Reflect the Molecular Heterogeneity of Advanced Disease an--d Serve as Models for Evaluating Cancer Therapeutics.* Prostate, 2017. **77**(6): p. 654-671.
242. Ebeling, S.B., et al., *Development and application of quantitative real time PCR and RT-PCR assays that discriminate between the full-length and truncated herpes simplex virus thymidine kinase gene.* J Virol Methods, 2003. **109**(2): p. 177-86.
243. Schmittgen, T.D. and K.J. Livak, *Analyzing real-time PCR data by the comparative C(T) method.* Nat Protoc, 2008. **3**(6): p. 1101-8.
244. Triezenberg, S.J., R.C. Kingsbury, and S.L. McKnight, *Functional dissection of VP16, the trans-activator of herpes simplex virus immediate early gene expression.* Genes Dev, 1988. **2**(6): p. 718-29.
245. Emami, K.H. and M. Carey, *A synergistic increase in potency of a multimerized VP16 transcriptional activation domain.* EMBO J, 1992. **11**(13): p. 5005-12.
246. Brodu, V., et al., *A UAS site substitution approach to the in vivo dissection of promoters: interplay between the GATAb activator and the AEF-1 repressor at a Drosophila ecdysone response unit.* Development, 2001. **128**(13): p. 2593-602.